



TAMPEREEN TEKNILLINEN YLIOPISTO
TAMPERE UNIVERSITY OF TECHNOLOGY

AAPO TERVONEN
MODELING DIFFUSION ACROSS THE BLOOD-RETINAL
BARRIER AND MASS TRANSFER IN A HALF-PERFUSION
CHAMBER

Master of Science Thesis

Examiners: professor Jari Hyttinen
and postdoctoral researcher Soile
Nymark

Examiners and topic approved in
the Faculty of Natural Sciences
council meeting on February 6th
2013

TIIVISTELMÄ

TAMPEREEN TEKNILLINEN YLIOPISTO

Biotekniikan koulutusohjelma

TERVONEN, AAPO: Veri-verkkokalvo esteen läpäisevän diffuusion ja puoliperfuusiokammiossa tapahtuvan massan siirtymisen mallintaminen

Diplomityö, 73 sivua, 4 liitesivua

Toukokuu 2013

Pääaine: Biokuvantaminen

Ohjaajat: professori Jari Hyttinen, tutkija Iina Vainio ja tutkijatohtori Soile Nymark

Tarkastajat: professori Jari Hyttinen ja tutkijatohtori Soile Nymark

Avainsanat: veri-verkkokalvo este, diffuusio, läpäisevyys, puoliperfuusiokammio, matemaattinen mallintaminen, silmänpohjan ikärappeuma

Väestön keskimääräisen eliniän kasvaessa vanhenemiseen liittyvät silmän sairaudet, kuten silmänpohjan ikärappeuma (age-related macular degeneration, AMD), muodostavat vakavan ongelman. AMD:n patogeneesin aikana verkkokalvon takana sijaitsevan veri-verkkokalvoeste (blood-retinal barrier, BRB) rakenne ja toiminta muuttuvat. BRB:llä on monia tärkeitä tehtäviä normaalin näkökyvyn ylläpitämisessä, ja se koostuu kolmesta osasta: verkkokalvon pigmenttiepiteelistä (retinal pigment epithelium, RPE), Bruchin kalvosta ja suonikalvon kapillaarien endoteelistä. Matemaattinen mallintaminen tarjoaa yksinkertaisen työkalun BRB:n ominaisuuksien tutkimiseen ja täten uusien hoitokeinojen kehittämiseen AMD:lle. Kokeellisessa tutkimuksessa hyödynnetään usein niin sanottuja diffuusiokammioita BRB:n esteominaisuuksiin tutkimiseen. Tässä työssä luodaan kaksi mallia: 1) passiivinen diffuusiomalli BRB:n läpäisevyydestä perustuen BRB:n ja diffundoituvan molekyylin fysikaaliskemiallisiin ominaisuuksiin (BRB-malli), ja 2) malli minityarisoidusta puoliperfuusiokammio ja tiettyjen parameterien vaikutuksesta sen toimintaan (kammiomalli).

BRB-malli rakennettiin yhdistämällä fysikaalisia teorioita kirjallisuudesta kuvaamaan diffuusion hidastumista eri tyypisissä ympäristöissä. Pää tavoitteina oli rakentaa malli ja validoida se kokeellisten tulosten perusteella, sekä tutkia BRB:n ja BRB:n osien esteominaisuuksien käyttäytymistä suhteessa diffundoituvan molekyylin ominaisuuksiin. Kammiomalli on elementtimenetelmämalli, ja se rakennettiin käyttämällä COMSOL Multiphysics mallinnusohjelmaa. Mallin tarkoituksena on tutkia systeemin mittojen ja muiden parametrien vaikutusta kammion toimintaan.

BRB-mallin tulokset osoittavat, että malli ennustaa oikein BRB:n läpäisevyyden kokuokan, mutta ei kykene kuvaamaan tarkemmin molekyyliominaisuuksista, kuten lipofiilisyydestä ja koosta, johtuvaa käyttäytymistä. RPE muodostaa suurimman esteen BRB:ssä, mutta Bruchin kalvo vaikuttaa hyvin lipofiilisiin molekyyliin. Kammiomallin tulokset näyttävät, että tämän tyyppisen kammion tarkkuutta rajoittaa molekyylin vapaa diffuusionopeus. Kammion mittojen ja muiden parametrien diffuusionopeudesta riippumaton vaikutus on pieni.

BRB-malli on ensimmäinen tyyppiään BRB:lle. Mallissa on ongelmia, mutta pienillä parannuksilla sitä voidaan hyödyntää BRB:n esteominaisuuksien tutkimisessa. Tulevaisuudessa mallia voidaan viedä moneen suuntaan, kuten dynaamiseen säätelyyn tai tautimallinnukseen. Kammiomalli osoittaa tämän tyyppisen kammion ongelman: diffuusionopeuden, joka yhdessä suurien diffuusiomatkojen kanssa tuottaa suuren mittausvirheen. Diffuusiokammioiden yleinen kyky mitata minkä tahansa epiteelin läpäisevyyttä tulisi ottaa huomioon mittauksia tehdessä.

ABSTRACT

TAMPERE UNIVERSITY OF TECHNOLOGY

Master's Degree Programme in Biotechnology

TERVONEN, AAPO: Modeling diffusion across the blood-retinal barrier and mass transfer in a half-perfusion chamber

Master of Science Thesis, 73 pages, 4 appendix pages

May 2013

Major: Bioimaging

Supervisors: professor Jari Hyttinen, researcher Iina Vainio and postdoctoral researcher Soile Nymark

Examiners: professor Jari Hyttinen and postdoctoral researcher Soile Nymark

Keywords: Blood-retinal barrier, diffusion, permeability, half-perfusion chamber, mathematical modeling, age-related macular degeneration

Retinal diseases, especially age-related macular degeneration (AMD), are becoming a large issue as life expectancy increases. Blood-retinal barrier (BRB) is located adjacent to the retina and has many important functions in normal vision and it is the main site associated with AMD pathogenesis. BRB consists of retinal pigment epithelium (RPE), Bruch's membrane (BrM) and choriocapillaris endothelium. Mathematical modeling provides a tool to study the properties of the BRB and thus new treatment options for AMD. In experimental research, the BRB barrier function is usually measured with a so-called diffusion chamber. In this thesis, two models are constructed: 1) a passive diffusion model across the BRB based on the physicochemical properties of the BRB (BRB model) and 2) a model of a miniaturized half-perfusion chamber concept to study the effects of different parameters to the functionality of the system (chamber model).

The predictive BRB model was constructed by combining physical theories from the literature to describe the hindered diffusion within a certain type of geometry. The main objectives were to construct the model, to study the behavior of the permeability of the whole BRB and its parts as a function of different molecular properties as well as to validate the model by using experimentally measured permeabilities. The chamber model was done by using finite element method (FEM) and by utilizing Comsol Multiphysics FEM modeling software. The main interest was on the effects of certain system dimensions and other chamber parameters to the error caused by the measurement system.

The results of the BRB model indicate that it predicts the correct magnitudes of the BRB permeabilities, but fails to predict the more accurate behavior based on the molecular properties of the diffusing molecule, such as molecular size and lipophilicity. As assumed, the model confirms that RPE forms the most significant barrier in the BRB, as the BrM has affects only the very lipophilic molecules. With the chamber model, the results show that the functionality of this kind of half-perfusion chamber is limited by the free diffusion rate. The chamber dimensions and other parameters are less significant, as they mainly just change the diffusion distances.

The proposed BRB model is the first model of this kind for the BRB. It can be utilized to study the barrier properties in normal function and in disease, especially with little refinements. There are several directions towards which the model can be taken in the future, such as dynamic regulation of the permeability. The chamber model clearly suggests that the free diffusion rate is the main issue with this kind of half-perfusion chamber. The ability of the diffusion chambers to measure the actual absolute values of permeability, and to provide reliable results, should be viewed with caution.

PREFACE

This thesis was done at Tampere University of Technology (TUT), in the departments of Biomedical Engineering in 2012 and Electronics and Communications in 2013. The constructed models are part of two projects. The BRB model is done for a project called *Modeling and assessment of epithelial function – towards validation of tissue engineering products and personalized therapies* and is financed by the Academy of Finland, and the chamber model is part of the *Human spare parts* project financed by TEKES.

First and foremost, I would like to thank my supervisors, Iina Vainio, Jari Hyttinen and Soile Nymark. Especially Iina has been a invaluable help and support during the last ten months. In addition, I would like to thank my family, friends and coworkers for support. Special thanks to my father Antero Tervonen, for his advices, and friends Hilla Hirvonen and Julia Johansson, who kindly proofread the thesis. Also, Antti Jylhä and Kati Juuti-Uusitalo from the Ophthalmology group in the Institute of Biomedical Technology in University of Tampere, as well as Samu Hemmilä and Antti Mäki from the Micro- and Nanosystems group in TUT deserve acknowledgments for their helpful advices. I would like to begin this thesis with the words Iina said to me at the beginning of this process: *“If this was easy, everybody would do it”*.

Aapo Tervonen, Tampere 6th of May, 2013

TABLE OF CONTENTS

1	Introduction.....	1
2	Theoretical background.....	3
2.1	Anatomy of the eye and blood-ocular barriers.....	3
2.2	Outer blood-retinal barrier (BRB).....	5
2.2.1	Retinal pigment epithelium (RPE).....	5
2.2.2	Tight junctions of the RPE.....	7
2.2.3	Bruch's membrane (BrM).....	9
2.2.4	Choriocapillaris endothelium (CE).....	11
2.2.5	Regulation of the BRB permeability.....	12
2.3	Aging of BRB and ocular diseases.....	13
2.3.1	Aging of BRB.....	13
2.3.2	Age-related macular degeneration and other retinal diseases.....	14
2.3.3	Prevention and treatment of retinal diseases.....	15
2.4	Epithelial transport and permeability research.....	16
2.4.1	Molecular characteristics.....	16
2.4.2	Epithelial transport.....	17
2.4.3	Studying the BRB permeability.....	19
2.4.4	Diffusion chamber.....	20
2.5	Physics of diffusion and permeability.....	21
2.5.1	Diffusion.....	21
2.5.2	Permeability.....	23
2.5.3	Hindered diffusion.....	25
2.6	Mathematical modeling.....	30
2.6.1	Mathematical modeling of physiological systems.....	30
2.6.2	Finite element method.....	31
2.6.3	Mathematical models of BRB and corresponding structures.....	32
3	Models of the blood-retinal barrier and half-perfusion chamber.....	34
3.1	Model of the outer blood-retinal barrier (BRB model).....	34
3.1.1	Retinal pigment epithelium.....	36
3.1.2	Bruch's membrane.....	39
3.1.3	Choriocapillaris endothelium.....	41

3.1.4	Properties of the solute molecules.....	42
3.1.5	Parameters.....	42
3.1.6	Calculations.....	44
3.2	Model of the half-perfusion chamber (chamber model).....	47
3.2.1	Geometry.....	47
3.2.2	Physics and boundary conditions.....	48
3.2.3	Simulations and calculations.....	49
4	Results.....	52
4.1	BRB model.....	52
4.1.1	Comparison between the solute radii.....	52
4.1.2	Parameter behavior analysis.....	53
4.1.3	Validation with the measured data.....	55
4.1.4	Sensitivity analysis.....	56
4.2	Chamber model.....	58
4.2.1	Parameter-based errors in permeability.....	58
4.2.2	Measurability of acceptor chamber concentration.....	61
5	Discussion.....	62
5.1	BRB model.....	62
5.1.1	Assessment of the results.....	63
5.1.2	Model assumptions and simplifications.....	66
5.1.3	Summary and future prospects.....	69
5.2	Chamber model.....	70
5.2.1	Assessment of the results.....	70
5.2.2	Model limitations.....	72
5.2.3	Summary.....	72
5.3	The models together.....	73
6	Conclusion.....	74
	References.....	75
	Appendix 1: molecules of the BRB model, their properties and measured permeabilities.....	85
	Appendix 2: Results of the BRB model validation.....	88

NOTATION, ABBREVIATIONS AND TERMS

A_{probe}	Probe area (m ²)
A_{BRB}	BRB area (m ²)
c	Concentration (mol)
c_{ac}	Acceptor chamber concentration (μl ml ⁻¹)
c_{dc}	Donor chamber concentration (μl ml ⁻¹)
D	Diffusion coefficient (m ² s ⁻¹)
D_0	Free diffusion coefficient (m ² s ⁻¹)
D_B	Diffusion coefficient within a barrier (m ² s ⁻¹)
$D_{B,eff}$	Effective diffusion coefficient within a barrier (m ² s ⁻¹)
D_{BRBpc}	BRB-channel distance (m)
D_c	Diffusion coefficient in the chamber model (m ² s ⁻¹)
$D_{CF,ICL}$	Diffusion coefficient within collagen fibril matrix in ICL (m ² s ⁻¹)
$D_{CF,OCL}$	Diffusion coefficient within collagen fibril matrix in OCL (m ² s ⁻¹)
$D_{CF,ICL,eff}$	Effective diffusion coefficient within collagen fibril matrix in ICL (m ² s ⁻¹)
$D_{CF,OCL,eff}$	Effective diffusion coefficient within collagen fibril matrix in OCL (m ² s ⁻¹)
D_{cyt}	Cytoplasmic diffusion coefficient (m ² s ⁻¹)
$D_{cyt,eff}$	Effective cytoplasmic diffusion coefficient (m ² s ⁻¹)
d_{dcBRB}	Chamber-BRB distance (m)
d_{ICL}	OCL thickness (m)
D_m	Diffusion coefficient within the matrix m (m ² s ⁻¹)
$D_{m,eff}$	Effective diffusion coefficient within the matrix m (m ² s ⁻¹)
d_m	Fiber matrix thickness (m)
d_{OCL}	OCL thickness (m)
$D_{PG,ICL}$	Diffusion coefficient within proteoglycan matrix in ICL (m ² s ⁻¹)
$D_{PG,OCL}$	Diffusion coefficient within proteoglycan matrix in OCL (m ² s ⁻¹)
$D_{PG,ICL,eff}$	Effective diffusion coefficient within proteoglycan matrix in ICL (m ² s ⁻¹)
$D_{PG,OCL,eff}$	Effective diffusion coefficient within proteoglycan matrix in OCL (m ² s ⁻¹)
d_{RPE}	RPE cell flat-to-flat diameter (m)
d_{TJp}	TJ pore separation (m)
d_{TJss}	TJ strand separation (m)
F	Faraday constant (9.65×10 ⁴ C mol ⁻¹)

ΔG	Change in free energy
ΔG_f	Change in free energy of the fiber
ΔG_s	Change in free energy of the solute particle
ΔG_{sf}	Change in free energy between the solute particle and fiber
f	Adjusted fiber volume fraction
H_m	Hydrodynamic interactions in matrix m
h	Separation distance between the fiber and particle (m)
h_{fen}	Fenestration height (m)
h_{LS}	Lateral space height (m)
$H_p(\lambda_p)$	Pore hindrance factor
h_{pc}	Perfusion channel height (m)
h_{RPE}	RPE cell height (m)
$H_s(\lambda_s)$	Slit hindrance factor
h_{TJ}	TJ region height (m)
h_{TJs}	TJ strand height (m)
\mathbf{I}	Unit matrix
J	Diffusional flux ($\text{mol m}^{-2} \text{s}^{-1}$)
k_B	Boltzmann's constant ($1.38 \times 10^{-23} \text{ J K}^{-1}$)
K_a	Association constant of the melanin binding reaction (μM^{-1})
K_D	Octanol-water distribution coefficient
K_P	Octanol-water partition coefficient
l_B	Barrier thickness (m)
l_{cb}	Cell boundary length per unit area (m m^{-2})
l_p	Pore length (m)
l_s	Slit length (m)
M	Cumulative amount of substance (mol)
m_{fr}	Perfusion flow rate ($\mu\text{l min}^{-1}$)
M_s	Solute's molecular mass (Da)
m_V	Membrane volume selectivity (mol cm^{-3})
n_{TJs}	TJ strand number
P	Permeability coefficient (m s^{-1})
p	Pressure (Pa)
P_{BRB}	BRB permeability coefficient (m s^{-1})
$P_{BRB,c}$	BRB permeability coefficient in the chamber model (m s^{-1})
P_{BrM}	BrM permeability coefficient (m s^{-1})
P_{CE}	CE permeability coefficient (m s^{-1})
P_{cyl}	Cytoplasm permeability coefficient (m s^{-1})
P_{fen}	Fenestration permeability coefficient (m s^{-1})
P_{ICL}	ICL permeability coefficient (m s^{-1})

P_{LS}	Lateral space permeability coefficient (m s^{-1})
P_{mem}	Membrane permeability coefficient (m s^{-1})
P_{OCL}	OCL permeability coefficient (m s^{-1})
P_{para}	Paracellular permeability coefficient (m s^{-1})
P_{RPE}	RPE permeability coefficient (m s^{-1})
P_{TJ}	TJ permeability coefficient (m s^{-1})
P_{trans}	Transcellular permeability coefficient (m s^{-1})
$P^*_{BRB,c}$	Simulated permeability coefficient based on the flux over BRB (m s^{-1})
$P^*_{out,c}$	Simulated permeability coefficient based on the flux through the outlet (m s^{-1})
$q_{A,f}$	Fiber's surface charge density (C m^{-2})
$q_{A,PG}$	Proteoglycan surface charge density (C m^{-2})
$q_{A,s}$	Particle's surface charge density (C m^{-2})
q_s	Solute molecule's charge
R	Universal gas constant ($8.31 \text{ J mol}^{-1} \text{ K}^{-1}$)
r_{CF}	Collagen fibril radius (m)
r_{dia}	Diaphragm pore radius (m)
r_f	Fiber radius (m)
r_p	Pore radius (m)
r_{PG}	Proteoglycan radius (m)
r_s	Solute particle radius (m)
r_{SE}	Stokes-Einstein radius (m)
r_{Su}	Sutherland radius (m)
r_{TJp}	TJ pore radius (m)
S_m	Steric interactions in matrix m
T	Absolute temperature (K)
t	Time (s)
\mathbf{u}	Velocity field (m s^{-1})
V	Van der Waals volume ($\text{cm}^3 \text{ mol}^{-1}$)
W_{LS}	Lateral space half-width (m)
W_s	Slit half-width (m)
W_{TJ}	TJ region half-width (m)
β	Dimensionless fiber radius
ϵ	Absolute permittivity (F m^{-1})
ϵ_0	Permittivity of vacuum ($8.85 \times 10^{-12} \text{ F m}^{-1}$)
ϵ_{dia}	Relative surface area of the diaphragm pores
ϵ_{LS}	Relative surface area of the lateral space
ϵ_{open}	TJ open part size
ϵ_p	Relative surface area of the pores
ϵ_r	Relative permittivity
ϵ_s	Relative surface area of the slit

ϵ_{TJo}	Relative surface area of the open TJ part
ϵ_{TJp}	Relative surface area of the TJ pores
ϵ_{TJss}	Relative surface area of the space between the strands
η	Dynamic viscosity (Pa s)
κ_D	Reciprocal of Debye screening length (m^{-1})
ζ	Viscous frictional coefficient ($N\ s\ m^{-1}$)
μ	Dimensionless separation distance
Φ_m	Partition coefficient between the matrix m and solvent
$\Phi_{m,e}$	Partition coefficient between the matrix m and solvent including the electrostatic interactions
$\varphi_{CF,ICL}$	Collagen fibril volume fraction in ICL
$\varphi_{CF,OCL}$	Collagen fibril volume fraction in OCL
φ_f	Fiber volume fraction
$\varphi_{PG,ICL}$	Proteoglycan volume fraction in ICL
$\varphi_{PG,OCL}$	Proteoglycan volume fraction in OCL
ρ	Fluid density ($kg\ m^{-3}$)
σ_f	Dimensionless fiber's surface charge density
σ_s	Dimensionless particle's surface charge density
τ	Dimensionless particle radius
τ_{LS}	Lateral space tortuosity
Da	Dalton, a unit used to indicate molecular mass (1 Da = 1.66×10^{-23} kg)
Å	Ångstrom, a unit used to indicate molecular sizes (1 Å = 1×10^{-10} m)
AMD	Age-related macular degeneration
BAB	Blood-aqueous barrier
BBB	Blood-brain barrier
BC	Boundary condition
BRB	Blood-retinal barrier/outer blood-retinal barrier
BrM	Bruch's membrane
Ch-BRB	Choroid and blood-retinal barrier
Ch-BrM	Choroid and Bruch's membrane
CE	Choriocapillaris endothelium
CE-BL	Basal lamina of the choriocapillaris endothelium
CNV	Choroidal neovascularization
ECM	Extracellular matrix
EL	Elastic layer
FITC	Fluorescein isothiocyanate
GAG	Glycosaminoglycan
iBRB	Inner blood-retinal barrier

ICL	Inner collagenous layer
OCL	Outer collagenous layer
PEDF	Pigment epithelium-derived growth factor
PEG	Polyethylene glycol
POS	Photoreceptor outer segment
RPE	Retinal pigment epithelium
RPE-BL	Basal lamina of the retinal pigment epithelium
TER	Transepithelial/endothelial electric resistance
TJ	Tight junction
VEGF	Vascular endothelial growth factor
Diaphragm	A fiber structure covering the fenestrations
Fenestration	A pore through an endothelium
Hydrodynamic interactions	Mechanical interactions mediated by liquid
Lipophilicity	Ability of chemical compound to dissolve in fats
Melanin	Pigment found e.g. in the RPE
Paracellular	Space between the cells
Steric interactions	Mechanical interactions caused by the obstacles
Transcellular	Transport pathway through the cells

1 INTRODUCTION

In this thesis, two mathematical models are constructed to predict the permeability of the blood-retinal barrier (BRB) and the functionality of a permeability measurement system. BRB is a layer in the eye, located just behind the retina, which has important roles in normal retinal function. In addition, it is the primary location for many retinal diseases, most notably age-related macular degeneration (AMD). This disease causes impairment of vision or even blindness, and thus forms a risk for the aging population due to increasing life expectancy. AMD is the third most common cause of blindness in the world after cataract and glaucoma (Pascolini & Mariotti 2012), and the most common cause of adult blindness in developed countries (Augood et al. 2006). It has been estimated that in the United States 1.75 million people and more than 10 % of the people older than 80 years have AMD (Friedman et al. 2004). The percentages are similar in Europe (Augood et al. 2006).

During AMD pathogenesis, many of the BRB functions are impaired, among them the barrier function, due to the compositional changes in the BRB. To enable the development of novel treatments for AMD, it is important to be able to study the BRB in normal function and in disease. Mathematical models present one useful method for studying this barrier function without the need for any cells or tissues. Currently, the mathematical modeling of the BRB is in its infancy. Models that include the BRB are generally pharmacokinetic models (Mac Gabhann et al. 2007; Amrite et al. 2008; Ranta et al. 2010) and represent the BRB only with one simple constant permeability value. There are some more accurate models of other barrier structures, such as the cornea (Edwards & Prausnitz 1998; 2001) and skin (Mitragotri 2003). In addition to mathematical models, so-called biological *in vitro* models can be constructed to further decrease the need for animal tissues. To be able to study the properties of *in vitro* models, proper tools are needed. Traditionally, diffusion chambers are used to study the molecular permeability across the BRB (Hussain et al. 2002; Pitkänen et al. 2005; Steuer et al. 2005; Cheruvu & Kompella 2006; Kadam et al. 2011). However, these devices have certain problems, such as large tissue areas and volumes, which require large amount of cells and expensive drugs. One option to overcome these problems is to miniaturize the chamber.

The main aim of this thesis is to create models, that predict the BRB permeability and describe the functionality of one type of diffusion chamber. To meet this aim, two computational models are constructed 1) a model of passive diffusion across the BRB based on the physicochemical properties of the BRB and diffusing molecule (BRB model), and 2) a model of a conceptual half-perfusion chamber for the BRB permeability studies (chamber model). The objectives of the first model (*BRB model*) are to construct and validate the model as well as to use it to determine the importance of different

parts of the BRB as barriers. The objectives of the second model (*chamber model*) are to predict the importance of certain dimensions and other parameters for the functionality of the chamber. The chamber model was constructed using COMSOL Multiphysics FEM software (v4.3) and all the calculation for both models were carried out with Mathworks MATLAB (R2012a). These models are part of an ongoing research on BRB conducted by Tampere University of Technology and University of Tampere.

The structure of the thesis is as follows. First, the basic background theory of the anatomy and physiology of the eye and BRB, aging of the BRB and AMD pathology as well as general epithelial transport concepts are introduced. These are followed by the description of the physics of diffusion and permeability. In addition, the general principles of modeling physiological systems are discussed. Then, the two models are presented, followed by results and discussion.

2 THEORETICAL BACKGROUND

This chapter describes the basic theoretical background of biology, physics and modeling concerning this thesis. First, the basic anatomy of the eye and the blood-ocular barriers is introduced, followed by the anatomy and physiology of the BRB and its components. Then, the BRB aging process and related AMD pathology are described. The next section will go through the epithelial transport mechanisms and methods of studying the BRB permeability. This is followed by the introduction of basic physics concerning diffusion. Finally, the concepts of a model and mathematical modeling are explained, followed by the description of the current state of BRB modeling.

2.1 Anatomy of the eye and blood-ocular barriers

As the organ responsible for one of the most important senses, the eye has a highly complex function and structure. As light comes into the eye, it passes through the cornea, after which the lens focuses it to the retina at the back of the eye. The retina has two types of photoreceptor cells – cones and rods – which are located in the outermost part of the retina, away from the incoming light. Cones mediate the color vision and work better in bright light conditions. In humans, they are mostly concentrated around the central part of the retina where the light is focused by the lens. This region is highly pigmented and is known as the macula and it is responsible for the sharp vision. Rods function in less intense lighting and can not distinguish colors. They are more numerous in the peripheral regions of the retina. Photoreceptors form the input of the retina and the output is formed by retinal ganglion cells. Between the two, specialized cells process the signal. The axons of ganglion cells form the optic nerve, which leaves the eye through the optic disc and transmits the signal to the brain. (Marieb 2009.)

Ocular blood supply is provided by the vascular layer located just outside the retina. In the anterior parts of the eye, the vascular layer is known as the ciliary body and in the posterior parts the choroid. Between the choroid and the retina, there is an important cell monolayer called retinal pigment epithelium (RPE). The outermost protective layer of the eye consists of two parts: the anterior cornea and posterior sclera. Inside of the eye is filled with fluid, which is divided into two segments by the lens. The anterior segment is known as the aqueous chamber and it is filled with clear water-like fluid. The posterior segment is called the vitreous and it contains gel-like vitreous humor. (Marieb 2009.) The gross anatomy of the eye is presented in Figure 2.1A.

It is important to maintain the right physicochemical environment inside the eye to enable the normal operation of the retinal cells. The structures mainly responsible for this function are called blood-ocular barriers. The two main barriers are categorized ac-

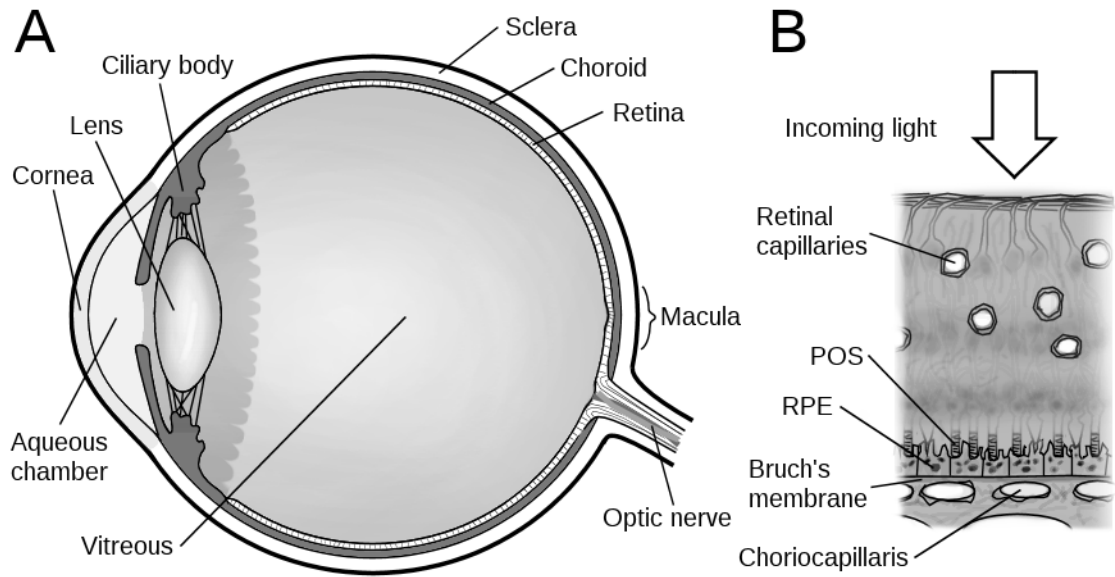


Figure 2.1. *A: The gross anatomy of the human eye. Redrawn from Marieb (2009) B: A more detailed anatomy of the locations of the retinal capillaries, RPE, Bruch's membrane and choriocapillaris in relation to the retina. Note that the dimensions are not correct. (POS: photoreceptor outer segments; RPE: retinal pigment epithelium)*

According to their location: the blood-retinal barrier (BRB) and blood-aqueous barrier (BAB). (Cunha-Vaz 1997.) They are both considered being part of the more studied blood-brain barrier (BBB), which is formed by the endothelial cells of the brain capillaries and which maintains the homeostasis inside the central nervous system (Rizzolo et al. 2011). The constant chemical and osmotic changes in systemic blood circulation mean that the BRB and BAB must restrict the movement of fluid and molecules between the vasculature and the eye. One important aspect of this function is the outwards transport of the waste products from the metabolically active tissues. (Cunha-Vaz 1997.)

In some mammals, such as humans and pigs, the retinal blood supply comes from two sources. The inner part of the retina is supplied by the retinal capillaries and the outer part by the choriocapillaris network. (Steuer et al. 2005.) The BRB is thus divided into two parts: the inner BRB (iBRB) and outer BRB, of which the latter is discussed in the next section. iBRB is formed by the endothelial cells of the retinal capillaries and the tight junctions (TJs) between them. The endothelial cells reside on a basal lamina and are covered by the processes of astrocytes and Müller cells, which regulate the tightness of the iBRB according to the changes in the retinal microenvironment. (Cunha-Vaz 2009.) BBB and iBRB are structurally very similar: they are both orders of magnitude tighter than the capillaries in systemic circulation and they have no fenestrations. Some species, e.g. horses and rabbits, lack the retinal capillaries and thus they also lack the iBRB. (Steuer et al. 2005.) Figure 2.1B presents the locations of the retinal capillaries in the retina.

BAB comprises the iris blood vessel endothelium and the ciliary epithelium. These barriers are more permeable than the BRBs, as they allow a small concentration of plasma proteins to diffuse into the aqueous humor. There are no diffusion barriers be-

tween the aqueous and vitreous humor or the vitreous humor and the retina. Hence the BAB is an important component in the regulation of the retinal microenvironment. (Cunha-Vaz 1997.)

2.2 Outer blood-retinal barrier (BRB)

The blood supply to the outer part of the retina – including the metabolically highly active photoreceptors – comes from the choriocapillaris network. The barrier between the choriocapillaris and other retina is formed by the outer blood-retinal barrier, which from now on will be referred to as the BRB. This barrier ensures the correct physicochemical conditions in the outer retina and especially around the photoreceptors. BRB includes three layers: the choriocapillaris endothelium (CE), Bruch's membrane (BrM) and retinal pigment epithelium (RPE). The tightness of the BRB is mainly due to the RPE and its TJs. BRB is structurally analogous to the ventricular part of the BBB: the main barrier is formed by the epithelium, not the endothelium. (Rizzolo et al. 2011.) BRB is extremely important to the retinal well-being, and in species without retinal capillaries, this tissue is alone responsible for the maintenance of the whole retina. The location of the RPE, BrM and choriocapillaris in relation to retina is presented in Figure 2.1B and Figure 2.2 shows the BRB in more detail.

2.2.1 Retinal pigment epithelium (RPE)

RPE is a monolayer of polarized and pigmented RPE cells that are connected to each other by tight junctions (TJs). The TJs form an important part of the barrier function of the whole BRB. (Rizzolo et al. 2011.) RPE is located between the photoreceptor cells of the retina and the choroid. The cells are anchored to BrM on their basal side and are in close contact with the photoreceptor outer segments (POS) on the apical side. At the peripheral regions of the retina, RPE continues as the membrane of the ciliary body. (Bhutto & Luttly 2012.) Among all epithelial tissues, RPE is a rare epithelium since the apical side does not face a lumen, but a solid tissue. (Rizzolo et al. 2011.)

Characteristics of the RPE cells

RPE cells are hexagonal in shape and in humans they have an average height and diameter of 8 and 16 μm , respectively (Garron 1963). In the macular region, the cells are slimmer and higher with the height and diameter of 11–14 and 10–14 μm , respectively (Garron 1963; Boulton & Dayhaw-Barker 2001). In the peripheral regions, the cells are more irregularly shaped, flatter and the diameter can be as large as 60 μm (Boulton & Dayhaw-Barker 2001).

The apical surface of the RPE cells has two types of microvilli: long and thin ones with the length of 5–7 μm , and shorter ones that are more specifically shaped and form a sheath around the POS's. (Boulton & Dayhaw-Barker 2001.) The basal surface of the cells has infoldings that extend up to 1 μm into the cell cytoplasm. Both the microvilli

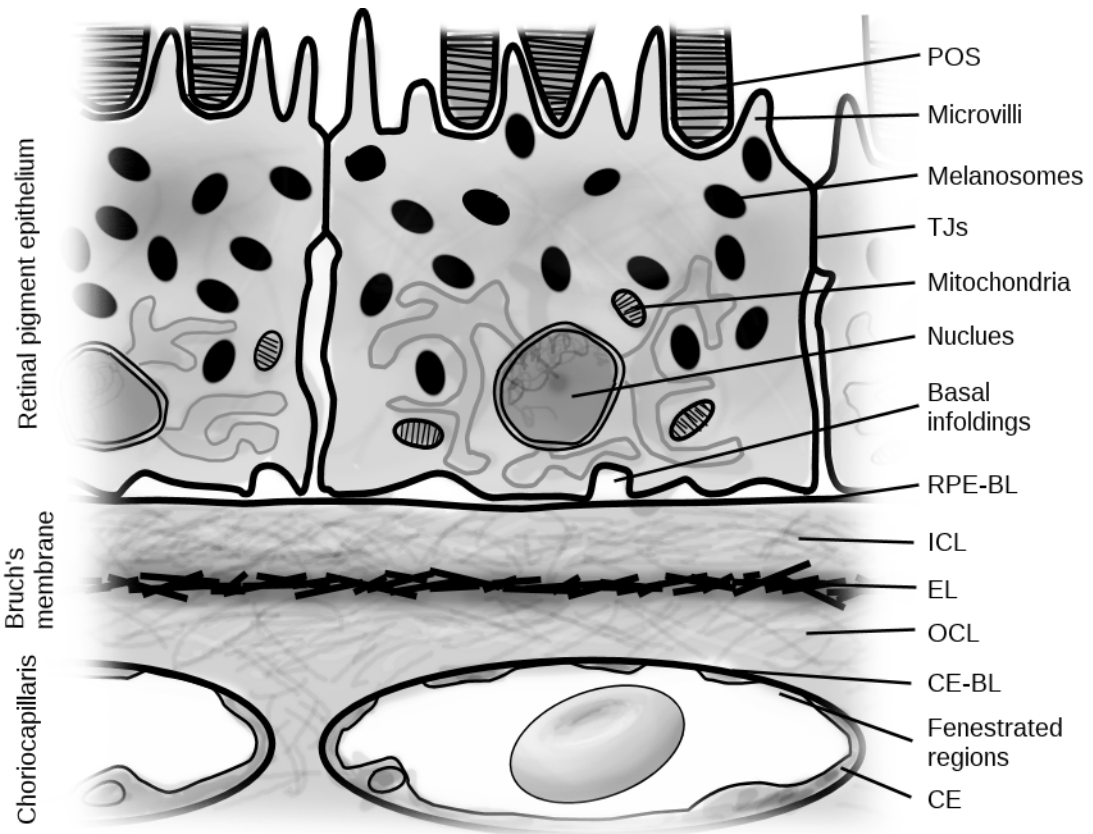


Figure 2.2. The main components of BRB: Retinal pigment epithelium, Bruch's membrane and choriocapillaris. (POS: photoreceptor outer segments; TJs: tight junctions; RPE-BL: basal lamina of RPE; ICL: inner collagenous layer; EL: elastic layer; OCL: outer collagenous layer; CE-BL: basal lamina of choriocapillaris endothelium; CE: choriocapillaris endothelium)

and infoldings increase the respective surface areas and thus facilitate the transport properties of the cells. (Garron 1963.)

The nucleus and most of the usual organelles, such as the abundant mitochondria, reside near the basal surface of the RPE cells. The melanin pigment is packed into granules, known as melanosomes. They are located near the apical surface and sometimes inside the microvilli. (Garron 1963.)

Functions of the RPE

RPE has multiple roles. In addition to being a barrier, it functions as a bidirectional transporter. The polarization of different membrane transport proteins is essential for this role. Important actively transported molecules from retina to blood vessels are metabolic end products of the photoreceptors, such as lactic acid. The transport of glucose and retinol (vitamin A) from blood to retina is essential for the visual function. Ions – such as Cl^- , K^+ , Na^+ and HCO_3^- – are transported to form electrochemical gradients, which are then used to drive the passive fluid transport outwards from the retina together with the molecular transport. The RPE ion-transport also creates a buffer for the subretinal space between the RPE and photoreceptors to compensate for the fast changes in the ion composition due to retinal signaling. (Strauss 2005.)

In addition to the transport properties, RPE has an essential role in the photoreceptor visual cycle. In photoreceptors, the light sensitive molecule is the chromophore 11-*cis* retinal. The conformation of 11-*cis* retinal changes to all-*trans* retinal due to light absorption. This chromophore in all-*trans* conformation is reduced to all-*trans* retinol and transported into the RPE cells, which have the enzymes to isomerize it to the active form, thus enabling the recycling of the chromophore. Retinal is also isomerized from retinol transported from blood circulation. (Strauss 2005.)

POS's consist of discs which are packed of visual pigment. These discs and the tips of the POS's need to be renewed constantly as they are damaged from concentrated light energy. One major role of the RPE cells is to phagocytose and degrade the shed POS segments. (Strauss 2005.) One RPE cell interacts with 20–30 POS's (Bhutto & Luty 2012) as well as phagocytoses and degrades 300 million discs during its 70-year life-span (Marshall 1987). The concentrated light energy and oxygen-rich environment, coupled with the reactive oxygen species produced by the degradation of the POS discs, create hazardous conditions for the proteins, lipids and DNA in the RPE cells. They protect themselves by three mechanisms: the light absorbing melanosomes, antioxidants and ability to repair damaged biomolecules. (Strauss 2005.)

RPE cells also produce many growth factors, e.g. vascular endothelial growth factor (VEGF) and pigment epithelium-derived growth factor (PEDF). These growth factors are not only important for the well-being and correct function of the photoreceptors, but also for the choriocapillaris. (Strauss 2005.)

2.2.2 Tight junctions of the RPE

Tight junctions (TJs) are essential for the barrier function of the RPE, as they seal the space between the RPE cells and thus retard the paracellular diffusion of molecules. (Rizzolo et al. 2011.) Paracellular refers to movement between the cells, as opposed to transcellular which refers to movement through them. TJs, also known as zonula occludens, are cell-cell adhesions that encircle the apical end of the lateral surface of epithelial cells. They connect the cell membranes of adjacent epithelial cells together, thus sealing the lateral space. (Alberts et al. 2008.)

Structure of the TJs

TJs are made out of a continuous belt of parallel strands that create a seal around the cells. The TJ strand structure is schematically presented in Figure 2.3. When viewed at the plane of the membrane, the branching strands form a web-like pattern. The number of the parallel strands and complexity of this network differs between epithelia. (Schneeberger & Lynch 2003.) For example, the mean number of parallel strands in the RPE of a late chicken embryo was measured to be five (Rahner et al. 2004).

TJs consist of three classes of proteins: transmembrane proteins which form the seal, adapter proteins which help to form the structure, and effector proteins which regulate the TJs. The main transmembrane protein families are claudins and occludins. The bar-

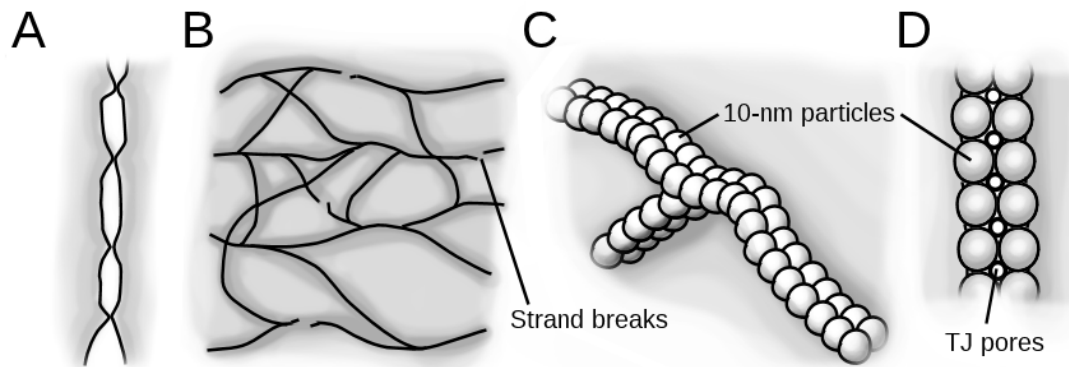


Figure 2.3. *The structure of the TJs. A: A cross section view of TJs between two cells. B: TJs viewed at the plane of the membrane, showing the web-like structure and strand breaks. C: Strands are formed by 10-nm particles (the other cell membrane is not shown). D: There are small TJ pores between the 10-nm particles. A and B redrawn from Rizzolo et al. (2011), C and D redrawn from Van Itallie & Anderson (2004).*

rier function is mainly created by claudins, as the presence of occludins is not necessary. (Schneeberger & Lynch 2003.) The TJ strands are formed by rows of so-called 10-nm particles consisting of claudins, seen in Figure 2.3C. Small pores shown in Figure 2.3D are formed in this particle structure, enabling the movement of ions and small molecules. These pores are ion and charge selective, a property which arises from the extracellular loops of the claudins. There are 24 members identified in the claudin family, and they have different selectivities. In addition to the selectivity, some claudins make the TJs leakier than others. (Anderson & Van Itallie 2009.) Claudin-19 is the prominent claudin in the human RPE TJs (Peng et al. 2011).

Functions and characteristics of the TJs in the RPE

As a part of the intercellular junctional complex, the TJs' main function is the regulation of the diffusion from one side of the cells to the other. This way they separate the two compartments. One important function is the creation of the apical-basolateral membrane polarity by restricting the lateral diffusion of membrane proteins and lipids. (Schneeberger & Lynch 2003.) In addition to TJs, the RPE intercellular junctional complex includes adherens junctions, that provide a mechanical connection between the cells, and gap junctions, that connect the cytoplasms of adjacent cells (Hudspeth & Yee 1973).

Despite their name, TJs can be tighter or leakier depending on the tissue. Epithelial or endothelial tightness is usually described by transepithelial or transendothelial electrical resistance (TER). TER describes how much the cell layer resists the movement of ions from one side to the other. As ions diffuse mainly through the paracellular pathway, TJs form the major component in TER. However, also the transcellular pathway through ion channels has an impact. (Krug et al. 2009.) The TER value of the RPE is around 135–600 $\Omega \text{ cm}^2$, varying between species, and it is somewhere between leaky and tight epithelia. The extreme ends of the scale are the leaky capillaries of the systemic circulation and tight BBB with values between 5–10 $\Omega \text{ cm}^2$ and 1000–2000 $\Omega \text{ cm}^2$, respec-

tively. (Rizzolo et al. 2011.) TER value does not measure tissue quality as such, as each epithelium or endothelium has its own function with suitable TER value for it (Rizzolo 2007). The relationship between the number of parallel TJ strands and TER vary among different studies. Claude (1978) found a logarithmic correlation between them, but Stevenson et al. (1988) found over tenfold difference in TER with two cell lines with a similar strand numbers.

Although they have differences in structure and TER values, the permeability of drug molecules through the BBB and whole BRB is fairly similar, as shown by Steuer et al. (2005) in an *in vitro* study. There are two diffusion pathways through the TJs. Small molecules are able to diffuse through the small structural pores. The radius of these pores was measured to be around 0.4 nm by Van Itallie et al. (2008) by using polyethylene glycol (PEG) oligomers with different molecular masses. In spite of the small radius of the pores, also larger molecules are able to cross the TJs. This is due to the highly dynamic TJ structure: the strands constantly break down and form new contacts. Larger molecules are able to permeate through these temporary breaks. The existence of multiple parallel strands forming the web-like structure restricts the diffusion through this pathway, even if one of the strands breaks. (Sasaki et al. 2003.)

In conclusion, TER and molecular permeability of the TJs are independently regulated and measure different TJ functions. Because of this, neither of them fully defines the TJ tightness. (Rizzolo 2007.)

2.2.3 Bruch's membrane (BrM)

Located between the RPE and choriocapillaris network, BrM is an acellular extracellular matrix (ECM) layer with different roles in the retinal function and especially in aging and pathology (Booij et al. 2010). It consists of five layers and has a total thickness of 2–4 μm (Bhutto & Luttj 2012). The composition and thickness of the tissue vary across the retina. For example, the thickness of the whole BrM decreases (Garron 1963) and the thickness of the central elastic layer increases in the peripheral regions of the retina (Booij et al. 2010).

Layers of BrM

The five layers are from the innermost to the outermost: the basal lamina of the RPE, inner collagenous layer, elastic layer, outer collagenous layer and basal lamina of the CE. The characteristic anatomical features of these layers change with age and the dimensions given in this section are determined from a young, healthy eye. (Booij et al. 2010). The layers are schematically presented in Figure 2.2.

The basal lamina of the RPE (RPE-BL) is 0.14–0.15 μm in thickness. It consists of type IV collagen, laminin, fibronectin, and heparan sulfate as well as chondroitin/dermatan sulfate proteoglycans. The inner collagenous layer (ICL) has a thickness of approximately 1.4 μm and it is composed of collagen types I, III and V. (Booij et al. 2010.) The collagen fibrils are tightly interwoven and randomly oriented in the plane of the

layer with occasional lengthwise attachments to each other (Goldbaum & Madden 1982). The fibrils have a diameter of 60 nm, and the space between them is filled with ground substance consisting mainly of hyaluronic acid, chondroitin sulfate and dermatan sulfate proteoglycans. The elastic layer (EL) is 0.8 μm thick and is formed by varying sizes of elastic fibers consisting of elastin. The fibers form a perforated sheet with large holes. In addition, EL contains other ECM components, such as type VI collagen and fibronectin. The collagen fibrils of the collagenous layers frequently cross the EL. The outer collagenous layer (OCL) is 0.7 μm thick and it is compositionally identical to the ICL. (Booij et al. 2010.) However, the collagen fibrils are less tightly interwoven than in the ICL (Goldbaum & Madden 1982). The OCL is also continuous with the ECM of the choroid, thus forming the choroidal intercapillary pillars (Moore & Clover 2001). The basal lamina of the CE (CE-BL) is approximately 0.14 μm thick and it is not a continuous layer of BrM, as it only covers the surfaces of the endothelial cells. It consists of laminin, heparan sulfate proteoglycan and collagen types IV, V and VI. (Booij et al. 2010.)

In BrM, as well as in other tissues of the body, collagens are the most common family of proteins in ECM. Collagens are found in different conformations. Of the types found in the BrM, types I, III and V are fibrillar, type IV forms a sheet-like network, and type VI has an important role in maintaining tissue integrity. (Hulmes 2008.) The fibrillar collagen molecules are made of three polypeptide chains wrapped helically around each other. The collagen molecules in turn form larger units known as collagen fibrils, which can have a diameter of 10–300 nm. Fibrils can further form aggregates known as collagen fibers. Proteoglycans compose of glycosaminoglycan (GAG) chains covalently linked to a core protein. GAGs, like chondroitin sulfate, dermatan sulfate and heparan sulfate, are linear polysaccharide chains made out of repeating disaccharide units. One of the sugars in the unit is an amino sugar, which is usually sulfated. Due to the sulfates and carboxyl groups in the sugars, GAGs have a highly negative charge in the physiological pH. The GAG chains occupy a high volume compared to their mass, and they form gels that fill most of the extracellular space. (Alberts et al. 2008.)

Functions of BrM

BrM has three main functions: 1) to act as a passive diffusion barrier between the choriocapillaris and RPE, 2) to form a platform for adhesion, migration as well as maybe for the differentiation of the RPE cells, and 3) to form a barrier restricting the migration of cells from one side to the other (Booij et al. 2010). The diffusion barrier properties of BrM are considered the most important ones for this thesis.

The diffusion through BrM is highly affected by the molecular composition, which changes with age (Hussain et al. 2010). Starita et al. (1997) found that the site of major fluid flow resistance is the ICL. It is possible, that the ICL also forms the main resistive layer against the diffusion of biomolecules. In the molecular scale the proteoglycans – especially chondroitin and dermatan sulfate – form the most significant barrier with their negative surface charges. The negative charge causes proteoglycans to bind water,

cations and positively charged molecules, and to repel negatively charged molecules. (Booij et al. 2010.)

The relationship between the molecular size and BrM permeability is an inverse relationship with small molecules permeating orders of magnitude faster than macromolecules (Hussain et al. 2010; Zayas-Santiago et al. 2011). The size exclusion limit of BrM was found to be over 200 kDa in the young tissue and this limit decreases with age. The limit is sufficient for the diffusion of retinol, which is transported in a complex with a molecular mass of 75 kDa and which is essential to the visual cycle. (Moore & Clover 2001.) In addition to the properties of the molecule and the matrix composition, the BrM permeability depends on the surrounding hydrostatic and osmotic pressures (Booij et al. 2010) and pH (Guymer et al. 1998).

2.2.4 Choriocapillaris endothelium (CE)

The choroidal blood comes from the ophthalmic artery, which branches into short posterior and long anterior ciliary arteries. These arteries in turn branch into small arteries and eventually terminate in the choriocapillaris. (Anand-Apte & Hollyfield 2011.) The choriocapillaris network lies in a single plane under BrM and is arranged in a lobular manner (Bhutto & Luty 2012). The blood perfusion of the choriocapillaris is very high in comparison with other tissues: $1400 \text{ ml min}^{-1} 100 \text{ g tissue}^{-1}$ (Strauss 2005). The arterioles and venules connect to this plane at right angles in the macular region and they lie in the choriocapillaris plane in the peripheral region (Bhutto & Luty 2012). The venous collecting vessels exit the eye through the vortex veins (Anand-Apte & Hollyfield 2011).

The choriocapillaris have large, elliptical lumen, with a major axis diameter of nearly $20 \mu\text{m}$ in the macular region and $18\text{--}50 \mu\text{m}$ in the peripheral region (Anand-Apte & Hollyfield 2011). The wall of the choriocapillaris composes of the endothelial cells (CE) and basal lamina. The nuclei and most of the cytoplasm of the CE cells are on the choroidal side. (Bernstein & Hollenberg 1965.) The CE cells are fenestrated with circular openings across the cells connecting the choriocapillaris lumen to the ECM of the choroid. The fenestrations of the choriocapillaris have diaphragm spanning over them (Anand-Apte & Hollyfield 2011). The fenestrations and a diaphragm are presented in Figure 2.4. The diaphragm consists of radial fibrils, that interweave in the center and particles that line the edges of the pore. This leaves triangular openings between the fibrils. (Bearer & Orci 1985.) The diameter of choriocapillaris fenestrations is approximately 80 nm and the open space in the radial direction is approximately 12 nm . The fenestrations are usually grouped together into clusters, where the cytoplasm is attenuated. (Melamed et al. 1980.) The fenestrations are more prevalent in the retinal side. Also the vascular endothelial growth factor (VEGF) receptors in the cell membrane are expressed in the retinal side, indicating polarization towards the RPE. (Bhutto & Luty 2012.)

Due to the fenestrations, the choriocapillaris are leaky, and the significance of paracellular and transcellular transport is small (Michel & Curry 1999). The fenestrations

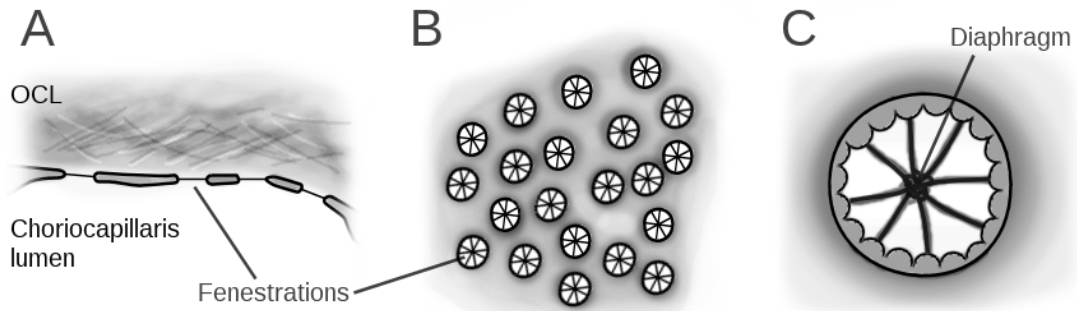


Figure 2.4. Fenestrations of the choriocapillaris. *A: A cross section view of the fenestrations between the lumen and OCL. B: A view on the plane of the endothelium of the fenestrations. C: A more detailed view of a diaphragm, showing the radial fiber structure. Adapted from Bearer & Orci (1985). (OCL: outer collagenous layer)*

readily enable the diffusion of small molecules, but Pino & Essner (1981) found that the diffusion of macromolecules with a radius larger than 3.2 nm is greatly hindered in the eye of a rat. However, the size of the retinol transportation complex has a radius of 3.7 nm, which means that there is some other means of transport, like transcellular vesicular pathway (Pino & Essner 1981).

2.2.5 Regulation of the BRB permeability

The BRB permeability is mainly regulated by the RPE, as it is the tightest layer of the BRB. Paracellular RPE permeability is regulated by the TJs and transcellular RPE permeability by the cell membrane transport proteins as well as by metabolic modification. (Rizzolo 2007.) The BrM regulation of permeability is based on passive mechanisms, such as changes in composition (Booij et al. 2010), which are relatively slow compared to the regulation done by the RPE.

The permeability and selectivity of the TJs can be regulated physiologically and pharmacologically. The photoreceptors are able to regulate the function and structure of the RPE TJs due to the close interaction between the two tissues. In addition to the tissue-tissue interactions between the RPE and the retina, the regulation is also mediated by diffusible factors secreted by the retinal cells. (Peng et al. 2003.) The retina can regulate the RPE by affecting the protein synthesis, degradation and distribution to the apical and basolateral membranes, as well as the barrier function of the TJs. The factor secreted by retina affect the expression of claudin and occludin genes, thus affecting the TJs. The half-lives of the claudins and occludins are around 4–12 h and 1.5 h, respectively. The short half-lives, especially that of occludins, facilitate a fast regulation of the TJ permeability and selectivity, and enable fast reaction to physicochemical changes. (Rizzolo et al. 2011.)

The function of cell membrane carrier proteins can be regulated in different ways. The regulation can happen at protein synthesis stage, as for example with glucose transport proteins during the development. Different types of glucose transporters are expressed during different stages of development due to different needs. The regulation can happen by directly regulating the protein functions. For example, the transportation

of some ions, like Na^+ , create electrochemical gradient that drive the transport proteins. Thus, by controlling the movement of Na^+ , the active transcellular transport can be regulated. Also, as TJs affect the movement of ions, they affect this transport pathway. (Rizzolo 2007.) The different methods of transcellular transport are discussed in detail later.

2.3 Aging of BRB and ocular diseases

The boundary between a normal aging process and an eye disease is not always clear. Therefore, main focus of this section is in the age-related changes occurring in the BRB and in the effects of diseases on the BRB and its permeability.

2.3.1 Aging of BRB

During the life-span of the BRB, there are dramatic changes in the structure and functionality of the RPE, BrM and choriocapillaris. Many of these changes lead to impairment in the functions of the whole BRB.

Changes in the RPE

The main changes in the RPE are more compositional and functional than structural. The main morphological age-related changes in the RPE cells are a loss of cell shape, hyperplasia, atrophy and areas of hyper- and hypopigmentation. (Boulton & Dayhaw-Barker 2001).

One of the main sources for the changes in the RPE is oxidative stress, caused for example by the degradation of the POS's. The highly oxidative environment leads to oxidative modification of lipid-related molecules that are transported to choriocapillaris or accumulate to form deposits in the BrM. (Booij et al. 2010.) The degradation process also creates lipofuscin pigment, which accumulates in melanosomes forming melanolipofuscin granules. Melanosomes are degraded by fusion with lysosomes, resulting in a decrease in the number of melanosomes. The accumulation of lipofuscin and other cytotoxic molecules to cytoplasm continues with age and can eventually lead to adverse effect, such as apoptosis. (Strauss 2005.)

Changes in BrM

The main changes in the BRB permeability during aging result from changes in BrM. The structural changes in the BrM encompass changes in molecular composition and thickening. The main compositional changes are the increase in collagen cross-linking, changes in proteoglycan synthesis, formation of mineral deposits, accumulation of advanced glycation end-products, lipids and oxidized metabolic end-products from the RPE as well as formation of drusens (Booij et al. 2010). Drusens are extracellular deposits that form between the RPE and BrM and contain incompletely digested material from the RPE, like lipids and oxidized end-products of the POS degradation. They tend to form on top of the intercapillary pillars, where there is no blood flow underneath.

(Bhutto & Luty 2012.) The thickness of the RPE increases by 135 % in normal lifespan due to the compositional changes, mainly in the ICL (Ramrattan et al. 1994).

These structural changes lead to functional changes resulting for example in loss of elasticity (Booij et al. 2010), decrease in hydraulic conductivity (Moore et al. 1995) and decrease in molecular permeability (Hussain et al. 2002; Hussain et al. 2010). The main structural changes that influence the molecular permeability are the increased collagen cross-linking and solubility, accumulation of lipids and the formation of drusens. The collagen cross-linking increases the density of the collagen network, thus decreasing the permeability. The lipids accumulate into ICL and EL and form a so-called lipid wall, which affects especially the permeability of hydrophilic molecules. (Booij et a. 2010.) The changes in proteoglycan synthesis, meaning that the relative amount of different proteoglycans change, may have an effect to permeability (Hewitt et al. 1989). Although the congestion of BrM is the main reason for dysfunction of the BRB, the source of all the debris accumulating into BrM comes mainly from the RPE and its high metabolic activity.

Changes in choriocapillaris

During aging the density of the choriocapillaris network almost halves and the diameter of the vessels decrease by one third, thus widening the intercapillary pillars (Ramrattan et al. 1994). This also leads to the decrease in blood volume and flow in the choroid, thus decreasing the transport of waste products from RPE and impairing the import of nutrients to the RPE. (Bhutto & Luty 2012.)

2.3.2 Age-related macular degeneration and other retinal diseases

The age-related changes in the layers of the BRB have a significant role in the development of age-related macular degeneration (AMD). This disease causes a decline, and in some cases, a total loss of sharp central vision. The two major forms of AMD are dry (non-exudative) and wet (exudative) AMD. (Bhutto & Luty 2012.) The determinants contributing to AMD are both genetic and environmental. Mutations in certain genes are found to increase the risk of AMD, but it most probably is a complex polygenic disorder. Some discovered environmental factors that increase the risk of AMD are smoking, diet and exposure to light. (Booij et al. 2010.) Figure 2.5 shows schematically the effects of dry and wet AMD compared to normal tissue.

Dry AMD is more common and, although it causes substantial visual impairment, it does not always lead to the loss of central vision. The formation of large drusens and abnormal pigmentation cause distorted and dimmed vision, and are the signs of an early form of dry AMD. In the later stages, RPE begins to atrophy. This atrophy leads to the loss of the RPE and thinning of the retina and finally results in the loss of central vision. The atrophy of the RPE is related to decreased permeability of BrM. At the moment there is no treatment to dry AMD. Dry AMD can lead to the wet form of the disease. (Bhutto & Luty 2012.)

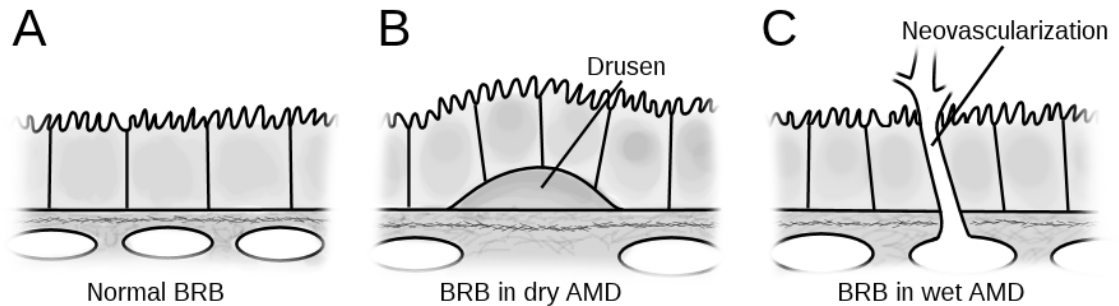


Figure 2.5. The effects of dry (B) and wet (C) AMD to BRB compared to the normal tissue (A). In dry AMD, drusens form between RPE and BrM, and in wet AMD, the choriocapillaris break through BRB in neovascularization.

Only about 10–15 % of AMD cases are wet form. It is characterized by choroidal neovascularization (CNV), which causes abnormal blood vessels migration through BrM and into the retina. With no barrier between the blood circulation and retina, blood begins to leak into the retina, causing distortions and blind spots. Central vision is lost as the abnormal vessels eventually result in disciform scar. The main reason for CNV is the rise of pro-angiogenic factor levels, such as VEGF, compared with anti-angiogenic factor levels, such as PEDF and endostatin. One factor increasing the production of VEGF is hypoxia, which may be caused by the decrease in choriocapillaris density and the congestion of BrM. (Bhutto & Luty 2012.) Elastin in the EL binds endostatin and forms one barrier against the vessel migration, so the break down of the EL might be one reason for CNV (Mullins & Sohn 2012). Additionally, inflammation and complement system activation are partial causes of AMD (Bhutto & Luty 2013).

In addition to AMD, there are many other diseases that affect BRB, such as diabetic retinopathy and some form of *retinitis pigmentosa* (Thrimawithana et al. 2011). However, AMD is the most common of these diseases (Pascolini & Mariotti 2012).

2.3.3 Prevention and treatment of retinal diseases

The efforts to prevent and treat diseases such as AMD are focused on four areas: fat metabolism, oxidative stress, complement activation and VEGF induced neovascularization. Easy ways to prevent or at least postpone AMD is to stop smoking, to have a diet high with anti-oxidants and to wear sunglasses. (Booij et al. 2010.)

There are some drug therapies that have shown promising results against AMD. The drug targets are for example the accumulation of retinol-based toxins into the RPE and restoration of pro/anti-angiogenic factor imbalance. (Booij et al. 2010.) The main challenge with drug-based therapies is the delivery of the drug to the retina and RPE. BRB forms a barrier against a drug delivered through systemic circulation. The easiest way to avoid it is to use eye drops, but even this way, the amount of drug reaching the retina is a very small percentage. Other viable option is intravitreal injection, with which the drug is invasively injected straight into the vitreous. The main problem with this is the invasive injection, which means that the drug should maintain its therapeutic concentration over a long period to minimize the number of injections. (Del Amo & Urtti 2008.)

There are two options for the drug delivery routes that include the permeation through BRB: periocular drug delivery and systemic administration. The drug molecules have to be lipophilic for these routes to enable the crossing of the BRB. In periocular drug delivery, the drug is either injected outside the eye or a drug-releasing implant is positioned next to it, usually in the posterior segment. With these methods, the choroidal blood circulation forms an additional barrier against the delivery. Systemic delivery is also challenging, as large concentrations are needed to enable the sufficient drug concentration in the retina. (Ranta et al. 2010.)

Another way to restore the functionality of BRB is to use tissue engineering. RPE transplantation has shown some success in animal models, but the main remaining challenges are the restoration of the RPE-retina interactions and re-establishment of the BRB (Bhutto & Lutty 2012). One promising cell source for this application is human embryonic stem cells, which can be differentiated towards the RPE direction. The problem with the earlier studies using a stem cell derived RPE cell as cell transplants was that cell were injected only as a suspension into the subretinal space, which did not lead to normal epithelial structure. The use of biodegradable scaffolds with cells has proven to be a better alternative, and the search for a good biomaterial is underway. (Hynes & Lavik 2010.)

The main interest in retinal repair is directed towards the RPE and photoreceptor cells. However, the main site of AMD pathology is BrM. Booij et al. (2010) lists two options for local BrM therapy, which are the removal of the pathogenic compound from the BrM or natural bioremediation by using enzymes to restore the BrM functions.

2.4 Epithelial transport and permeability research

Certain molecular properties govern which of the two pathways – paracellular or transcellular – does a molecule take through an epithelium. Molecules can move through epithelium either by passive or active transport. In passive transport, the molecular movement is passive, non-specific and its direction is governed by the electrochemical gradient of the molecule. With active transport, on the other hand, molecules are transported to a specific direction while consuming energy. In addition to the epithelial transport properties, this section also introduces the methods usually used to measure the BRB permeability.

2.4.1 Molecular characteristics

Important molecular characteristics affecting transport through an epithelium are molecule's size, charge and lipophilicity (Ho et al. 2003). The size of the molecule can be expressed in many ways: with radius, molecular mass or molecular volume. Different methods of determining the molecule's radius are reviewed later.

Molecular charge is based on the pK_a values of the functional groups in the molecule structure and the surrounding pH. If pH is below the pK_a value of a function group, it is in its protonated form. For acidic groups, this means positive charge and for basic

groups neutral form. When pH is above the pK_a value, the functional groups are deprotonated, meaning neutral for acidic groups and negative for basic groups. (Nelson 2008.)

Lipophilicity, or hydrophobicity, describes how well a molecule mixes with water, and it is based on the molecule's ability to form hydrogen bonds with water molecules. The more lipophilic the molecule, the less likely it is to form these bonds and thus to mix with water, and vice versa. Lipophilicity can be expressed by two parameters: a partition coefficient and distribution coefficient. They both describe the molecule's partitioning between aqueous and hydrophobic phases in equilibrium. The partition coefficient is the relationship between the non-ionized molecule concentration in a hydrophobic phase to that of the aqueous phase. Therefore, a higher partition coefficient refers to higher lipophilicity. (Mälkiä et al. 2004.)

The distribution coefficient includes also the ionized species, and it has smaller value than the partition coefficient, as ionized species tend to remain in the aqueous phase. The level of ionization depends on both the molecule's pK_a value and the solvent's pH. The hydrophobic phase is usually represented by octanol, and partition and distribution coefficient are expressed as $\log P$ and $\log D$, respectively. Logarithmic scale is used as the size differences between values can be large. (Mälkiä et al. 2004.) Molecules with $\log P < 1$ can be considered hydrophilic and $\log P > 2.5$ highly lipophilic (Kadam et al. 2011). In this thesis, partition and distribution coefficients are denoted as $\log K_p$ and $\log K_D$, respectively, to prevent confusion with permeability and diffusion coefficients discussed later.

2.4.2 Epithelial transport

Movement through the paracellular pathway is always passive, but the movement through the transcellular pathway is more complex, as there are three main mechanisms for it. First of all, molecules can diffuse passively across the cells with two mechanisms. Molecules can permeate straight through the cell membrane, cell cytoplasm and other cell membrane. The second mechanism is to partition into the hydrocarbon core of the cell membrane and to diffuse within it to the other side of the cell. The third and more active mechanism is carrier-mediated transport, which is done by two types of transmembrane proteins: channels and transporters. (Ho et al. 2003.) Channels are a form of passive transport, as they only facilitate the diffusion across the plasma membrane along the molecule's or ion's electrochemical gradient. Transporters function by changing their conformation while transporting molecules across the membrane. The transport may be passive along the molecule's electrochemical gradient or active against it. The energy for active transport comes from the movement of other molecules, known as coupled transport, ATP or light energy. Coupled transport is usually driven by the electrochemical gradient of ions, such as Na^+ . (Alberts et al. 2008.) As a fourth mechanism, the molecules can be transported using vesicles, a process known as transcytosis, and it may be specific or non-specific. (Ho et al. 2003.) The different mechanisms of epithelial transport are summarized in Figure 2.6.

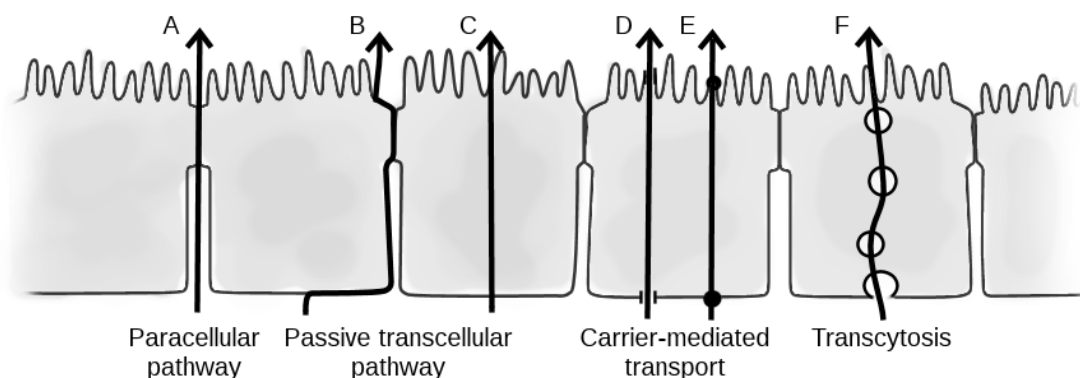


Figure 2.6. The different mechanisms of epithelial transport. A: Paracellular transport; B: Transcellular transport within the hydrocarbon core; C: Transcellular through the cytoplasm; D: Facilitated diffusion through the channels; E: Active transport using energy or coupled transport; F: Transcytosis.

The pathway a molecule takes across an epithelium depends on its physicochemical properties. Active transport is always specific to a molecule, depending on its specific interactions with the transporter, whereas passive movement is non-specific. Also, molecules transported actively do move passively across an epithelium. As the present work is only concerned with the passive movement of molecules, the active transport mechanisms are excluded from the following discussion.

The size of the molecule restricts the passive diffusion through both the paracellular and transcellular pathways. Small molecules can diffuse through the small structural TJ pores and larger ones through the dynamic strand breaks (Anderson & Van Itallie 2009). The diffusion through the transcellular pathway is also dependent on the molecular size. It defines how large opening there must be in the cell membrane for the molecule to diffuse through. Molecules that have molecule mass under 400 Da – which makes them smaller than lipids – can cross the membrane through the small gaps formed between fluctuating lipids. Molecules larger than this diffuse slower as a larger and energetically more unfavorable gap must be formed between the lipids. (Mitragotri 2003.)

The lipophilicity of the molecule has no effect on the paracellular pathway, as molecules do not cross any lipophilic barriers. However, in the transcellular pathway it has a major role. The hydrocarbon core of the cell membrane greatly restricts the diffusion of hydrophilic molecules, whereas for lipophilic molecules this is the favored pathway. The permeation of hydrophilic, and especially charged, molecules across the cell membrane is energetically very unfavorable. As a basic rule, small and hydrophilic molecules permeate through the paracellular pathway, and larger and lipophilic molecules through the transcellular pathway. In addition to the permeation across the cell membrane, lipophilic molecules can remain inside the membrane and diffuse within the hydrocarbon core around the cell cytoplasm. In this case the transmembrane proteins, such as the TJ claudins, hinder the diffusion. (Ho et al. 2003.)

Melanin pigment in the RPE cells contributes an additional barrier to the transcellular pathway. It is fairly well established that lipophilic and basic drugs tend to bind reversibly to melanin. The binding interactions usually arise from electrostatic and van

der Waals forces. (Leblanc et al. 1998.) Lipophilicity is one major component influencing the molecule's binding affinity, but correlations between the two alone are quite weak (Kadam & Kompella 2010). Also, there are differences in binding affinities between synthetic melanin and natural bovine ocular melanin (Pitkänen et al. 2007), and natural melanin from *Sepia officinalis* and porcine eyes (Pescina et al. 2012).

2.4.3 Studying the BRB permeability

There are a few different ways to study the permeability in eyes. Some methods can be utilized *in vivo* and some *in vitro*. Clinically the permeability can be measured by vitreous fluorometry. In this method, fluorescein is administered to systemic circulation and the permeated concentration is measured from vitreous using a fluorometer. (Cunha-Vaz 2004.) Another way is using a so-called retinal uptake index, analogous to a more commonly used brain uptake index. Tracer molecules are injected into test animals, after which they are sacrificed and the tissues in interest are removed. The concentration in the retina is then compared with the injected concentration. (Hosoya et al. 2010.) The problem with above methods in relation to the present study is that the tracer molecules can permeate into the retina through both the outer and inner BRB. Some studies utilize tracer molecules that can be seen using an electron microscope, like ferritin. After injection and sacrifice, thin sections of BRB are prepared to observe the permeability qualitatively. (Essner & Gordon 1983.)

More common way of measuring the permeability of a tissue is to use a diffusion chamber, which can be used study molecule permeation through excised tissues *in vitro*. The basic idea of a diffusion chamber is to place a planar tissue, usually an epithelium, so that it separates a chamber into two half-chambers (Clarke 2009). This method is widely used to measure the permeability of BRB and different parts of it (Hussain et al. 2002; Hillenkamp et al. 2004; Pitkänen et al. 2005; Cheruvu & Kompella 2006; Kadam et al. 2011). The permeated concentration can be measured by different methods: UV or fluorescence detectors (Hussain et al. 2002; Pitkänen et al. 2005; Cheruvu & Kompella 2006), mass spectrometry (Kadam et al. 2011) or scintillation counter with radio-labeled tracers (Hillenkamp et al. 2004; Cheruvu & Kompella 2006). In addition to the molecular permeability measurements, TER is sometimes measured during the experiments. This is done to monitor the RPE cell viability and quality of the BRB. (Hillenkamp et al. 2004; Pitkänen et al. 2005)

Depending on the properties of the BRB or its parts studied, the used molecules vary. Some basic molecules used to study the general permeability are fluorescent tracers, such as fluorescein (Cheruvu & Kompella 2006), carboxyfluorescein (Pitkänen et al. 2005) or Rhodamine tracers (Steuer et al. 2005; Cheruvu & Kompella 2006). The permeated concentration is easily determined using a fluorometer. When studying the influence of the molecular size on permeation, series of differently sized but otherwise similar molecules are used. Usually used molecule series are FITC-dextrans (fluorescein isothiocyanate) (Pitkänen et al. 2005) and amino acids (Hussain et al. 2002). The FITC-dextrans are branched polysaccharide chains and have a size scale of over 1 kDa,

whereas amino acids are around 100-200 Da and have more compact conformation. To study the effect of lipophilicity on the permeability, usually β -blockers are utilized. This is because they have similar molecular masses and pK_a values, but a wide range of different lipophilicities (Kadam & Kompella 2009). Studies using β -blockers (Pitkänen et al. 2005; Kadam et al. 2011) measure the permeability of all the β -blockers simultaneously, a method known as the cassette analysis, as this saves time and effort. However, when using a mixture of β -blockers, they have to be separated from each other during the analysis. This is usually done using high-performance liquid chromatography, which is found to be a good method for the separation (Ranta et al. 2002; Kadam & Kompella 2009).

2.4.4 Diffusion chamber

In a diffusion chamber, a planar tissue or cell layer on biomaterial insert is placed between two half-chambers, as schematically shown in Figure 2.7. One of the half-chambers (donor chamber) is filled with a solution including the studied drug molecules and the other (acceptor chamber) is filled with a solution without the drug. (Li et al. 2004.) By placing the epithelium between the two chambers, the transport from one chamber to the other takes place only through it. To enable this, the system has to be tight, so there is no leak from chamber to the other through any other pathway than the epithelium. The drug concentration in the acceptor chamber can then be studied by the analysis techniques discussed earlier.

Although there are different forms of diffusion chambers, the basic principles are the same. Some chambers include perfusion on both sides of the tissue instead of the static fluids. (Li et al. 2004.) One type of diffusion chamber is called Ussing chamber, which is largely used for this kind of studies, but especially to measure TER of the BRB.

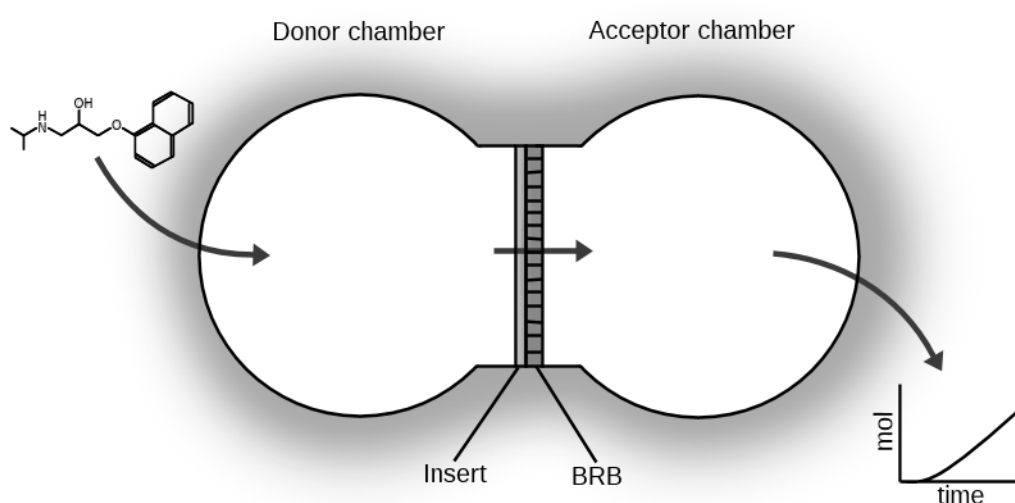


Figure 2.7. A schematic presentation of the function of the diffusion chamber. The drug solution is placed into the donor chamber and a solution without the drug in the acceptor chamber. From the donor chamber the drugs diffuse through BRB and a possible insert into the acceptor chamber. Samples are taken from the acceptor chamber and analyzed to produce the permeability data.

(Clarke 2009.) Depending on the type of the chamber, different kind of tubing, stirring systems and electrodes are connected to the half-chambers (Li et al. 2004). The electrodes are connected to both sides of the epithelium, so that the TER over it can be measured. TER is used to monitor the quality of the epithelium as well as the tightness of the measurement system. (Griep et al. 2013.)

Although the diffusion chambers provide a good basic platform for the study of the transport properties of tissues, there are issues with the current diffusion chambers. Problems with some currently available chambers are the large tissue area and chamber volumes. By miniaturizing the whole system, the needed tissue areas and chamber volumes can be decreased. This means that smaller tissue pieces can be used and the amount of solutions and drugs decrease. (Griep et al. 2013.) Perfusion used in some chambers helps to minimize the hydrostatic pressure of large chamber and thus prevent tissue damage (Li et al. 2004).

2.5 Physics of diffusion and permeability

Diffusion is one of the basic methods of movement in the molecular scale. This section describes the physical basis of diffusion and the equations trying to capture its essence. In addition to diffusion, also permeability over barriers and hindered diffusion within different geometrical surroundings are represented.

2.5.1 Diffusion

Diffusion is a phenomenon that describes passive movement of molecules usually in liquid or in gas. The driving force of diffusion is the random thermal motion of the surrounding solvent or gas molecules. Diffusion is an important process in the cellular world, as it is a method of transport without any consumption of chemically stored energy. There are two scales that diffusion can be described in. In the molecular scale, the random motion of an individual molecule can be studied and modeled, and in the larger scale, diffusion is a process which leads to a complete mixing of molecules with concentration differences – or an equilibrium. (Nelson 2008.) The rate of diffusion is denoted with diffusion coefficient D , which has a unit of $\text{m}^2 \text{s}^{-1}$. The bigger the D is, the larger is the diffusion rate.

In the molecular scale the random motion of one molecule (referred as a solute particle from here on) is created by the interactions between the solvent molecules and the solute particle. As the small solvent molecules fluctuate due to the thermal energy and collide with the larger solute particle, they exert a small force on it. Generally, these small collisions have a little effect, as the size difference between the solute particle and small solvent molecules is large, and they tend to cancel each other out. Thus the particle remains stationary. However, at some time points a net force exists towards a random direction and the particle moves. This movement continues until, after a while, another net force is exerted towards another random direction. (Nelson 2008.) This motion can be described as a random walk and it is known as the Brownian motion, named after

a 19th century Botanist Robert Brown, who noticed the random motion of pollen grains suspended in water (Brown 1828).

Brownian motion can be modeled in many ways, most notably with equation derived by Albert Einstein in 1905. The small collisions creating the movement of the solute particle also diminish it as they generate resisting frictional force. Einstein's theory does not account the individual collisions, but represents the solvent with this force. Einstein related the parts creating and diminishing the diffusion to one equation, known as Einstein's relation or fluctuation-dissipation theorem

$$\zeta D = k_B T, \quad (2.1)$$

where ζ is the viscous friction coefficient, which is the relation of the frictional force to the particle's drift velocity (N s m^{-1}), k_B is Boltzmann's constant ($1.38 \times 10^{-23} \text{ J K}^{-1}$) and T is the absolute temperature (K). This relation is universal, as it does not depend on the solute particle or solvent. (Nelson 2008.)

To relate the diffusion coefficient to the particle, especially to its size, the viscous frictional coefficient has to be defined. The most commonly used form of this coefficient was derived by Sir George Stokes for a rigid spherical particle diffusing in a continuum of solvent, and it is known as Stokes' law

$$\zeta = 6 \pi \eta r_s, \quad (2.2)$$

where η is the solvents dynamic viscosity (Pa s) and r_s is the solute particle radius (m). The value of η at 37°C is $6.92 \times 10^{-4} \text{ Pa s}$. Equations (2.1) and (2.2) can be combined into Stokes-Einstein equation

$$D = \frac{k_B T}{6 \pi \eta r_{SE}}, \quad (2.3)$$

where the subscript of r_{SE} denotes that this is Stokes-Einstein radius. As can be seen from Equation (2.3), a small particle has large D and vice versa. Nowadays it is possible to measure the diffusion coefficients and Equation (2.3) is usually used to calculate the size of the solute particle. (Nelson 2008.)

It is important to notice that the Stokes-Einstein radius does not always correspond to the actual size of the molecule, just the radius of a spherical particle with the diffusion coefficient D . There are many other and more complex approximations for this relationship, but Equation (2.3) is very simple and quite accurate. The important assumptions of Stokes' law are that the particle is spherical and has a radius of more than five times the radius of the solvent molecules. (Cussler 2009.) These assumptions are good for large globular proteins, but not for linear proteins or small drug molecules. The assumption of a spherical particle is seldom very accurate, but it is a mandatory simplification, as it enables the description of solute particle's size with one parameter and the utilization of spherical symmetry. For particles smaller than five times the radius of the solvent molecule, Equation (2.3) fails.

This size restriction can be bypassed by using Sutherland correlation, which assumes that – contrary to Stokes-Einstein equation – the solvent molecules can slip past the surface of the particle (Sutherland 1905)

$$D = \frac{k_B T}{4 \pi \eta r_{Su}}, \quad (2.4)$$

where the subscript of r_{Su} emphasizes the difference with Stokes-Einstein radius. A common collective name for r_{SE} and r_{Su} is a hydrodynamic radius, but it is important to differentiate them as they are meant for different molecular size scales.

The diffusion covered so far describes the diffusion of one average particle in a continuum of solvent. In the larger scale, including multiple particles and concentration gradients, diffusion levels out the gradients and eventually leads to a complete equilibrium. Basically, diffusion erases order, so it has entropic nature. Diffusion in this scale is described by Fick's laws of diffusion, named after Physicist Adolf Fick. Fick's first law states that the number of solute particles diffusing per unit area per unit time, or diffusional flux, relates to the particle concentration gradient according to Equation

$$J = -D \nabla c, \quad (2.5)$$

where J is the diffusional flux ($\text{mol m}^{-2} \text{s}^{-1}$) and c is the concentration (mol m^{-3}). The symbol ∇ denotes the gradient and represents a partial derivation in three directions. Basically, Equation (2.5) states that the flux is directed towards the decreasing concentration with the rate defined by D . The basic reason behind the direction of the flux is the fact that there are more particles in the domain with high concentration diffusing towards the low concentration domains than in the other direction. Fick's first law assumes steady-state conditions, in which the flux is constant. Fick's second law omits the flux altogether and defines the rate of concentration change as

$$\frac{\partial c}{\partial t} = D \nabla^2 c. \quad (2.6)$$

This equation is also known as the diffusion law. (Nelson 2008.)

It is important to notice that diffusion coefficients in Stokes-Einstein or Sutherland equations are limited to infinitely dilute solutions, as they do not take into account the interactions between solute particles. Diffusion coefficients in liquids vary with the concentrations, sometimes by several hundred percents. (Cussler 2009.) The assumption of dilute concentration is usually made in mathematical models, although it is not necessarily always very accurate (Cu & Saltzman 2009).

2.5.2 Permeability

In cases where the particle diffuses through a barrier, for example an epithelium, a permeability coefficient is usually used instead of the diffusion coefficient. The permeabil-

ity coefficient is more case-specific and it is defined from the diffusion coefficient according to Equations

$$P = \frac{D_{B,eff}}{l_B}, \quad (2.7)$$

where

$$D_{B,eff} = D_B \Phi_B \quad (2.8)$$

and P is the permeability coefficient (m s^{-1}), $D_{B,eff}$ is the effective diffusion coefficient within the barrier ($\text{m}^2 \text{s}^{-1}$), l_B is the barrier thickness (m), D_B is the diffusion coefficient within the barrier ($\text{m}^2 \text{s}^{-1}$) and Φ_B is the partition coefficient between the solvent and the barrier. Usually, the experimentally measured permeability coefficients are denoted as apparent (P_{app}) or effective (P_{eff}) to highlight their uncertainty and dependence on experimental conditions. (Brodin et al. 2009.) The partition coefficient describes the amount of solute inside the matrix in relation with the free solution – that is, how favorable the matrix environment is for the molecule. Basically, it is analogous to the partition coefficient describing lipophilicity.

With permeability, Equation (2.5) can be written as

$$J = -P \frac{\nabla c}{l_B}, \quad (2.9)$$

which is analogous to Ohm's law, as J corresponds to current and ∇c to potential difference. This means that permeability is analogous to electrical conductivity. (Cussler 2009.) Thus when there are different diffusion pathways and diffusion barriers within a pathway, the permeabilities can be thought of as being connected in parallel or in series. If n number of pathways are connected in parallel, the individual permeabilities are combined to total permeability by using Equation

$$P_{tot} = \sum_{i=1}^n P_i. \quad (2.10)$$

Because in this case the permeabilities are additive, the relationship is straightforward: if there are pathways with permeabilities in different orders of magnitude, the pathway with the highest permeability dominates. (Yu & Amidon 2000.) For example the paracellular and transcellular permeabilities can be combined using this equation.

If n number of diffusion barriers are connected in series – arranged in successive manner – the total permeability is calculated with Equation

$$\frac{1}{P_{tot}} = \sum_{i=1}^n \frac{1}{P_i}. \quad (2.11)$$

When connected in series, the barrier with the lowest permeability mainly defines the

total permeability. (Yu & Amidon 2000.) The lateral space and TJs are connected in series in the paracellular pathway, the latter dominating with its low permeability.

2.5.3 Hindered diffusion

Diffusion taking place within the permeability barrier is slower than in free solution, because of the barrier structures hindering it. The interactions between the barrier structures and the solute particle can be divided into three types: hydrodynamic, steric and electrostatic.

Hydrodynamic interactions are mechanical interactions between the solute particle and structures that are mediated by the solvent. They enhance the frictional drag felt by the diffusing particle, thus decreasing the diffusion rate as seen from Equation (2.1). Also, the structures serve as steric obstacles that increase the diffusion path length. (Amsden 1998.) In addition to these more mechanical interactions, there may be electrostatic interactions that cause attraction or repulsion between the particle and its surroundings, thus affecting the diffusion rate.

Models for hindered diffusion within three different geometrical structures – slit, pore and fiber matrix – are presented next. Their geometries are presented in Figure 2.8.

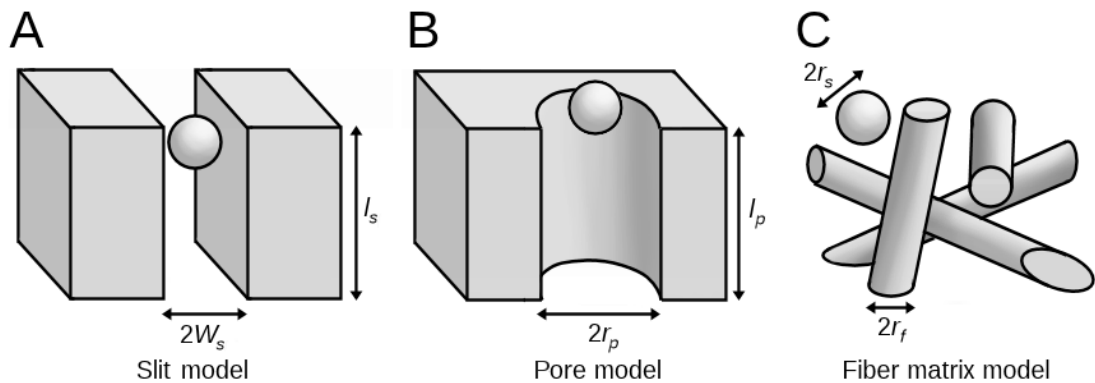


Figure 2.8. The geometrical idea of slit model (A), pore model (B) and fiber matrix model (C). (W_s : slit half-width; l_s : slit length; r_p : pore radius; l_p : pore length; r_s : solute particle radius; r_f : fiber radius)

Slit model

The basic geometry of the slit model is a space with a width of $2W_s$ between two parallel surfaces, as shown in Figure 2.8A. Essentially, the slit model is a modified version of Equation (2.7), as the permeability coefficient of the slit is given by Equations

$$P = \frac{\epsilon_s D_0 H_s(\lambda_s)}{l_s}, \quad (2.12)$$

where

$$\lambda_s = \frac{r_s}{W_s} \quad (2.13)$$

and ϵ_s is the relative surface area of the slit, D_0 is the free diffusion coefficient ($\text{m}^2 \text{s}^{-1}$), $H_s(\lambda_s)$ is the hindrance factor in a slit, l_s is the slit length (m) and W_s is the slit half-width (m). (Ho et al. 2003). The hindrance factor $H_s(\lambda_s)$ basically describes the sum of the partitioning into the slit, and hydrodynamic as well as steric interactions within the slit itself (Dechadilok & Deen 2006). There are many different approximations for $H_s(\lambda_s)$ with different value ranges of λ_s . The most accurate one was derived by Dechadilok & Deen (2006) and it is accurate within the range of $0 \leq \lambda_s \leq 0.80$:

$$H_s(\lambda_s) = 1 + \frac{9}{16} \lambda_s \ln \lambda_s - 1.19358 \lambda_s - 0.4285 \lambda_s^3 - 0.3192 \lambda_s^4 + 0.08428 \lambda_s^5 \quad (2.14)$$

Pore model

This model is very similar to the slit model, but the pore is formed by a cylinder, as shown in Figure 2.8B. Again, this is a modification of Equation (2.7) and is given as

$$P = \frac{\epsilon_p D_0 H_p(\lambda_p)}{l_p}, \quad (2.15)$$

where

$$\lambda_p = \frac{r_s}{r_p} \quad (2.16)$$

and ϵ_p is the relative surface area of the pores, $H_p(\lambda_p)$ is the hindrance factor in a pore, l_p is the pore length (m) and r_p is the pore radius (m) (Ho et al. 2003). Again, there are many different approximations for the hindrance factor in pores. Dechadilok & Deen (2006) derived one with a good accuracy range of $0 \leq \lambda_p \leq 0.95$:

$$H_p(\lambda_p) = 1 + \frac{9}{8} \lambda_p \ln \lambda_p - 1.56034 \lambda_p + 0.528155 \lambda_p^2 + 1.91521 \lambda_p^3 - 2.81903 \lambda_p^4 + 0.270788 \lambda_p^5 + 1.10115 \lambda_p^6 - 0.435933 \lambda_p^7 \quad (2.17)$$

Fiber matrix model

The fiber matrix model describes diffusion within a randomly oriented fiber matrix, as shown in Figure 2.8C. This theory was proposed by Ogston (1958) and it describes the polymer matrix with only the radius and fiber volume fraction. As shown in Equation (2.8), the partition coefficient and diffusion coefficient inside the matrix has to be defined to calculate the effective diffusion coefficient.

The partition coefficient for an uncharged, spherical particle in a randomly oriented fiber matrix can be calculated with Equation

$$\Phi_m = \exp \left[-\varphi_f \left(1 + \frac{r_s}{r_f} \right)^2 \right], \quad (2.18)$$

where φ_f is the fiber volume fraction and r_f is the fiber radius. Equation (2.18) is limited to dilute solutions, as it does not include the intermolecular interactions. (Ogston 1958.) Later Ogston et al. (1973) derived an equation for the diffusion coefficient within the matrix. The equation tends to overestimate as it includes steric interactions, completely ignoring the hydrodynamic interactions (Johnson et al. 1996).

The diffusion coefficient within the matrix includes the hydrodynamic and steric interactions between the particle and the matrix. Brady (1994) suggested a so-called effective medium model, which divides the two interactions into two separate factors

$$\frac{D_m}{D_0} = H_m S_m, \quad (2.19)$$

where D_m is the diffusion coefficient within the matrix ($\text{m}^2 \text{s}^{-1}$), and H_m and S_m are the hydrodynamic and steric interactions, respectively.

There are some different results for the hydrodynamic interactions between a spherical particle and randomly oriented fiber matrix. A widely used one was derived by Phillips et al. (1989) and it relates the hydrodynamic interactions to the matrix fluid permeability, called Darcy permeability. The problem with this model is that the Darcy permeability of the matrix must be known, or at least approximated. To counter this fact, Clague & Phillips (1996) derived an equation relating the interactions only to the fiber volume fraction, and fiber and solute particle radii

$$H_m = \exp(-a \varphi_f^v), \quad (2.20)$$

where a and v are fitted parameters and dependent of r_f and r_s . Amsden (1998) fitted the parameters using literature data of diffusion in hydrogels as

$$a = \pi \quad (2.21)$$

and

$$v = 0.174 \ln \left(59.6 \frac{r_f}{r_s} \right). \quad (2.22)$$

The two models have been compared with varying results (Amsden 1998; Phillips 2000). When r_s and r_f have similar magnitude, both models have practically identical behavior across the whole volume fraction range. However, when the fiber radius is much larger than that of the solute particle, their behavior is very different.

The steric interactions can be calculated by using an equation derived by Johansson & Löfroth (1993) for diffusion through straight, randomly oriented fiber network, because they ignored the hydrodynamic interactions:

$$S_m = \exp(-0.84 f^{1.09}) \quad (2.23)$$

and

$$f = \varphi_f \left(1 + \frac{r_s}{r_f}\right)^2, \quad (2.24)$$

where f is the adjusted fiber volume fraction. Basically Equation (2.24) describes the volume fraction of fibers with a radius of $r_s + r_f$. Equation (2.23) was derived using Brownian dynamic simulations and it is valid when $f < 3$ (Johansson & Löfroth 1993). There are also other results for S with different fiber arrangements, for example those derived for hexagonal and square arrays of cylinders by Perrins et al. (1979).

In addition to the hydrodynamic and steric interactions, there can be electrostatic interaction between the solute particles and fibers. In ionic solutions, charged surfaces are surrounded by ions with an opposite charge. This ion cloud screens the surface charge, and Debye screening length characterizes the distance after which the surface seems neutral. (Nelson 2008.) Debye screening length depends on the ionic strength of the solution. Electrostatic interactions lose their significance as the radius of the fiber is much larger than Debye screening length. (Stylianopoulos et al. 2000a.) There are small electrostatic interactions even though other object is uncharged, as it still influences the ion cloud surrounding the charged object (Johnson & Deen 1996).

To incorporate the electrostatic interactions, the basic fiber matrix theory has to be modified. Johnson et al. separately measured the effective diffusion and partition coefficients of molecules with different charges diffusing through agarose gel. They concluded that the electrostatic interactions mainly affect the partition coefficient, not the diffusion coefficient within the matrix. (Johnson et al. 1995.) The mathematical model to predict this behavior was constructed by Johnson & Deen (1996). Equation (2.18) was originally derived from Equations

$$\Phi_m = \int_0^{\infty} g(h) dh \quad (2.25)$$

and

$$g(h) = \frac{2\varphi_f(h+r_s+r_f)}{r_f^2} \exp\left[-\frac{\varphi_f(h+r_s+r_f)^2}{r_f^2}\right], \quad (2.26)$$

where h is the separation distance between the particle and a fiber (m) (Ogston 1958). To include the electrostatic interactions into the partition coefficient, Johnson & Deen (1996) introduced Boltzmann factor into Equation (2.25) to describe the relative probability of different energy states between the solute particle and the fiber so that

$$\Phi_{m,e} = \int_0^{\infty} g(h) \exp(-E(h)) dh \quad (2.27)$$

and

$$E(h) = \frac{(RT/F)^2 \epsilon r_s}{k_B T} \Delta G(h), \quad (2.28)$$

where R is the universal gas constant ($8.31 \text{ J mol}^{-1} \text{ K}^{-1}$), F is Faraday constant ($9.65 \times 10^4 \text{ C mol}^{-1}$), ϵ is the solvent's absolute permittivity (F m^{-1}) and ΔG is the change in free energy (J). The absolute permittivity is defined as $\epsilon = \epsilon_0 \epsilon_r$, where ϵ_0 is the vacuum permittivity ($8.85 \times 10^{-12} \text{ F m}^{-1}$) and ϵ_r is the relative permittivity, which is 74.2 for water at 37 °C. The change in free energy can be divided into three components: the first describing the free energy change between the particle and fiber (ΔG_{sf}) and the other two describing the changes in the ion clouds surrounding the particle (ΔG_s) and fiber (ΔG_f) resulting in Equation

$$\Delta G(h) = \Delta G_{sf}(h) + \Delta G_s(h) + \Delta G_f(h). \quad (2.29)$$

Electrostatic interactions in ionic solutions are described by Poisson-Boltzmann equation. A linearized version of this equation was used by Johnson & Deen (1996) to determine the electrical potentials and it was solved using a finite element method. The resulting expression is of the form

$$\Delta G(\mu, \tau, \beta, \sigma_s, \sigma_f) = A_1(\mu, \tau, \beta) \sigma_s \sigma_f + A_2(\mu, \tau, \beta) \sigma_s^2 + A_3(\mu, \tau, \beta) \sigma_f^2, \quad (2.30)$$

where

$$A_i(\mu, \tau, \beta) = a_i \tau^{b_i} \beta^{c_i} \exp(-d_i \mu) \quad (2.31)$$

and a_i , b_i , c_i and d_i are constants shown in Table 2.1. The rest of the factors in Equations (2.30) and (2.31) are the dimensionless separation distance μ , particle radius τ , fiber radius β , particle's surface charge density σ_s and fiber's surface charge density σ_f . They are defined by Equations

$$\mu = h \kappa_D, \quad (2.32)$$

$$\tau = r_s \kappa_D, \quad (2.33)$$

$$\beta = \frac{r_f}{r_s}, \quad (2.34)$$

$$\sigma_s = \frac{r_s F}{\epsilon R T} q_{A,s} \quad (2.35)$$

and

$$\sigma_f = \frac{r_f F}{\epsilon R T} q_{A,f}, \quad (2.36)$$

Table 2.1. The values of constants a_i , b_i , c_i and d_i in Equation (2.31) (Johnson & Deen 1996).

i	a_i	b_i	c_i	d_i
1	2.3523	0.7599	1.2472	1.0956
2	0.3570	0.5052	0.9512	3.7684
3	0.4473	0.9310	1.1512	2.4987

where κ_D is reciprocal of Debye screening length (m^{-1}), and $q_{A,s}$ and $q_{A,f}$ are the particle's and fiber's surface charge densities (C m^{-2}), respectively. (Johnson & Deen 1996.) The value of κ_D^{-1} is 0.79 nm in the physiological ionic strength of 0.15 M (Stylianopoulos et al. 2010a).

The permeability coefficient of a fiber matrix barrier with a thickness of d_m can be calculated as

$$P_m = \frac{D_{m,eff} \Phi_m}{d_m} = \frac{D_0 H_m S_m \Phi_m}{d_m}, \quad (2.37)$$

where Φ_m is replaced with $\Phi_{m,e}$ if the electrostatic interactions are included.

2.6 Mathematical modeling

The importance of mathematical modeling of biological processes and systems has rapidly increased in recent years (Gavaghan et al. 2006). This section describes the basics of models, mathematical modeling and a technique known as the finite element method. Also, the current state of mathematical modeling of the BRB and similar anatomical structures are presented shortly.

2.6.1 Mathematical modeling of physiological systems

A model is a presentation of a real system. It is practically impossible to model a real system perfectly: there has to be some approximations. A mathematical model expresses the real system with mathematical equations. (Cobelli & Carson 2008.) Mathematical modeling is an important tool in life sciences as it enables the study of physiological processes and features with a reduced need to study the real system, which is in some cases difficult and expensive as well as includes the usage of test animals. Models can also be used to rule out some unneeded experimental studies and enable the experimental researchers to concentrate only on the important studies.

Another kind of important type of model in life sciences is an *in vitro* model. In an *in vitro* model, a physiological system is modeled by constructing a close biological equivalent system. In the case of the epithelial research, this usually means using cultured cells to form the epithelium, as opposed to using excised tissues from test animals or deceased humans. *In vitro* models allow the study of important properties of a physiological system easily and decrease the need of test animals (Barar et al. 2009).

Modeling of a physiological system is quite different from modeling mechanical systems. Physiological systems are complex, which rises for example from the number of components, interconnectivity in the system and nonlinearity. They are also dynamic and stochastic, so the behavior is sometimes difficult to predict. As in all models, the real system must be simplified, only accounting the important and governing components relating to the studied function. (Cobelli & Carson 2008.)

Models are used for different purposes and they can be categorized into four classes: descriptive, interpretive, predictive and explanatory. Descriptive models are used to express quantitative relationships between variables with equations. For example, Stokes-Einstein equation is a descriptive model, as it relates the diffusion rate to particle size. Interpretive models are used to interpret experimental results using mathematical equations. Predictive models are used to predict the output of the system with a known input. Explanatory models can be used to explain changes in a system by studying the effects of modeling parameters linked to system properties. (Cobelli & Carson 2008.)

There are two distinct approaches to mathematical modeling. Data-driven, or black-box modeling uses the known input and output of the system to determine a mathematical representation of the system using parameters without any connection with the real system. This is a good approach if there is little knowledge about the system or if a more accurate representation of the system is not needed. The other approach is to actually model the system. This approach needs prior knowledge of the system, but is generally more dynamic and related to the real system. After the model is created, it has to be validated. This is done by comparing its behavior with the real system and, in some cases, alternative models. Validation is also done during the model construction, as the quality of approximations has to be determined. A complete model can be used to study different scenarios by simulating the system response to specific inputs (Cobelli & Carson 2008.)

2.6.2 Finite element method

As a computational technique, the finite element method (FEM) can be used to obtain approximate solution to engineering problems. Real systems are continuous, and it is impossible to compute the value of a variable in every point of a volume. With FEM, this problem is avoided by dividing the system domain into small, finite-sized elements, so only a finite number of values have to be calculated. (Hutton 2003.)

FEM is applied to solve so-called boundary value problems, in which depending values must satisfy the governing differential equations everywhere in a system domain with known boundary conditions (BCs). Material properties are an important part of FEM modeling as they define how a specific material behaves. (Hutton 2003.) For example, when modeling diffusion as a boundary value problem, the dependent variable is concentration, governing differential equation is Fick's second law, a BC might be that there is no flux out of the system and material properties might be the viscosity of water as well as diffusion coefficient of the solute.

The elements are usually triangular in two dimensions and tetrahedral in three dimensions. The variables are usually calculated in the vertices of the elements, known as nodes, and the values of all the other points in the system are approximated by interpolation from the node values. The system's number of the degrees of freedom depends on both the number of the nodes and dependent variables in the system. (Hutton 2003.)

The process of discretization is called meshing and the element structure is called a mesh. The element number of the mesh defines the accuracy of the approximation of the real system. By increasing the element number, the size of each element decreases and approaches infinitesimal volume, or a point. The problem with increasing the element number is that the amount of degrees of freedom is also increasing, thus increasing the computational load. (Hutton 2003.)

The basic FEM modeling process is divided into three parts: preprocessing, solution and postprocessing. Preprocessing means the definition of the model: e.g. its geometry, material properties and BCs. In the solution phase a FEM software, like COMSOL Multiphysics, is used to compute the results. The postprocessing includes the analysis and evaluation of the results. One important part of the postprocessing is the determination of the result reasonability. (Hutton 2003.)

2.6.3 Mathematical models of BRB and corresponding structures

Most of the current mathematical models of the BRB are so-called pharmacokinetic models. They are constructed from anatomically-based compartments and rate constants that describe the drug transport between the compartments (Gallo 2003). Mac Gabhann et al. (2007) constructed a pharmacokinetic model of protein transport into the eye after periocular injection. In their model, BRB is only represented by the RPE with just one permeability coefficient (Mac Gabhann et al. 2007). A different approach was taken by Amrite et al. (2008), as they simply connected sclera, choroid and RPE into one compartment and had rate constant for transport into and out of this compartment. Ranta et al. (2010) related their compartmental model more to the properties of the solutes. They used three different molecule types: small lipophilic, small hydrophilic and macromolecule. They still gave these three types constant permeability coefficients based on *in vitro* and *in vivo* experiments.

In addition to pharmacokinetic compartmental models, there are some FEM models of drug movement within the eye, but only few of them include BRB. Balachandran & Barocas (2008) constructed a FEM model of periocular delivery of fluorescein into the eye. In addition to the passive diffusion, they included the active transport of fluorescein outwards from the eye. As their model also included the geometry of the eye, it resembled more the actual physiological system. (Balachandran & Barocas 2008.)

More accurate models relating the physicochemical properties of the diffusing molecule with the permeability have been constructed for anatomical barriers. Edwards & Prausnitz (1998; 2001) combined physical theories into a model describing hindered diffusion in the cornea. Their model consisted of three parts: corneal endothelium, stroma and epithelium. For the stroma they used the fiber matrix model, and both the

Table 2.2. *A summary of the permeability models that include the BRB or its parts. Please note that the last model is not of the BRB, but of cornea.*

Type	Model	Properties	Benefits and drawbacks
Pharmacokinetic	Mac Gabhann et al. 2007	RPE presented by one diffusion coefficient	Simple, but no relationship between molecular properties and permeability
	Amrite et al. 2008	Sclera, choroid and RPE form a single compartment, rate constants for inwards and outwards movement	Simple, but no relationship between molecular properties and permeability
	Ranta et al. 2010	RPE presented by three diffusion coefficient for three types of molecules	Simple and some relationship between the molecular properties and permeability, but cannot be used for a specific molecule
FEM	Balachandran & Barocas 2008	Transport of fluorescein into the eye, including active transport and a realistic geometry	More complex and includes the geometry, but constructed only for one molecule
Model based on physicochemical properties	Edwards & Prausnitz 1998; 2001: cornea	Based on the properties of the cornea and diffusing molecule	Can relate the permeability to molecular properties, but quite complex

endo- and epithelium were modeled with three pathways. The paracellular pathway was modeled with the slit model and the transcellular pathway was divided into two sub-pathways: diffusion through the cytoplasm and diffusion within the cell membrane around the cytoplasm. (Edwards & Prausnitz 1998; 2001). The current models including the BRB, their benefits and drawbacks are presented in Table 2.2.

3 MODELS OF THE BLOOD-RETINAL BARRIER AND HALF-PERFUSION CHAMBER

This thesis consists of two models. At first, a passive diffusional model across the BRB, based on the physicochemical properties of both the BRB and diffusing molecule, was constructed. The second model was a FEM model of a general concept of a chamber having a stationary fluid on one side of the BRB membrane and perfusion on the other side. Both models are mathematical models, can be classified as predictive and are based on the knowledge of the systems.

3.1 Model of the outer blood-retinal barrier (BRB model)

This model is a steady-state model of passive diffusion across the BRB. The mathematical framework and physical theories used in this model are largely based on the works of Edwards & Prausnitz (1998; 2001), who constructed a model by combining physical theories derived by others to predict the permeability of cornea to drug molecules. The present model of BRB is modified in aspects related to the different structural and compositional features between the BRB and the cornea. Also, the behavior of the equations used by Edwards & Prausnitz is assessed in this application and compared with alternative equations to find the most suitable ones for this model. A new feature proposed in this BRB model is a structurally more detailed model of the TJs.

The present model is based on the BRB in the human macular region. Only the passive diffusion pathways are included and the facilitated diffusion through the RPE cell membrane channels is ignored. The major parts of the model are presented in Figure 3.1. The RPE consists of paracellular and transcellular pathways connected in parallel. Further, the paracellular pathway includes the lateral space and TJs connected in series. The transcellular pathway consists of the two cell membranes and the cytoplasm, including the melanin binding, connected in series. BrM includes the ICL and OCL connected in series and CE only includes the fenestrations. The permeabilities of the RPE, BrM, CE and whole BRB can be calculated as

$$P_{RPE} = P_{para} + P_{trans} = \left(\frac{1}{P_{LS}} + \frac{1}{P_{TJ}} \right)^{-1} + \left(\frac{2}{P_{mem}} + \frac{1}{P_{cyt}} \right)^{-1}, \quad (3.1)$$

$$P_{BrM} = \left(\frac{1}{P_{ICL}} + \frac{1}{P_{OCL}} \right)^{-1}, \quad (3.2)$$

$$P_{CE} = P_{fen} \quad (3.3)$$

and

$$P_{BRB} = \left(\frac{1}{P_{RPE}} + \frac{1}{P_{BrM}} + \frac{1}{P_{CE}} \right)^{-1}. \quad (3.4)$$

In this chapter, the parts of the model are described. The way the geometry of the biological structure is modeled is explained at the beginning of each part. Also, the major simplifications and reasoning behind them are given. Next, the way that Edwards & Prausnitz modeled the corresponding part of the cornea and the equations they used are introduced. The way the present model calculates the diffusion in the geometry in question is then described.

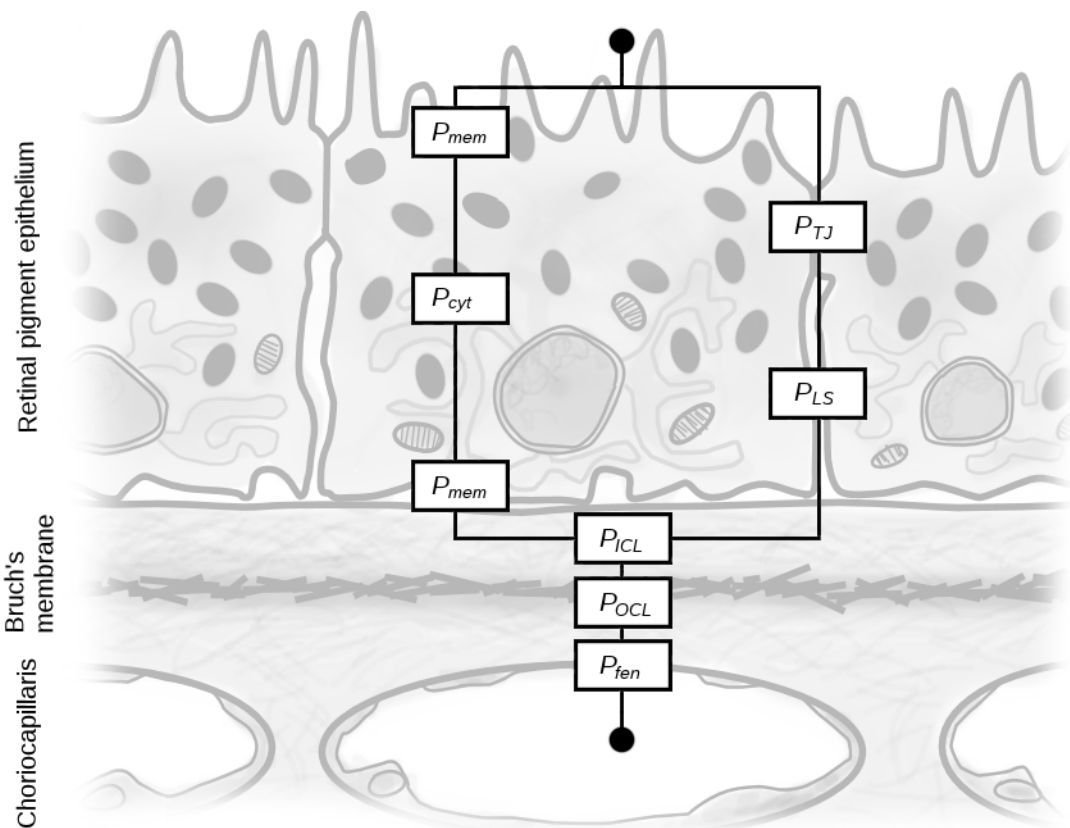


Figure 3.1. The main permeability components of BRB. The molecules first permeate through the choriocapillaris endothelial fenestrations (P_{fen}), and then through OCL (P_{OCL}) and ICL (P_{ICL}) of BrM. RPE is divided into two pathways: paracellular and transcellular. In the paracellular pathway the solute molecules permeate through the lateral space (P_{LS}) and TJs (P_{TJ}), and in the transcellular pathway through the cell membrane (P_{mem}), cytoplasm including the effect of melanin (P_{cyt}) and cell membrane (P_{mem}). To calculate the total BRB permeability, Equations (2.10) and (2.11) are used to combine different permeabilities in parallel or in series.

3.1.1 Retinal pigment epithelium

RPE is modeled by connecting the paracellular and transcellular diffusion pathways in parallel. The geometrical idea of the model is presented in Figure 3.2. The cells are organized into a hexagonal array leaving a small gap between them as shown in Figure 3.2A. The main assumption of this model is that the solute molecules can only diffuse along one pathway. Thus, molecules cannot diffuse into lateral space and change the pathway by transversing the lateral cell membrane. The microvilli and basal infoldings are also ignored.

Edwards & Prausnitz modeled two cell layers: corneal epithelium and endothelium. Their paracellular pathway consisted of a lateral space connected in series with a narrower part, representing the TJs. For the transcellular pathway, they included two permeation pathways. In the first one the molecules permeate through the basal cell membrane, cytoplasm and apical cell membrane. In the second one the molecules partition into the cell membrane's hydrocarbon core and diffuse around the cytoplasm within the membrane and partition out of the membrane in the apical side. Edwards & Prausnitz used the slit model for the lateral space (Equations (2.12) and (2.13)) with different and less accurate equation for the hindrance factor $H_s(\lambda_s)$. Other equations used by Edwards & Prausnitz or based on equations used by them are Equations (3.5), (3.10), (3.11), and (3.12). (Edwards & Prausnitz 2001.)

Paracellular pathway

The paracellular pathway is modeled with the lateral space and TJs connected in series, and the basic geometry is presented in Figure 3.2B. The lateral space is modeled with the slit model (Equations from (2.12) to (2.14)). The parameters needed for the slit model are the relative surface area of the lateral space, lateral space length and lateral space half-width W_{LS} (m). The effective lateral space length is $\tau_{LS}h_{LS}$, where τ_{LS} is the lateral space tortuosity and h_{LS} is the lateral space length (m). Parameter h_{LS} can be defined as $h_{RPE} - h_{TJ}$, where h_{RPE} is the RPE cell height (m) and h_{TJ} is the TJ region height (m).

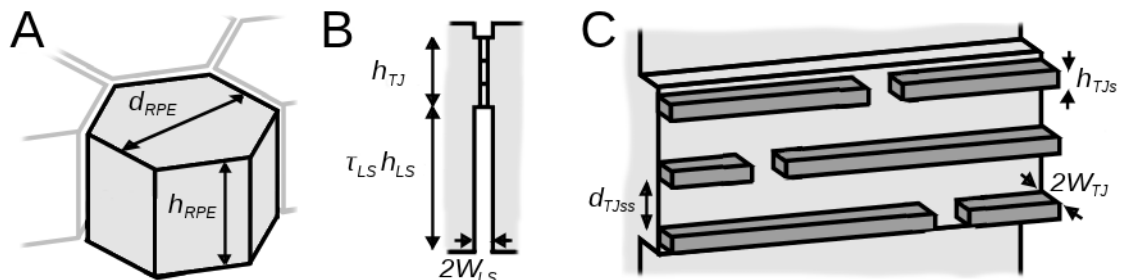


Figure 3.2. The basic geometrical idea of the RPE model. *A:* The hexagonal array of RPE cells (d_{RPE} : RPE cell flat-to-flat diameter; h_{RPE} : RPE cell height). *B:* The lateral space and TJs between the RPE cells (h_{TJ} : TJ region height; τ_{LS} : lateral space tortuosity; h_{LS} : height of the lateral space without the TJ complex; W_{LS} : half-width of the lateral space). *C:* A section of the TJ structure in the model without the other cell membrane. Each strand (darker parts) is represented with an intact part with small pores and an open part reflecting the strand breaks. (d_{TJss} : TJ strand separation; l_{TJs} : TJ strand height; W_{TJ} : TJ region half-width).

The relative surface area of the lateral space, ϵ_{LS} , for Equation (2.12) can be determined by multiplying the width of the slit with the length of the cell boundaries per unit area (Edwards & Prausnitz 1998). For hexagonal cells this can be written as

$$\epsilon_{LS} = 2 W_{LS} l_{cb} = 2 W_{LS} \left[\left(\frac{1}{\sqrt{3} d_{RPE}^2 / 2} \right) \left(\frac{12 \sqrt{3} d_{RPE}}{3} \right) \frac{1}{2} \right], \quad (3.5)$$

where l_{cb} is the cell boundary length per unit area (m m^{-2}) and d_{RPE} is the hexagonal cell flat-to-flat diameter (m). The part in the brackets is simply the cell density multiplied by the circumference of one cell and divided by two to encounter the fact that all boundaries between two cells are calculated twice.

The basic TJ geometry used is shown in Figure 3.2C. The TJ model proposed here is novel, and it applies the slit pore model already utilized for the lateral space and pore model (Equations from (2.15) to (2.17)). The narrow part in the lateral space represents the TJ region, where the TJ complex resides. Each strand is modeled with an intact part and open part, which represent the dynamic breaks. The slit model is used to model the diffusion in the open parts and in the parts between two strands. The parameters needed for the slit model are the TJ region half-width W_{TJ} (m), TJ strand height h_{TJs} (m) for the open parts and TJ strand separation d_{TJss} (m) as well as the relative surface areas of the open parts ϵ_{TJo} and space between the strands ϵ_{TJss} . Parameter ϵ_{TJo} is calculated as

$$\epsilon_{TJo} = 2 W_{TJ} l_{cb} \epsilon_{open}, \quad (3.6)$$

where l_{cb} is calculated as in Equation (3.5) and ϵ_{open} is a parameter describing the open part size. Although the web-like structure of the strands is omitted in the geometry, its influence is incorporated into parameter ϵ_{open} , as the structure greatly hinders the diffusion rate. Parameter ϵ_{TJss} is calculated as in Equation (3.5) with W_{TJ} .

The intact part has periodically-located small structural pores through it, which are modeled using the pore model. Parameters needed for the pore model are the TJ pore radius r_{TJp} (m), relative surface area of the TJ pores ϵ_{TJp} , and h_{TJs} . Parameter ϵ_{TJp} can be calculated as a multiplication of the area of one pore and the number of pores per unit area

$$\epsilon_{TJp} = \pi r_{TJp}^2 \frac{l_{cb} (1 - \epsilon_{open})}{d_{TJp}}, \quad (3.7)$$

where d_{TJp} is the pore separation (m).

The permeability of each strand can be calculated by connecting the intact and open parts in parallel

$$P_{TJs} = P_{TJp} + P_{TJo}, \quad (3.8)$$

where P_{TJp} is the TJ pore permeability (m s^{-1}) and P_{TJo} is the open part permeability (m s^{-1}). The permeability coefficient of the space between two strands, P_{TJss} (m s^{-1}), is also calculated with the slit model, with the relative surface area of the narrowed TJ re-

gion ϵ_{TJss} calculated as in Equation (3.5). Now the total TJ permeability coefficient is calculated as

$$P_{TJ} = \left(\frac{n_{TJs}}{P_{TJs}} + \frac{(n_{TJs} - 1)}{P_{TJss}} \right)^{-1}, \quad (3.9)$$

where n_{TJs} is the strand number and P_{TJss} (m s^{-1}) is the permeability of the space between two strands. The paracellular permeability coefficient is calculated as shown in Equation (3.1).

Transcellular pathway

The transcellular pathway is modeled with two cell membranes and cytoplasm connected in series. The plasma membrane permeability was modeled by Edwards & Prausnitz (2001) by utilizing the experimental result of red blood cell membrane permeability, measured by Lieb & Stein (1986). Lieb & Stein defined the permeation across plasma membrane as

$$P_{mem} = P_{mem}^0 10^{-m_v V}, \quad (3.10)$$

where P_{mem} has units of cm s^{-1} , P_{mem}^0 is the membrane permeability of a theoretical, infinitely small molecule (cm s^{-1}), m_v is the membrane volume selectivity (mol cm^{-3}) and V is the van der Waals volume of the diffusing molecule ($\text{cm}^3 \text{mol}^{-1}$). The value of m_v for red blood cell was found to be $0.0516 \text{ mol cm}^{-3}$. (Lieb & Stein 1986.) Edwards & Prausnitz used the test molecule data given in Lieb & Stein (1986) to fit the value of P_{mem}^0 as

$$\log(P_{mem}^0) = A \log(K_D) + B, \quad (3.11)$$

where K_D is the octanol/water distribution coefficient, and A and B are constants with the values 1.323 and -0.834 , respectively.

Two effects are taken into account in the diffusion across the cytoplasm: the intracellular structures, like mitochondria and endoplasmic reticulum which hinder the diffusion, and drug-binding melanin. Kao et al. (1993) determined the diffusion coefficient in the cytoplasm to be about 25 % of the free diffusion coefficient. So, the cytoplasmic diffusion coefficient is given by Equation

$$D_{cyt} = 0.25 D_0. \quad (3.12)$$

Binding to melanin can be very simply added to the model by a method recommended by Cheruvu & Kompella (2006) for modeling the effects of binding to matrix as

Table 3.1. A summary of the equations used in the RPE model.

Description	Equation
Paracellular pathway permeability	$P_{para} = \left(\frac{1}{P_{LS}} + \frac{1}{P_{TJ}} \right)^{-1} \quad (3.1)$
Lateral space	$P_{para} = \frac{\epsilon_{LS} D_0 H_{sp}(\lambda_{LS})}{\tau_{LS} l_{LS}} \quad (2.12)$
Tight junctions	$P_{TJ} = \left(\frac{n_{TJs}}{P_{TJs}} + \frac{(n_{TJs} - 1)}{P_{TJss}} \right)^{-1} \quad (3.9)$
Transcellular pathway permeability	$P_{trans} = \left(\frac{2}{P_{mem}} + \frac{1}{P_{cyl,eff}} \right)^{-1} \quad (3.1)$
Cell membrane	$P_{mem} = P_{mem}^0 10^{-m, V} \quad (3.10)$
Cytoplasm and melanin binding	$P_{cyl} = \frac{D_{cyl,eff}}{h_{RPE}}, \quad D_{cyl,eff} = \frac{D_{cyl}}{1 + K_a} \quad (2.7), (3.13)$
Total RPE permeability	$P_{RPE} = P_{para} + P_{trans} \quad (3.1)$

$$D_{cyl,eff} = \frac{D_{cyl}}{1 + K_a}, \quad (3.13)$$

where $D_{cyl,eff}$ is the effective cytoplasmic diffusion coefficient and K_a is the association constant of the melanin binding reaction (μM^{-1}). The cytoplasm permeability coefficient P_{cyl} is calculated with Equation (2.7) with h_{RPE} . The paracellular, transcellular and total RPE permeability coefficients are calculated as shown in Equation (3.1). The main equations of the RPE model are summarized in Table 3.1.

3.1.2 Bruch's membrane

BrM model includes only the ICL and OCL. Both are modeled as a homogeneous type I collagen layer with proteoglycan ground substance. All the other layers are neglected. This approximation is applicable as the collagenous layers form the bulk of BrM, and the ICL forms the site of the highest fluid resistance within BrM. Also, there is not much data about the structure or properties of the basal laminae or EL. The model is done in two scales: a smaller scale is used to describe the charged proteoglycan matrix and a larger one to describe the collagen fibril matrix. The difference between ICL and OCL is the tightness of the fiber matrices and layer thickness. The basic idea of the model is schematically presented in Figure 3.3.

Corneal stroma corresponds to BrM in the model by Edwards & Prausnitz. The corneal stroma has one additional structural level: collagen lamellae, which are layers of collagen fibrils oriented in the same direction, and usually perpendicular to the neighboring layers. The theory used for both proteoglycan and collagen fibrils in the present

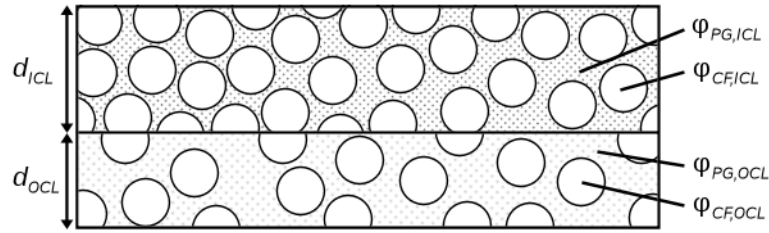


Figure 3.3. The basic idea and the material parameters concerning each layer in the BrM model. The white circles represent the collagen fibrils and the texture between them the proteoglycan ground substance (d_{ICL} : thickness of the ICL; d_{OCL} : thickness of the OCL; $\phi_{PG,ICL}$: volume fraction of the proteoglycans in the ICL, excluding collagen fibrils; $\phi_{CF,ICL}$: volume fraction of the collagen fibrils in the ICL; $\phi_{PG,OCL}$: volume fraction of the proteoglycans in the OCL, excluding collagen fibrils; $\phi_{CF,OCL}$: volume fraction of the collagen fibrils in the OCL).

model is based on the proteoglycan scale of the model by Edwards & Prausnitz, as fibers in both scales are assumed to be randomly oriented. The equations used by Edwards & Prausnitz are Equations (2.18), (2.19), (2.23) and (2.24), and in addition they used the electrostatic theory by Johnson & Deen (1996) (Equations from (2.27) to (2.36)). (Edwards & Prausnitz 1998.)

In both scales the fibers, proteoglycan and collagen, are approximated with cylinders, ignoring the finer surface characteristics. In addition, both fiber matrices are approximated with randomly oriented fibers, which is accurate for the proteoglycan matrix but less accurate for the collagen matrix. In a real BrM, the collagen fibrils are mostly aligned randomly within the plane, but the matrix includes some more aligned fibril bundles, which can be thought to create a more ordered micro-environment. Stylianopoulos et al. (2010b) studied the effect of network orientation to diffusion with stochastic model and found very little practical difference between different magnitudes of fiber alignment.

Both scales are modeled using the fiber matrix model (Equations from (2.18) to (2.36)). The parameters needed for the model are proteoglycan radius r_{PG} and collagen fibril radius r_{CF} as well as the proteoglycan volume fraction $\phi_{PG,i}$ and collagen fibril volume fraction $\phi_{CF,i}$, for both the ICL and OCL, denoted by the subscript i . Also, as proteoglycan scale includes the electrostatic interactions, the proteoglycan surface charge density $q_{A,PG}$ is needed. The two scale model enables the calculation of the separate effects of the proteoglycan and collagen matrices. First, the effective diffusion coefficient within the proteoglycan ground substance $D_{PG,i,eff}$ is calculated as in Equation (2.8) by determining the effects of hydrodynamic, steric and electrostatic interactions on the molecule's free diffusion coefficient and partitioning between the barrier and the free solution. While this is done, the presence of the collagen fibril is neglected.

Then, the same process is done with the collagen matrix, but replacing D_0 with $D_{PG,i,eff}$, and calculating the effective diffusion coefficient collagen matrix $D_{CF,i,eff}$. The electrostatic interactions between the diffusing molecule and collagen fibrils are ignored, because the electrostatic interactions are more significant with small fibers

Table 3.2. A summary of the equations used in the BrM model. The subscript i denotes either ICL or OCL and the subscript m used in the fiber matrix model is replaced by the respective matrix.

Description	Equation
Effective diffusion coefficient in PG scale	$D_{PG,i,eff} = \Phi_{PG,i,e} D_{PG,i}, i = ICL \text{ or } OCL$ (2.8)
Diffusion coefficient	$D_{PG,i} = D_0 H_{PG,i} S_{PG,i}$ (2.19)
Partition coefficient	$\Phi_{PG,i,e} = \int_0^{\infty} g(h) \exp[-E(h)] dh$ (2.27)
Effective diffusion coefficient in CF scale	$D_{CF,i,eff} = \Phi_{CF,i} D_{CF,i}$ (2.8)
Diffusion coefficient	$D_{CF,i} = D_{PG,i,eff} H_{CF,i} S_{CF,i}$ (2.19)
Partition coefficient	$\Phi_{CF,i} = \exp \left[-\Phi_{CF,i} \left(1 + \frac{r_s}{r_{CF}} \right)^2 \right]$ (2.18)
Total BrM permeability	$P_{BrM} = \left(\frac{d_{ICL}}{D_{CF,ICL,eff}} + \frac{d_{OCL}}{D_{CF,OCL,eff}} \right)^{-1}$

(Stylianopoulos 2010a). The values of $D_{CF,i,eff}$ are calculated both in the ICL and OCL, and the separate values are shown with respective subscripts.

The permeability coefficients of both the ICL and OCL are then calculated using Equation (2.37), with the ICL and OCL thicknesses d_{ICL} and d_{OCL} , respectively, and the total BrM permeability using Equation (3.2). The equations used for BrM model are summarized in Table 3.2. The subscript m used in the fiber matrix model is replaced by the respective matrix.

3.1.3 Choriocapillaris endothelium

The fenestrations of the CE are the major diffusion pathways for small molecules through the endothelium. The fenestrations, paracellular and transcellular pathways are connected in parallel. Therefore, the one with the highest permeability dominates. Also, the permeability of openings of this kind is many orders of magnitude higher than the permeability of RPE. Due to these reasons the CE model is simplified by ignoring the paracellular and transcellular pathways. The present endothelium model is not based on the model by Edwards & Prausnitz, as corneal endothelium lacks fenestrations.

The fenestrations are modeled with the diaphragms, which span over the fenestration leaving triangular holes between fibers. The triangular holes are modeled with circular holes which fit inside the sectors seen in Figure 2.4. Because of the circular pores, the fenestrations can be modeled using the pore model. The parameters needed for the model are diaphragm pore radius r_{dia} (m), fenestration height h_{fen} (m) and relative surface area of the diaphragm pores ϵ_{dia} . The CE permeability coefficient is equal to fenestration permeability, as it is the only diffusion pathway, and it is calculated as shown in Equation (3.3).

3.1.4 Properties of the solute molecules

The diffusing solute molecules are approximated as spherical particles. Basically four things are needed to predict the BRB permeability of a molecule: its size, free diffusion coefficient, charge and lipophilicity.

Molecule's size and diffusion coefficient are linked together, as presented by Equations (2.3) and (2.4). The problem with these equations is that very rarely the radius or the diffusion coefficient of drug molecules are known. Fortunately, the diffusion coefficient can be measured, so an empirical relationship between the molecular mass and diffusion coefficient can be derived, as done by Avdeef (2010) at 37 °C as

$$D_0 = 9.9 \times 10^{-5} M_s^{-0.453}, \quad (3.14)$$

where M_s is the molecular mass of the molecule (Da) and D_0 has a unit of $\text{cm}^2 \text{s}^{-1}$. Equation (3.14) was fitted using 147 molecules with molecular mass between 30–1,200 Da and with $R^2 = 0.94$ (Avdeef 2010). Due to the size limitations of Equation (2.3), Equation (2.4) is used to calculate the radius of the molecules. The solute molecule charge q_s was determined using Marvin Calculator Plugins (MarvinSketch 5.10.1, 2012, ChemAxon, <http://www.chemaxon.com>) by choosing the most common species at pH 7.4.

The lipophilicity values are calculated using Marvin Calculator Plugins. Both, the partition coefficient ($\log K_p$) and distribution coefficient in pH 7.4 ($\log K_D$), are calculated.

To model the binding to melanin, the binding association constants (K_a) are needed. Kadam & Kompella (2010) measured the affinities of eight β -blockers to natural melanin, but found only correlation of $R^2 = 0.10$ with lipophilicity. The present model of the melanin binding is very simplified, and it is important to get the right magnitude for the association constants. Due to this reason, the values by Kadam & Kompella (2010) are used to fit the association constants with lipophilicity, as their range of eight molecules is quite large in comparison with other studies. When the fitting is done with the $\log K_D$ values calculated using the Marvin Calculator Plugins, the resulting linear fit with $R^2 = 0.25$ is

$$K_a = 0.052 \log K_D + 0.2268, \quad (3.15)$$

where K_a has a unit of μM^{-1} .

3.1.5 Parameters

This chapter presents the parameter values used in the BRB model. Parameters found in literature or measured from images in literature are not discussed in detail, but are presented in Table 3.3 with the rest of the parameters. Parameters whose values are approximated or calculated are presented in more detail in the text.

Parameters for RPE

The parameters needed for the RPE are the RPE cell and lateral space dimensions as well as the parameters defining TJs. As the TJ strands are formed by 10-nm particles (Anderson & Van Itallie 2009), the strand height is taken as $l_{TJs} = 10$ nm. Since it is difficult to measure the frequency or size of the strand breaks or the effect of the network-like structure, an approximated value of $\epsilon_{open} = 0.001$ is used. This value is based on the comparison between the measured and calculated permeabilities of hydrophilic molecules. The TJ region half-width is approximated to be $W_{TJ} = 5$ nm, based on the 10-nm particle structure. The strand number is taken as $n_{TJs} = 5$ (Rahner et al. 2004). The TJ region height was measured by Rahner et al. (2004) to be $h_{TJ} = 0.30$ μm . The TJ strand separation is calculated by subtracting the TJ strands from h_{TJ} and dividing it to equally sized parts, thus resulting in $d_{TJss} = 65$ nm.

The TJ pore radius measured by Van Itallie et al. (2008) was determined by calculating the hydrodynamic radius of the PEG oligomer that barely made it through the small pores. The molecular mass of the oligomer with the radius of 0.4 nm is 323.80 Da (Van Itallie et al. 2008). The radius of that oligomer and that of the TJ pores – comparable to the molecules in this model – can be determined by using Equations (2.4) and (3.14) to be $r_{Tjp} = 0.68$ nm. The pore separation is approximated to be $d_{Tjp} = 10$ nm, based on the 10-nm particle size (Anderson & Van Itallie 2009).

Parameter for BrM

The parameters needed for the modeling of the BrM are the ICL and OCL thicknesses, the radii and fiber volume fractions of the proteoglycan and collagen fibrils in both the ICL and OCL as well as the proteoglycan surface charge density. The ICL and OCL thicknesses are taken as $d_{ICL} = 2$ μm and $d_{OCL} = 1.5$, calculated by roughly dividing the EL thickness equally and adding it to the real ICL and OCL thicknesses. This way, the total BrM thickness is taken into account, while still excluding EL. The proteoglycans are approximated only by the GAGs, neglecting the core proteins. Thus the proteoglycan radius is equal to the GAG radius.

There are no data about the fiber volume fraction in the literature, so they have to be approximated. The collagen volume fraction in the corneal stroma can be calculated from the hexagonal arrangement of the fibrils to be around 0.25, based on values given by Edwards & Prausnitz (1998). Based on the differences in images from the corneal stroma and BrM (Goldbaum & Madden 1982; Hirsch et al. 2001) and the fact that corneal stroma is transparent and much thicker than BrM, the values for the BrM are estimated higher. For collagen in the ICL and OCL, the values of $\phi_{CF,ICL} = 0.6$ and $\phi_{CF,OCL} = 0.3$ are approximated. As for the proteoglycan volume fractions, the approximated values are $\phi_{PG,ICL} = 0.25$ and $\phi_{PG,OCL} = 0.08$. It is important to note that $\phi_{PG,ICL}$ and $\phi_{PG,OCL}$ are the volume fractions when collagen fibrils are ignored, as they only describe the proteoglycan ground substance. These values correspond to volume fractions of 0.10 and 0.05 when including collagen fibrils, respectively.

Parameters for CE

Only a few parameters are needed for the CE: the fenestration height, diaphragm pore size and relative surface area of the diaphragm pores. The fenestrations are usually divided into eight segments by the diaphragm as shown in Figure 2.4. The diaphragm pore radius is calculated by using the sector angle of 45 degrees and sector radius of 12 nm (Melamed et al. 1980). The resulting diaphragm pore radius is $r_{dia} = 3.3$ nm.

The relative surface area of the diaphragm pores is determined as a product of the relative surface area of the fenestrated region in the endothelium, the fenestrations in a fenestrated region and the diaphragm pores in a fenestration. According to the investigation of Federman (1982) the choriocapillaris side facing the BrM has relative fenestrated area of 0.6 around the macular region. The surface area of the fenestrations inside the regions is calculated from rabbit endothelial cell membrane freeze-fractured figures (Melamed et al. 1980), and the resulting value is 0.25. The relative area of the diaphragm pores in a fenestration is calculated by assuming the fenestration radius of 40 nm, giving a resulting value of 0.05. The relative surface area of the diaphragm pores in the CE is $\epsilon_{dia} = 0.0075$. All the parameters of the BRB model are given in Table 3.3.

3.1.6 Calculations

The calculations to study the functionality of the BRB model are separated into four parts: 1) a comparison between the different methods of determining the solute radius, 2) a parameter behavior analysis to study the effects of molecular properties, 3) a comparison between the actual measured and predicted values to validate the model and 4) a sensitivity analysis of certain model parameters to study their importance in the model. All the calculations in the BRB model are done with Mathworks MATLAB software.

Melanin binding causes one problem to the model: the steady-state nature of the model cannot take into account the accumulation of the drug molecules to melanin. To model the accumulation, time and drug concentration would have to be included. Because of this, the BRB permeability is modeled with two modes: with and without melanin binding. The one with the binding represents the initial phase of the permeation when there is no drug bound to the melanin. The latter mode represents the later phase of the permeation, when the melanin is full of drug and can no longer bind any. These two values set the limits for the real permeability coefficient. This two-mode method is included in the parameter behavior analysis and validation.

Comparison between the molecular radii

The comparison between the solute radii is done by calculating the radii of ten molecules used in this model with different methods. The molecules are chosen based on their molecular masses. Equations (2.3) and (2.4) are used with the diffusion coefficient calculated by Equation (3.14). The radii are compared to approximate the physical dimensions of the molecules, calculated with Marvin Calculator Plugins. The physical

Table 3.3. *The parameter values in the BRB model.*

Description	Parameter	Value	Reference
Parameters of RPE			
RPE cell flat-to-flat distance	d_{RPE}	12 μm	Garron 1963, Boulton & Dayhaw-Barker 2001
RPE cell height	h_{RPE}	12 μm	Boulton & Dayhaw-Barker 2001
Lateral space half-width	W_{LS}	15 nm	Ban & Rizzolo 2000
Lateral space tortuosity	τ_{LS}	1.1	Garron 1963
TJ strand height	h_{TJs}	10 nm	Anderson & Van Itallie (2009)
Open part size	ϵ_{open}	0.001	See text
TJ region half-width	W_{TJ}	5 nm	See text
Strand separation	d_{TJss}	65 nm	See text
TJ strand number	n_{TJs}	5	Rahner et al. (2004)
TJ pore radius	r_{TJp}	0.68 nm	See text
TJ pores separation	d_{TJp}	10 nm	Anderson & Van Itallie (2009)
Parameters of BrM			
ICL thickness	d_{ICL}	2 μm	See text
OCL thickness	d_{OCL}	1.5 μm	See text
Proteoglycan radius	r_{PG}	0.5 nm	Ogston et al. 1973
Proteoglycan surface charge density	q_{PG}	-0.10 C m ⁻²	Mattern et al. 2008
Collagen fiber radius	r_{CF}	30 nm	Booij et al. 2010
Proteoglycan volume fraction in ICL	$\phi_{PG,ICL}$	0.25	See text
Proteoglycan volume fraction in OCL	$\phi_{PG,OCL}$	0.08	See text
Collagen fibril volume fraction in ICL	$\phi_{CF,ICL}$	0.60	See text
Collagen fibril volume fraction in OCL	$\phi_{CF,OCL}$	0.30	See text
Parameters of CE			
Fenestration height	h_{fen}	50 nm	Hogan & Alvarado 1967
Diaphragm pore radius	r_{dia}	3.3 nm	See text
Relative surface area of the diaphragm pores	ϵ_{dia}	0.0075	See text

size is approximated as an average of the radii of the maximum and minimum projection area of the molecule.

In addition, the radii tabulated by Prausnitz & Noonan (1998) are also presented for the molecules. They calculated the radii by determining the van der Waals volume of the molecules and approximating them as spheres.

Parameter behavior analysis

The behavior of the BRB model is studied by varying lipophilicity, molecular radius and charge. First, the behavior of paracellular and transcellular pathways in the RPE is studied alone. The value ranges used with the RPE for lipophilicity and radius are $\log K_D = -1 \dots 4$ and $r_s = 0.5 \dots 0.8$ nm, respectively. Other values are kept constant in each case, and values $r_s = 0.64$ nm and $\log K_D = 1.5$.

BrM is studied by varying radius and charge with values $r_s = 0.5 \dots 0.8$ nm and $q_s = -1, 0$ and 1 , respectively. CE is studied with the same radius range as the RPE and BrM.

Finally, the behavior of the whole BRB is studied together by changing lipophilicity and radius with the same value ranges.

Validation with the measured values

The model validation is done by using measured permeability coefficients from several studies for comparison with the calculated results. The solutes used for this model are for many species and BRB parts. These include Bovine choroid and BRB (Ch-BRB) (Steuer et al. 2004; Pitkänen et al. 2004; Kadam et al. 2011), bovine choroid and BrM (Ch-BrM) (Cheruvu & Kompella 2006), porcine Ch-BRB (Kadam et al. 2011), porcine Ch-BrM (Pescina et al. 2012), human Ch-BRB (Kadam et al. 2011), human BRB (Sanders et al. 2011), human RPE (Rajasekaran et al. 2003) and human Ch-BrM (Hussain et al. 2002).

The solutes used in the validation and their properties as well as measured permeability coefficients are presented in Appendix 1 Tables A1.1 and A1.1, respectively. If the permeability is measured in both apical-to-basal and basal-to-apical directions, the smaller is used, as the other might include some forms of active transport. In addition, in Pescina et al. (2012) the permeabilities were measured with multiple concentrations, producing different values. In this case, the largest values are used, as melanin binding has greater effect on smaller concentrations.

Sensitivity analysis

The sensitivity analysis is done by increasing and decreasing the values of specific model parameters and finding how much the change affects the permeability. The parameters are chosen based on their uncertainty. The parameters chosen for the RPE are the lateral space half-width (W_{LS}), open part size (ϵ_{open}), TJ region half-width (W_{TJ}), TJ pore radius (r_{Tjp}) and TJ pore separation (d_{Tjp}). The main focus in RPE is the paracellular pathway and the novelty of the TJ model. The parameters of transcellular pathway were already studied by Edwards & Prausnitz (2001). For BrM, the parameters are the proteoglycan surface charge density (q_{PG}) and proteoglycan and collagen fibril volume fractions in both ICL and OCL ($\phi_{PG,ICL}$, $\phi_{CF,ICL}$, $\phi_{PG,OCL}$ and $\phi_{CF,OCL}$). Due to the simplicity of the CE model, it is left out of the sensitivity analysis.

Each parameter value is increased and decreased by 25 %. The simulations are done with generic molecules. As there are no lipophilicity-dependent parts discussed here, only the molecular radius and charge vary between molecules. For the RPE, two molecules with the radii of $r_s = 5$ and 7 \AA are used. For BrM, four molecules of two sizes and charges are used. The radii are $r_s = 5$ and 7 \AA and charges $q_s = -1$ and 1 . The lipophilicity is kept constant at $\log K_D = 1.5$. The change in permeability is considered significant when it is larger than 20 %.

3.2 Model of the half-perfusion chamber (chamber model)

This model is a FEM model of half-perfusion chamber concept with a stationary fluid on one side of the BRB membrane and perfusion on the other side. The model is used to study the effect of certain dimensions and other system parameters on the functionality of the system. As a general concept, the geometry of the system is presented in Figure 3.4A. The upper part of the system is the donor chamber where the test molecules are placed. The bottom part is the perfusion channel. One end of the channel is inlet and the other is outlet, which leads to the acceptor chamber, where the samples are taken from. To function properly, the system should affect the BRB permeability measurement as little as possible and the concentration in the acceptor chamber should be measurable.

The model was done using COMSOL Multiphysics software and all the additional calculations were done with Mathworks MATLAB. First, the geometry, physics and boundary conditions of the model are described. Following that, the different simulation series are introduced.

3.2.1 Geometry

The large upper cylindrical part is the donor chamber to where the test molecules are placed. It has a radius of 4 mm and height of 10 mm, so the volume is approximately 500 μl . Below the donor chamber is the vertical channel where the BRB is placed, denoted here as the BRB channel. This channel has a radius of 1 mm. This channel is divided into two parts by the BRB. The length of the upper part between BRB and the

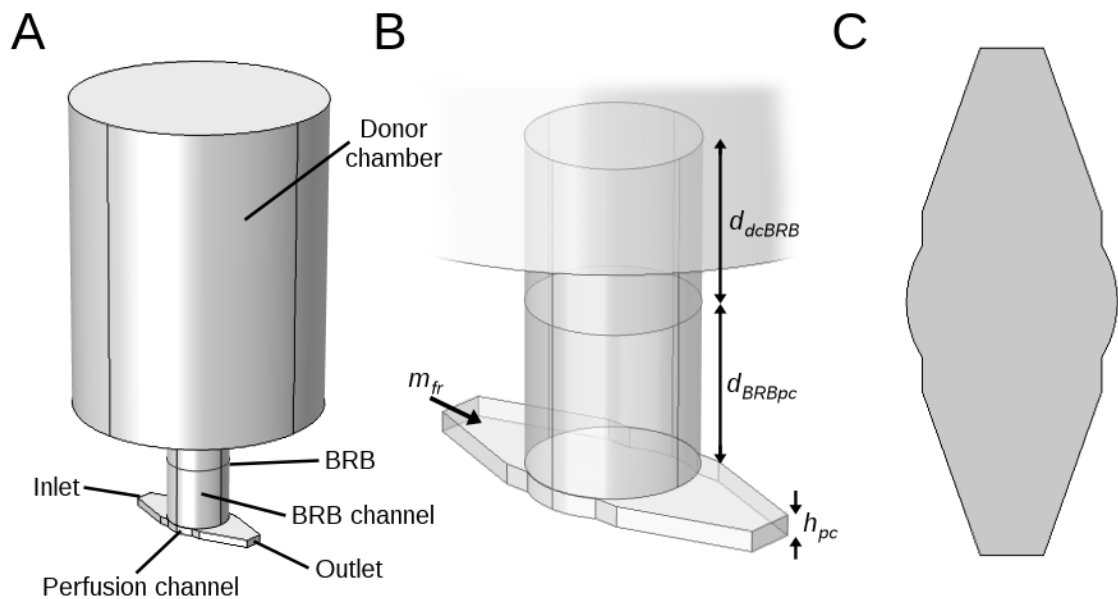


Figure 3.4. The geometry of the chamber model. A: The parts of the chamber. B: A detailed view of the BRB channel and the studied parameters (m_{fr} : flow rate; d_{dcBRB} : chamber-BRB distance; d_{BRBpc} : BRB-channel distance; h_{pc} : channel height). C: The layout of the channel from the top.

donor chamber is d_{dcBRB} (m) and the part between BRB and the perfusion channel is d_{BRBpc} (m). The BRB channel is presented in detail in Figure 3.4B.

Below the BRB channel and perpendicular to it, is the perfusion channel. Its shape is presented in Figure 3.4C. The channel has the height of h_{pc} (m). The circular part in the middle of the perfusion channel has the same radius as the BRB channel. The parts leading away from the middle are the inlet and outlet channels. The width of the channels at the ends is 0.6 mm. The sides of the channel do not continue directly to the sides of the circular BRB channel, because this would create very small elements on the upper surface of the channel near the sides of the BRB channel. This problem is avoided by creating the little cuts shown in Figure 3.4C.

Different parts of the geometry are meshed with different accuracies. Because the used dimensions vary and smaller dimensions need more elements, the accuracy of the mesh is set according to the needs of each part of the model. The mesh of the donor chamber is the least accurate, as it is only used to monitor the changes in drug concentration in it. The rest of the model is meshed more accurately, as there is combined fluid flow and diffusion. The smallest elements are found in the perfusion channel, as it has the smallest dimensions in the system.

3.2.2 Physics and boundary conditions

The model uses two COMSOL physics: Laminar Flow in Computational Fluid Dynamics module for the perfusion and Transport of Diluted Species in Chemical Reaction Engineering module for the diffusion. Each of these physics has its own equations and boundary conditions (BCs). Laminar Flow is modeled as stationary, because only the velocity field of constant flow is needed. Transport of Diluted Species is modeled as time-dependent, as the main interest is the diffusional behavior over time.

The governing differential equations in the Laminar Flow are Navier-Stokes equations and are given as

$$\rho(\mathbf{u} \cdot \nabla) \mathbf{u} = \nabla \cdot \left[-p \mathbf{I} + \eta (\nabla \mathbf{u} + (\nabla \mathbf{u})^T) - \frac{2}{3} \eta (\nabla \cdot \mathbf{u}) \mathbf{I} \right], \quad (3.16)$$

with

$$\nabla \cdot (\rho \mathbf{u}) = 0, \quad (3.17)$$

where ρ is the fluid density (kg m^{-3}), \mathbf{u} is the fluid velocity field (m s^{-1}), p is the pressure (Pa), \mathbf{I} is unit matrix, η is the dynamic viscosity (Pa s), T is temperature (K). BC in the outer boundaries is a no slip wall, except for the inlet and outlet channels. The inlet has a flow inlet BC, with a flow rate of m_{fr} ($\mu\text{l min}^{-1}$). The outlet BC allows free flow out of the system. The only inner BC is the interior wall for the boundary representing BRB, which restricts the fluid movements to the lower part of the system. The material used for the fluid is water.

Transport of Diluted Species is governed by Fick's second law, including convective part:

$$\frac{\partial c}{\partial t} + \mathbf{u} \cdot \nabla c = \nabla \cdot (D \nabla c), \quad (3.18),$$

where \mathbf{u} is the velocity field. All the outer boundaries have no flux BC, except for the outlet channel, for which the BC is outflow allowing the solute movement out of the system. Again, the only inner boundary having BC is the one representing the BRB. The BC for it is a thin diffusion barrier, which needs a permeability coefficient $P_{BRB,c}$. The initial concentrations for the parts below and above the BRB are 0 and c_{dc} ($\mu\text{g ml}^{-1}$), respectively. Concentrations with the unit of $\mu\text{g ml}^{-1}$ have to be converted into mol in the equations used. The free diffusion coefficient was chosen as $D_c = 0.75 \times 10^{-9} \text{ m}^2 \text{ s}^{-1}$, corresponding to the average of the free diffusion coefficient of the drug molecules used in the BRB model. The temperature used in both models is 37 °C.

Four probes are used to measure concentrations and fluxes in the system as functions of time. Two domain probes are used to monitor the concentrations: one in the whole donor chamber and second in the upper part of the BRB channel. Two boundary probes are used to measure the total flux magnitudes across the BRB boundary and outlet boundary.

3.2.3 Simulations and calculations

The functionality of the chamber is studied in two parts. First, the errors caused by certain system parameters to the functionality of the system are studied. Then, the measurability of the concentration in the acceptor chamber is calculated by varying donor chamber concentration as well as channel flow rate, and the results are compared to sensitivity of the analysis techniques.

Parameter-based errors in permeability

In the first part, the effects of the chamber-BRB distance d_{dcBRB} , BRB-channel distance d_{BRBpc} , channel height h_{pc} , flow rate m_{fr} and permeability coefficient $P_{BRB,c}$ to the measurement errors caused by the system are simulated. The simulations series are done by changing one or more parameters while keeping the others constant to show how each affects the system. The BRB permeability values are changed within every simulation series, and three values are used to represent different molecules and membranes. The values used for the permeability coefficient in each simulation series are $P_{BRB,c} = 1 \times 10^{-6}$, 1×10^{-5} and $1 \times 10^{-4} \text{ cm s}^{-1}$. The values of the parameters kept constant are given in Table 3.4.

In the first simulation series, the chamber-BRB distance is simulated with values $d_{dcBRB} = 0.5, 1, 2, 3, 4$ and 5 mm, each with the three different permeability coefficients. In the second simulation, the mutual effect of both the BRB-channel distance and perfusion channel height is studied. The used values are $d_{BRBpc} = 0.5, 1, 2, 3, 4$ and 5 mm, and $h_{pc} = 0.15, 0.25, 0.5, 0.75$ and 1 mm, resulting in 30 simulations per permeability coefficient. To ignore the effects of changes in flow rate due to the channel height changes,

Table 3.4. The values of the parameters kept constants during different FEM simulations.

Description	Parameter	Value
Chamber-BRB distance	d_{dcBRB}	2 mm
BRB-channel distance	d_{BRBpc}	2 mm
Channel height	h_{pc}	0.25 mm
Flow rate	m_{fr}	1 $\mu\text{l min}^{-1}$
Donor chamber concentration	c_{dc}	0.1 $\mu\text{g ml}^{-1}$

the flow velocity, instead of the flow rate, is kept constant between the simulations. In the third simulation series the flow rate is varied using values $m_{fr} = 0.1, 0.5, 1, 5$ and $10 \mu\text{l min}^{-1}$. The simulation time is taken as 6 hours, which shows the diffusional behavior in long experiments and corresponds to the time used by Kadam et al. (2011). The error simulations are summarized in Table 3.5.

Table 3.5. The simulation series of the chamber model. Each simulation is done with the three different permeability coefficient. The total number of simulation is 132.

Simulated parameter(s)	Values	Number of simulations
Parameter-based errors in permeability		
Chamber-BRB distance	$d_{dcBRB} = 0.5, 1, 2, 3, 4, 5 \text{ mm}$	18
BRB-channel distance and channel height	$d_{BRBpc} = 0.5, 1, 2, 3, 4, 5 \text{ mm}$ and $h_{pc} = 0.15, 0.25, 0.5, 0.75, 1 \text{ mm}$	90
Flow rate	$m_{fr} = 0.1, 0.5, 1, 5, 10 \mu\text{l min}^{-1}$	15
Measurability of donor chamber concentration		
Flow rate	$m_{fr} = 0.1, 0.5, 1, 5, 10 \mu\text{l min}^{-1}$	-
Donor chamber concentration	$c_{dc} = 0.01, 0.1, 1 \mu\text{g ml}^{-1}$	9

The results from the boundary probes in COMSOL are fluxes with a unit of $\text{mol m}^{-2} \text{s}^{-1}$. The idea is to determine the permeability coefficient (m s^{-1}) in similar fashion than in the experimental measurements. Basically this means that the fluxes have to be converted to show the cumulative amount of substance that has passed the boundary probe. The cumulative amount of substance as a function of time is calculated by Equation

$$M(t) = A_{probe} \int_t J_{probe}, \quad (3.19)$$

where M is the cumulative amount of substance (mol) and A_{probe} is the area of the respective probe boundary (m^2). The permeability coefficient is then calculated using Equation

$$P = \frac{1}{A_{BRB} \bar{c}} \frac{dM(t)}{dt}, \quad (3.20)$$

where A_{BRB} is the BRB area in both cases and \bar{c} is the mean concentration (Kadam et al.

2011). The derivative is determined as the slope of the linear section of the curve, even though the curves are non-linear in some cases.

For each simulation, two values are produced: the simulated permeability coefficient based on the flux over the BRB ($P_{BRB,c}^*$) and simulated permeability coefficient based on the flux through the outlet, ($P_{out,c}^*$). $P_{BRB,c}^*$ describes the system's ability to achieve the actual permeability of the BRB and $P_{out,c}^*$ the system's ability to measure the actual BRB permeability. When calculating $P_{BRB,c}^*$, the mean concentration is taken from the probe that monitors upper part of the BRB channel to define more accurate value for $P_{BRB,c}^*$. The total donor chamber mean concentration is used for $P_{out,c}^*$, as it is the concentration that is experimentally measurable. $P_{BRB,c}^*$ and $P_{out,c}^*$ could be calculated straight from the fluxes, as with the present method the fluxes are consecutively integrated and derived. However, using Equation (3.20) to determine the permeability coefficients resembles more accurately the method used in the experimental measurements. The results are presented as errors caused by the system to both permeability coefficients. The BRB error percentage is calculated as $(1 - P_{BRB,c}^*/P_{BRB,c}) \times 100\%$ and outlet error percentage as $(1 - P_{out,c}^*/P_{BRB,c}) \times 100\%$.

Measurability of acceptor chamber concentration

The measurability of the concentration in the acceptor chamber is studied by varying flow rate m_{fi} and donor chamber concentration c_{dc} . For c_{dc} , the simulations are done with the values $c_{dc} = 0.01, 0.1$ and $1 \mu\text{ ml}^{-1}$. The values of other system parameters used are those in Table 3.4. The three BRB permeability coefficients are also used with c_{dc} . The acceptor chamber concentration at time t can be calculated by Equation

$$c_{ac}(t) = \frac{M(t)}{m_{fi}t}. \quad (3.21)$$

The concentration at 3 hour time point is calculated and compared with sensitivity of the analysis techniques. Concentration limit for the sensitivity is taken as 0.1 ng ml^{-1} (Jylhä 2013). The concentration after 3 hours represents well the magnitude of the concentration with those parameters. The measurability simulations are summarized in Table 3.5. Total number of all the simulations is 132.

4 RESULTS

The results chapter is divided into two sections. In the first section, the results of the four parts of the BRB model functionality studies are presented, followed by the results of the chamber model simulations in the second section.

4.1 BRB model

The functionality of the BRB model was studied in four parts: 1) a comparison between the solute radius, 2) a parameter behavior analysis, 3) a validation with measured data and 4) a parameter sensitivity analysis.

4.1.1 Comparison between the solute radii

The comparison was done between Stokes-Einstein radius r_{SE} (Equation (2.3)), Sutherland radius r_{Su} (Equation (2.4)), van der Waals radius and average projection radius, corresponding to the real molecular size. The molecules and different solute radii are presented in Figure 4.1. The radii calculated with Equation (2.4) are generally a little higher than the average projection radius, but on average the magnitude is of similar

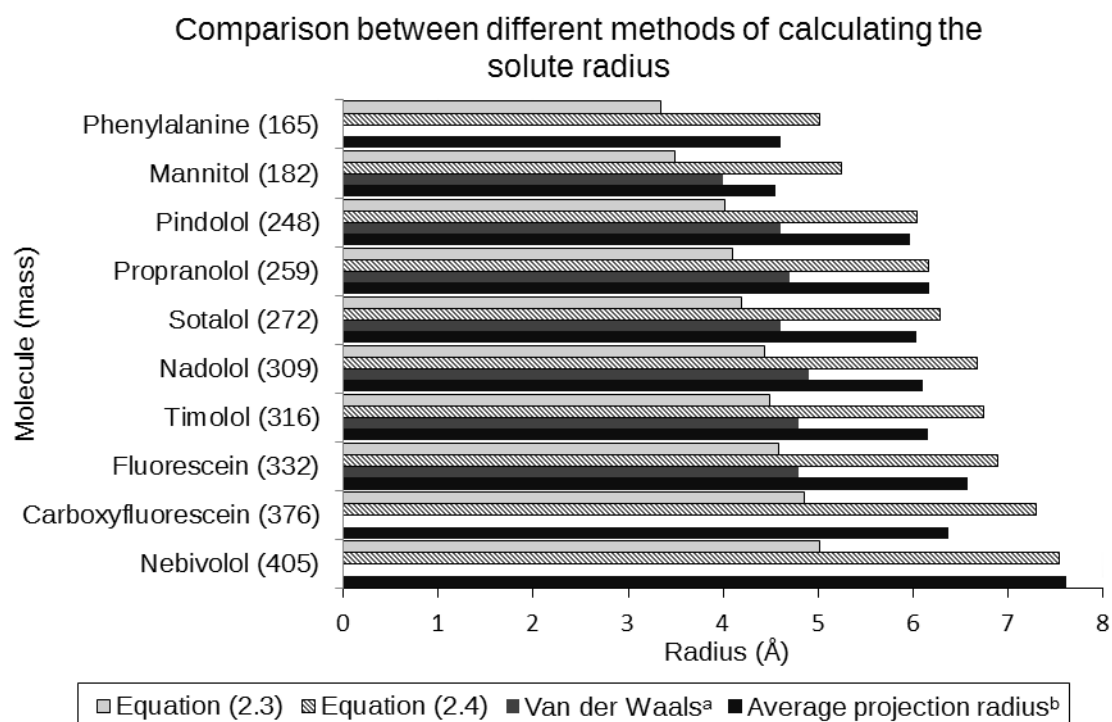


Figure 4.1. Radii of 10 molecules calculated by four different methods: Stokes-Einstein radius (Equation (2.3)); Sutherland radius (Equation (2.4)), Van der Waals radius, a: Prausnitz & Noonan 1998; Average projection radius, b: Marvin Calculator Plugin.

scale. Both Equation (2.3) and van der Waals produce consistently smaller values than the average projection radius.

4.1.2 Parameter behavior analysis

The parameter behavior analysis was done by calculating the effects of solute properties on the RPE, BrM, CE and total BRB permeabilities. In addition, with RPE the paracellular and transcellular permeabilities were also calculated. The studied solute properties were radius, lipophilicity and charge.

RPE, paracellular and transcellular permeabilities

The behavior of the total RPE, transcellular and paracellular permeabilities as functions of lipophilicity and solute radius are presented in Figures 4.2A and 4.2B, respectively. Lipophilicity has no effect in paracellular pathway, which can be clearly seen in Figure 4.2A. Transcellular pathway permeability increases with increasing lipophilicity, but after $\log K_D = 1$ the effect of melanin binding is clearly seen. Without melanin, the permeability increases logarithmically and around $\log K_D = 3$, the transcellular pathway becomes more permeable than the paracellular pathway. The total RPE permeability without melanin is defined by paracellular pathway when $\log K_D < 3$ and by transcellular pathway when $\log K_D > 3$. With melanin, the paracellular pathway totally defines the RPE permeability.

The paracellular pathway depends only on the solute radius, but the dependence is quite weak compared to the transcellular permeability as seen in Figure 4.2B. The paracellular permeability decreases with increasing solute radius. Without melanin, the transcellular permeability becomes more significant than the paracellular permeability when

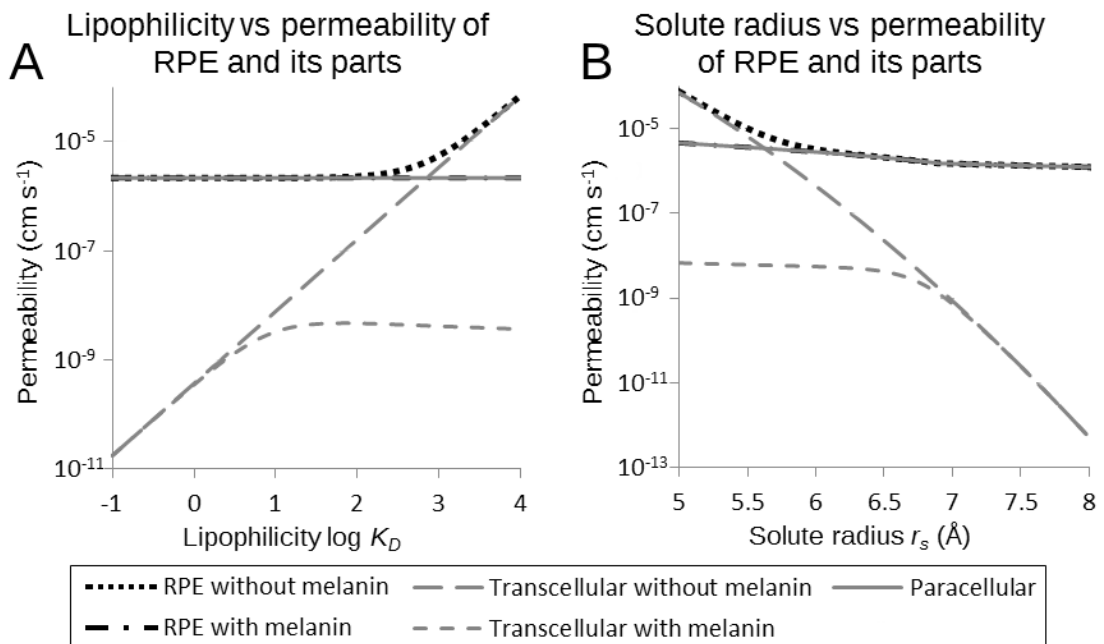


Figure 4.2: The behaviors of the total RPE, transcellular and paracellular permeabilities as functions of solute lipophilicity ($\log K_D$) (A) and radius (r_s) (B) with and without melanin. RPE within melanin can be seen under the paracellular curves.

$r_s > 5.6$ Å. With melanin, the transcellular permeability is always at least three orders of magnitude smaller than the paracellular permeability. With $r_s > 7$, the existence of melanin has no effect on the transcellular permeability. Without melanin, the total RPE permeability is defined by the transcellular pathway with small radii and by the paracellular pathway with $r_s > 5.6$ Å. With melanin, the paracellular pathway again totally defines the RPE permeability.

BrM and CE permeabilities

The behaviors of the BrM and CE permeabilities with increasing solute radius are presented in Figures 4.3A and 4.3B, respectively. The BrM permeability is also calculated with three different solute charges. Generally, the BrM permeability decreases logarithmically with increasing solute radius. Positive charge speeds up and negative charge retards the diffusion rate within the BrM matrix. The differences between charges begin to vanish with high solute radii. The CE permeability also decreases logarithmically as solute radius increases. However, the CE permeability is at minimum around 2 orders of magnitude higher than that of BrM.

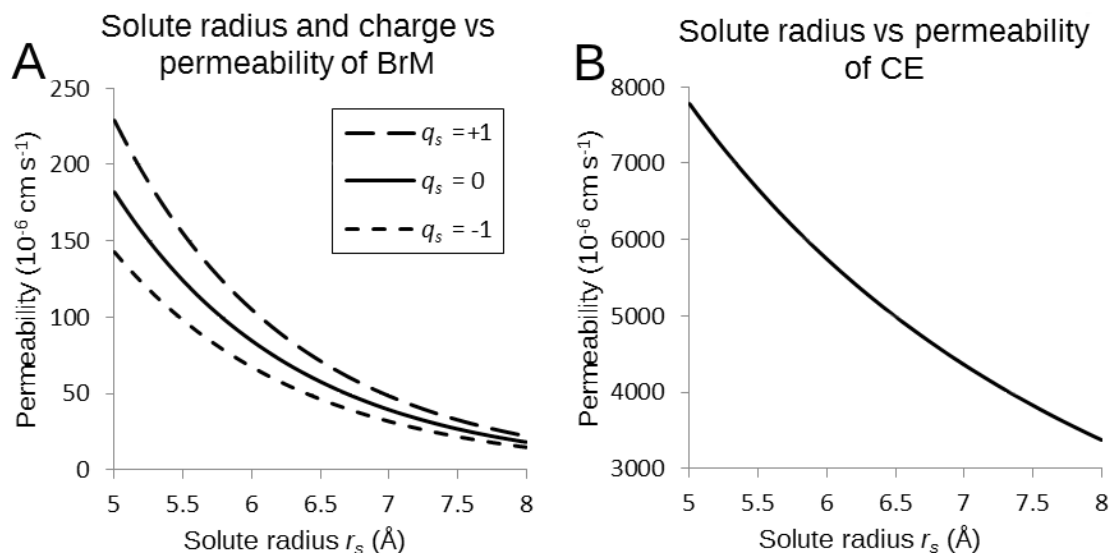


Figure 4.3: The behaviors of the BrM permeability as a function of solute radius (r_s) and charge (q_s) (A) and CE permeability as a function of solute radius (r_s) (B).

Total BRB permeability

The total BRB permeability, with and without melanin and as a function of lipophilicity and solute radius is shown in Figures 4.4A and 4.4B, respectively. In addition, the RPE (with and without melanin) and BrM permeabilities are presented. CE is ignored due to the high magnitude difference. In relation to lipophilicity, RPE with melanin is the limiting factor and defines the total BRB permeability. With melanin, the permeability is constant regardless of lipophilicity. Without melanin, the RPE permeability begins to increase rapidly at $\log K_D = 2$ and surpasses the BrM permeability near $\log K_D = 4$. So

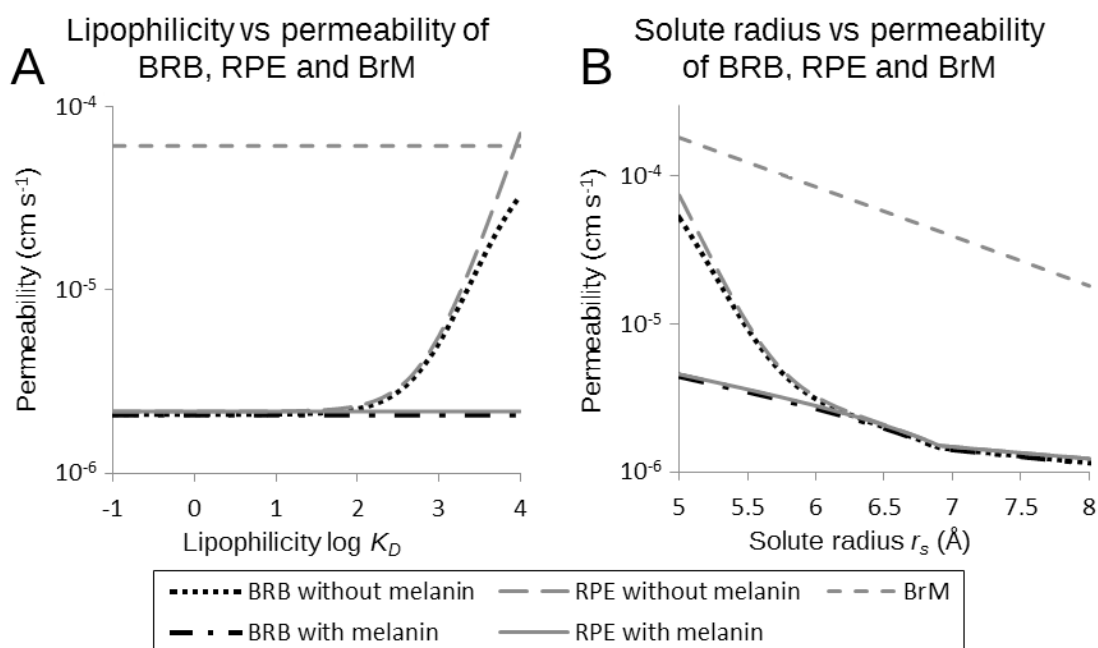


Figure 4.4: The behaviors of total BRB, RPE and BrM permeabilities as functions of solute lipophilicity ($\log K_D$) (A) and radius (r_s) (B) with and within melanin.

with highly lipophilic molecules and without melanin, BrM defines the BRB permeability.

In relation to solute radius, the BrM permeability is higher within the calculated range than the RPE permeability, with and without melanin. The effect of melanin binding can be seen with $r_s < 6$ Å as the BRB permeability without melanin begins to increase more rapidly than the BRB permeability with melanin. Also, around $r_s = 6.8$ Å there is a clear discontinuity in both cases of the BRB permeability.

4.1.3 Validation with the measured data

The validity of the BRB model was tested by comparing the calculated values to experimentally measured values. Figure 4.5A compares the measured permeability coefficients from bovine and porcine choroid-BRB (Ch-BRB) and human Ch-BRB, BRB and RPE with the calculated permeability coefficients from the BRB model with and without melanin. Most of the calculated values are within one order of magnitude from the measured values, presented by the dashed lines. The calculated values are mainly concentrated between values 1 and 10×10^{-6} cm s⁻¹, but measured values are more spread out through the whole range. The differences between values with and without melanin are small. There is a clear difference only between three molecules between the two cases: clonidine, fluorescein, Rhodamine 123. Also, there are no clear differences between animal species.

For the BrM, the comparison is presented in Figure 4.5B, and all the measured values are from the Ch-BrM. At higher permeabilities, the calculated and measured values are in similar scale, around 10 – 100×10^{-6} cm s⁻¹. The calculated permeability does not decrease with decreasing measured permeability, leading to differences of over two orders of magnitude. The interspecies differences are clear, as for porcine and human all

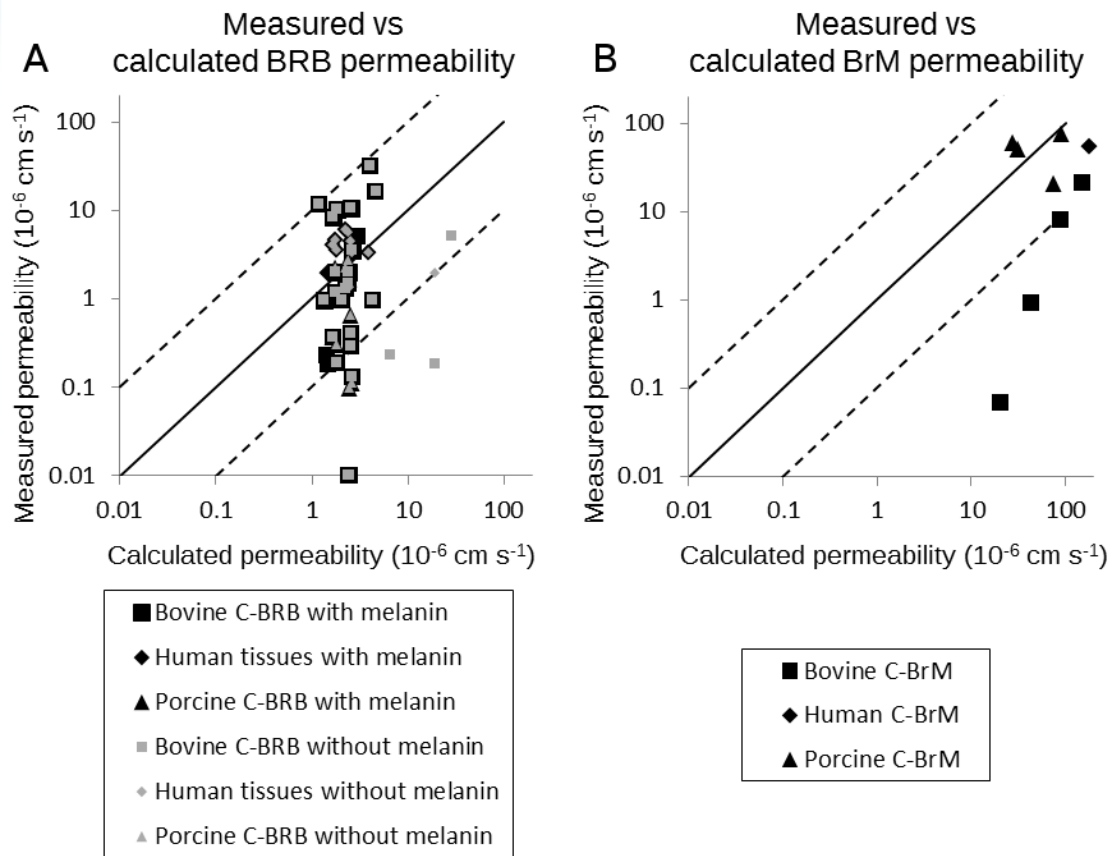


Figure 4.5: A: A comparison between the measured and calculated permeability coefficients from Ch-BRB from bovine or porcine as well as multiple human tissues. B: A comparison between measured and calculated permeability coefficient from bovine, human and porcine Ch-BrM. Human tissues include Ch-BRB, BRB and RPE.

the values are within one order of magnitude and for bovine the difference is generally greater. All the calculated permeabilities for the test molecules in the RPE, BrM, CE and BrM can be seen in Appendix 2 Table A2.1.

4.1.4 Sensitivity analysis

In the sensitivity analysis, the significance of specific model parameters was studied by varying their values by $\pm 25\%$ and calculating the change in permeability of the respective BRB component. Figure 4.6 shows the effect of the RPE parameters to the RPE permeability. Only the magnitude of the change is shown. The chosen parameters were lateral space half-width (W_{LS}), open part size (ϵ_{open}), TJ region half-width (W_{TJ}), TJ pores radius (r_{Tjp}) and TJ pore separation (d_{Tjp}). The changes were calculated for two solute sizes. The effect of W_{LS} is insignificant, as all the changes are under 3%. The effect is slightly higher with larger solutes and when the parameter value is decreased. With ϵ_{open} and W_{TJ} the effect is more pronounced with the larger solutes, as both changes in parameter value lead to a change of just under 25% and over 30%, respectively. Parameters ϵ_{open} and W_{LS} do not have any significant effect on the permeability of the smaller solutes. The effect of r_{Tjp} is very significant, as increasing its value by 25% leads to almost 120% increase in the large solute permeability. The decrease has no effect in the

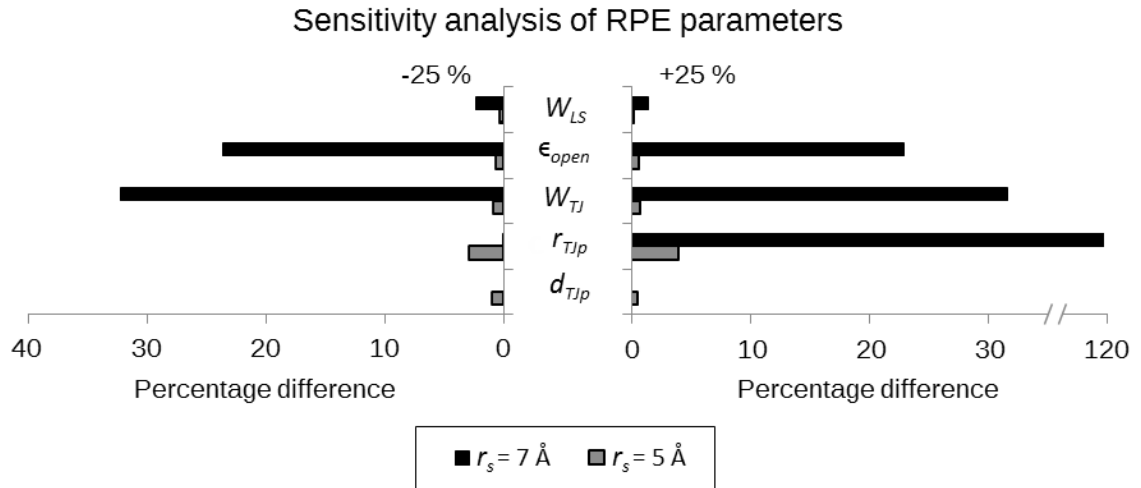


Figure 4.6: The sensitivity of five RPE parameters: lateral space half-width (W_{LS}), open part size (ϵ_{open}), TJ region half-width (W_{TJ}), TJ pores radius (r_{TJp}) and TJ pore separation (d_{TJp}). The values were increased and decreased by 25 % and the change in the RPE permeability of two molecules with different radius (r_s) was calculated. Only the magnitude of the change is shown.

large solute permeability. Also, for small solutes it is the most significant parameter as both decrease and increase lead to changes of 3–4 %. With large solutes, d_{TJp} has no effect at all, and with small solutes the effect is small.

The parameters chosen for BrM are the proteoglycan surface charge density (q_{PG}) as well as proteoglycan and collagen fibril volume fractions in both the ICL and OCL ($\phi_{PG,ICL}$, $\phi_{CF,ICL}$, $\phi_{PG,OCL}$ and $\phi_{CF,OCL}$). The results are shown in Figure 4.7. The analysis is

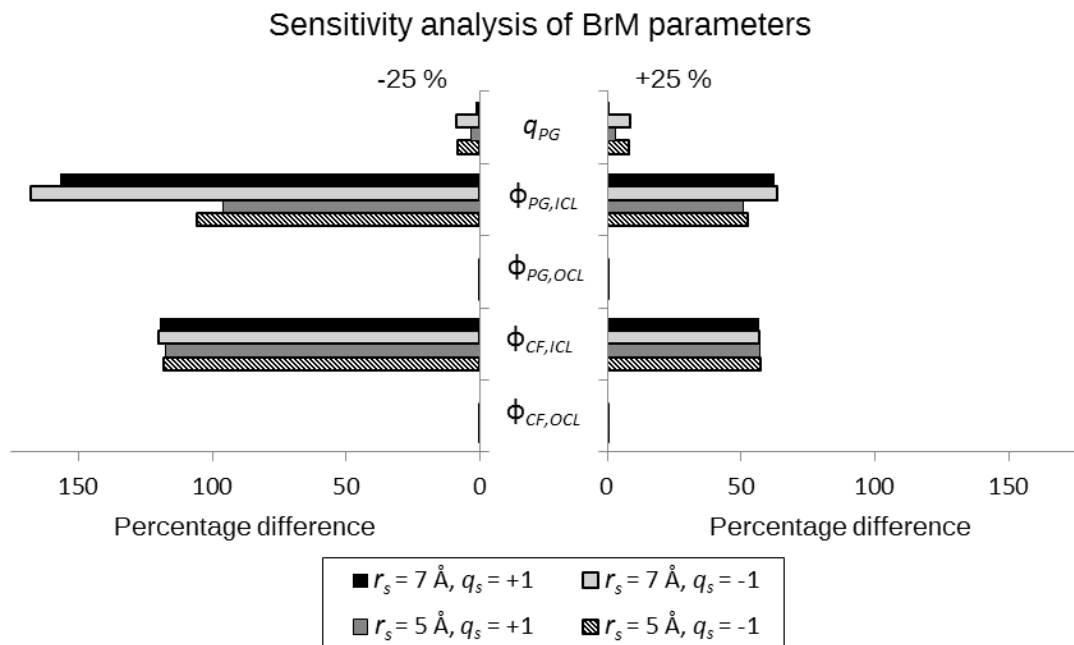


Figure 4.7: The sensitivity of five BrM parameter: proteoglycan surface charge density (q_{PG}) as well as proteoglycan and collagen fibril volume fractions in both ICL and OCL ($\phi_{PG,ICL}$, $\phi_{CF,ICL}$, $\phi_{PG,OCL}$ and $\phi_{CF,OCL}$). The values were increased and decreased by 25 % and the change in the BrM permeability of four molecules with different radius (r_s) and charge (q_s) was calculated. Only the magnitude of the change is shown.

done for four solutes with different radii and charges. The effect of q_{PG} is quite small for all the four solutes. However, it is more significant for negatively charged solutes, as their permeability changes by 8–9 %. With $\varphi_{PG,ICL}$ and $\varphi_{CF,ICL}$, there is a clear difference between decreasing and increasing the parameter value. Both changes of $\varphi_{PG,ICL}$ and $\varphi_{CF,ICL}$ by 25 % result in a change of 95–170 % and 50–65 % in the permeability, respectively. The effect of $\varphi_{PG,ICL}$ is more prominent with larger and negatively charged solutes in both directions. With $\varphi_{CF,ICL}$ the differences between solutes are small. The effects of both $\varphi_{PG,OCL}$ and $\varphi_{CF,OCL}$ are nonexistent for all the solutes.

4.2 Chamber model

The functionality of the half-perfusion chamber concept was studied by varying the values of certain parameters and monitoring how the changes affect the system function. After these simulations, the measurability of acceptor chamber concentration was studied.

4.2.1 Parameter-based errors in permeability

The errors caused by four parameters to the system function were tested by varying the value of each of them while keeping the others constant. The four parameters were the chamber-BRB distance (d_{dcBRB}), BRB-channel distance (d_{BRBpc}), channel height (h_{pc}) and perfusion flow rate (m_{fr}). In addition, the effect of the real permeability coefficient ($P_{BRB,c}$) was also simulated by using three different permeability values for each simulation. The results were calculated as BRB and outlet errors, first of which describes the systems ability to achieve the real permeability and latter the system's ability to measure the real permeability.

Effect of the chamber-BRB distance (d_{dcBRB})

The results for d_{dcBRB} simulations are shown in Figure 4.8 for the three different values of $P_{BRB,c}$. Figure 4.8A presents the behavior of the BRB error. Increasing d_{dcBRB} increases the BRB error with all the values of $P_{BRB,c}$. The increase in error is smaller with $P_{BRB,c} = 1 \times 10^{-6}$ cm s⁻¹, and in similar scale with the other two. Increasing $P_{BRB,c}$ increases the error considerably, as seen from the three curves.

Figure 4.8B presents the behavior of the outlet error in the same cases. The outlet errors behave similarly to the BRB errors, but are all slightly higher for each value of $P_{BRB,c}$. The difference between the errors in Figures 4.8A and 4.8B is most prominent when $P_{BRB,c} = 1 \times 10^{-6}$ cm s⁻¹.

Effects of the BRB-channel distance (d_{BRBpc}) and channel height (h_{pc})

The results for the effects of d_{BRBpc} and h_{pc} on the BRB and outlet errors with $P_{BRB,c} = 1 \times 10^{-6}$ cm s⁻¹ are shown in Figures 4.9A and 4.9B, respectively. In the case of the BRB error, the behavior of the error with $h_{pc} = 0.15$ mm is different from the others,

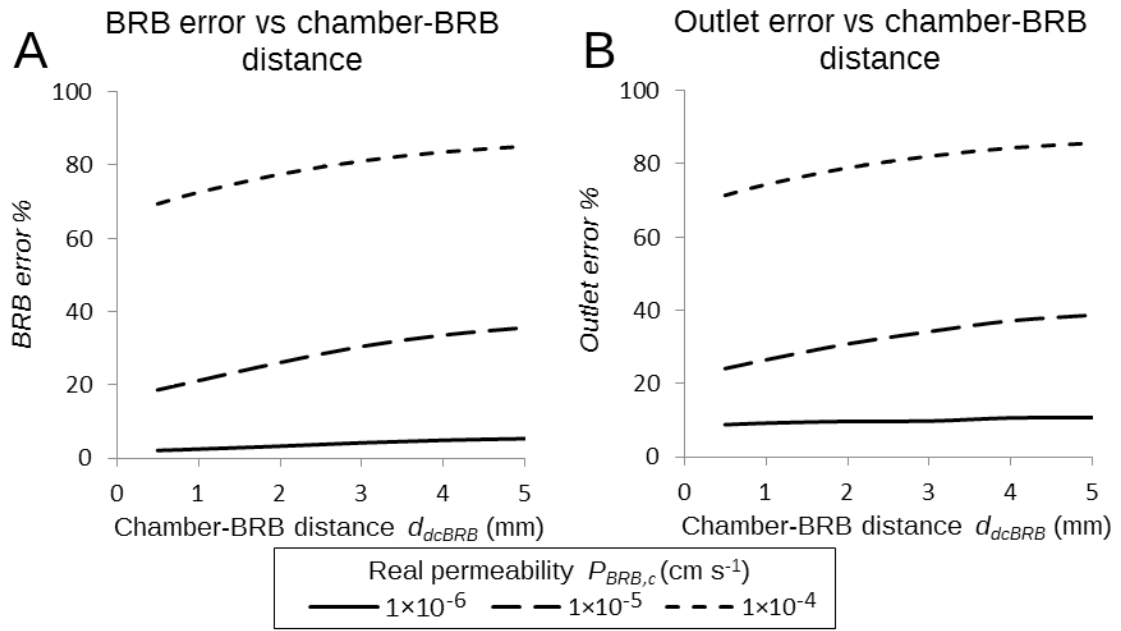


Figure 4.8: The effect of chamber-BRB distance (d_{dcBRB}) to BRB(A) and outlet errors (B), with the three different real permeability coefficients (P_{BRB}).

decreasing at first and increasing after $d_{BRBpc} = 1$ mm. The behavior of all the other values of h_{pc} is similar to each other, increasing as d_{BRBpc} increases and leveling out near $d_{BRBpc} = 5$ mm. Despite slightly different behavior of $h_{pc} = 0.15$ mm, the differences between the channel heights are minimal. With the outlet error, the differences between different values of h_{pc} are more clearly seen compared with the BRB error. At low values of d_{BRBpc} , the higher channels have lower error, but the differences vanish as d_{BRBpc} increases. Again, $h_{pc} = 0.15$ mm differs most from the rest. The outlet errors of all the channel heights begin to increase more rapidly after $d_{BRBpc} = 2-3$ mm. Also, when comparing the BRB and outlet errors, the effects of d_{BRBpc} and h_{pc} are more prominent with the outlet error.

The results for the effects of d_{BRBpc} and h_{pc} on the BRB and outlet errors with $P_{BRB,c} = 1 \times 10^{-5}$ cm s⁻¹ are shown in Figures 4.9C and 4.9D, respectively. With the BRB error, the differences between different values of h_{pc} are minimal, apart from $h_{pc} = 0.15$ mm, which shows a slightly lower error than the rest. With all the values of h_{pc} , the error increases with increasing d_{BRBpc} and levels out near $d_{BRBpc} = 5$ mm. For the outlet error, there is no clear trend with the different values of h_{pc} , but they increase quite linearly with the increasing d_{BRBpc} . The different behavior between the BRB and outlet error is clear, as the outlet errors increase to higher values than the BRB errors.

The results for the effects of d_{BRBpc} and h_{pc} on the BRB and outlet errors with $P_{BRB,c} = 1 \times 10^{-4}$ cm s⁻¹ are shown in Figures 4.9E and 4.9F, respectively. With the BRB error, the differences between values of h_{pc} are again minimal, apart from $h_{pc} = 0.15$ mm. The errors of all the values of h_{pc} increase with the increasing d_{BRBpc} and level out near $d_{BRBpc} = 5$ mm. With the outlet error, the value of h_{pc} has minimal effect on the error. All the values of h_{pc} similarly increase with the increasing d_{BRBpc} . The differences between the BRB and outlet errors are small compared to two lower values of $P_{BRB,c}$.

When the errors and behaviors between different values of $P_{BRB,c}$ are compared with each other as d_{BRBpc} and h_{pc} are changed, it is evident that the general error increases with

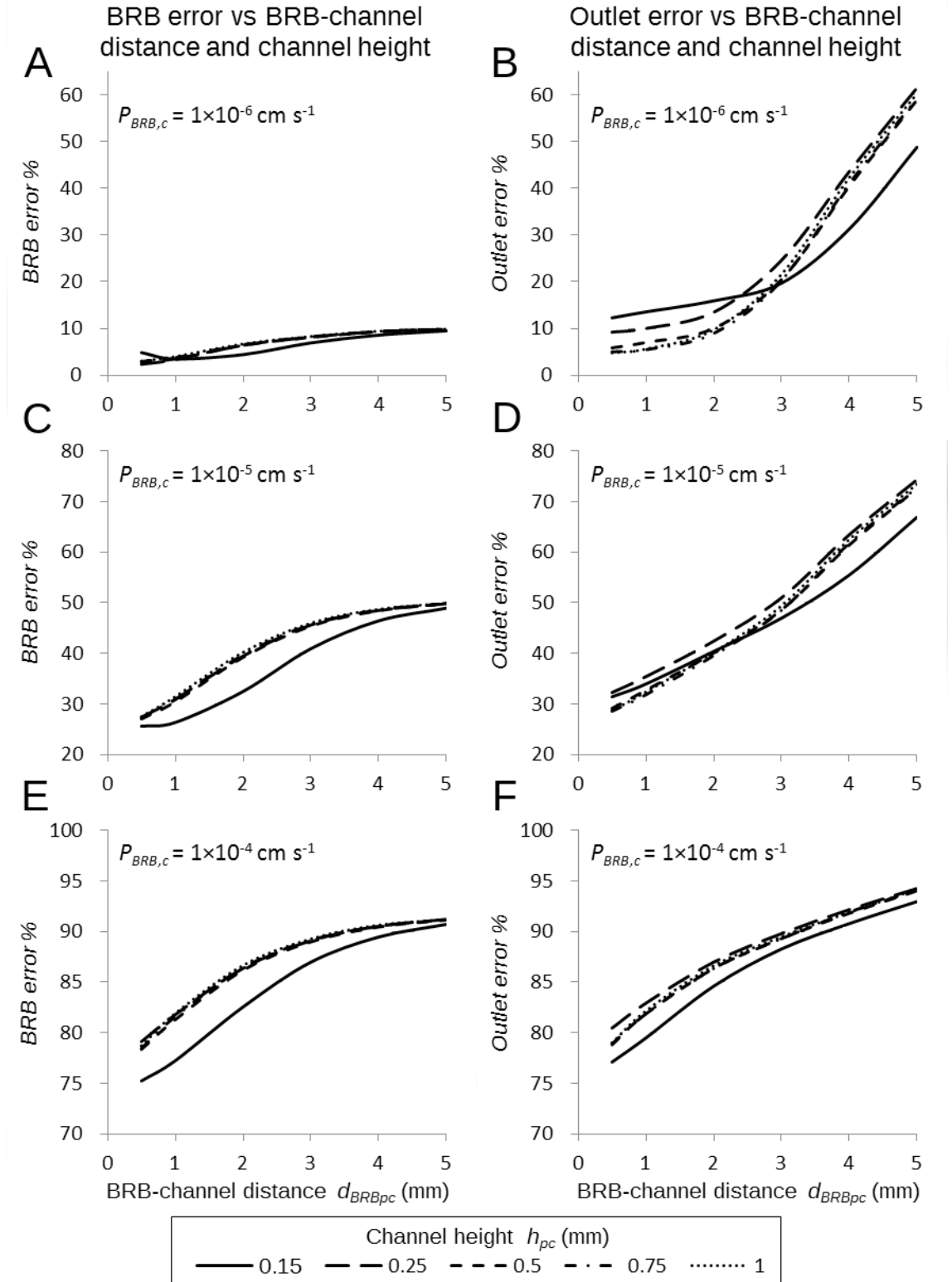


Figure 4.9: The effects of BRB-channel distance (d_{BRBpc}) and channel height (h_{pc}) to BRB and outlet errors percentages, with $P_{BRB} = 1 \times 10^{-6} \text{ cm s}^{-1}$ (A and B), $P_{BRB} = 1 \times 10^{-5} \text{ cm s}^{-1}$ (C and D) and $P_{BRB} = 1 \times 10^{-4} \text{ cm s}^{-1}$ (E and F). Note the scale of the y-axes.

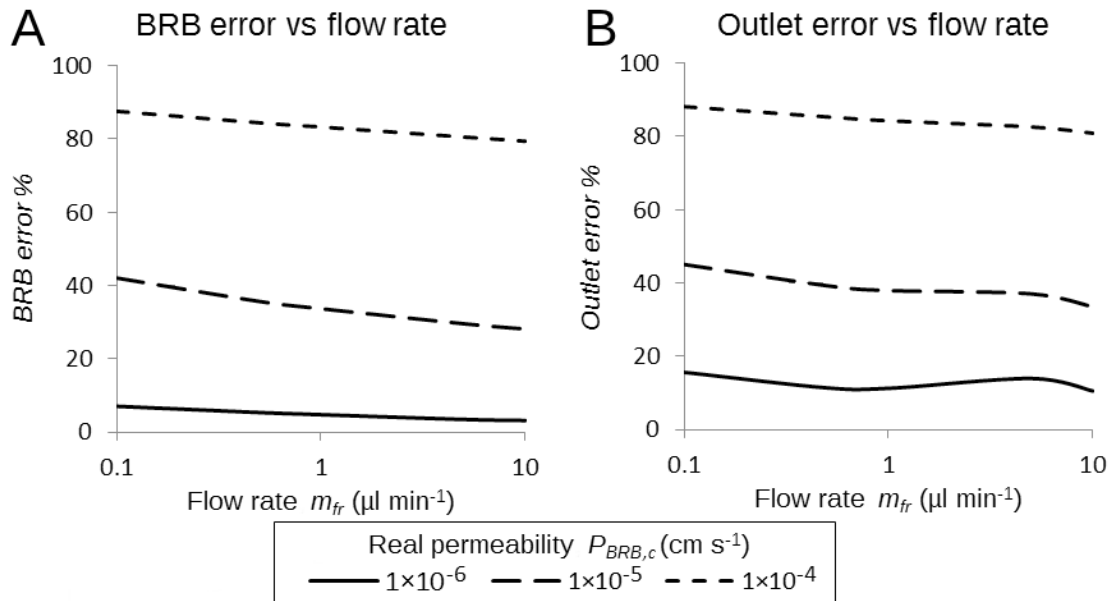


Figure 4.10: The effect of flow rate (m_{fr}) to BRB (A) and outlet errors (B), with the three real permeability coefficients ($P_{BRB,c}$). Note the logarithmic x-axis.

increasing $P_{BRB,c}$, as already seen in Figure 4.8. Also, the differences between the behaviors of the BRB and outlet errors are clearer with the small values of $P_{BRB,c}$.

Effect of the flow rate (m_{fr})

Figures 4.10A and 4.10B show the behavior of the BRB and outlet errors with the increasing value of m_{fr} , respectively. With all the values of $P_{BRB,c}$, the BRB errors decrease as m_{fr} increases. The decrease is fastest when $P_{BRB,c} = 1 \times 10^{-5} \text{ cm s}^{-1}$. With the outlet error, the behavior is not as straightforward, but the trend is clearly the same. With $P_{BRB,c} = 1 \times 10^{-6} \text{ cm s}^{-1}$, the error decreases until about $m_{fr} = 1 \text{ } \mu\text{l min}^{-1}$, after which it begins to increase and again decrease near $m_{fr} = 10 \text{ } \mu\text{l min}^{-1}$. The differences between the BRB and outlet errors are small, but more noticeable with the lower values of $P_{BRB,c}$. Again it is clearly seen in both Figures 4.10A and 4.10B that the increasing $P_{BRB,c}$ increases both errors.

4.2.2 Measurability of acceptor chamber concentration

To study the measurability of the acceptor chamber concentration, the concentrations with different flow rates (m_{fr}), donor chamber concentrations (c_{dc}) and BRB permeability coefficients ($P_{BRB,c}$) were calculated and compared to analysis technique sensitivity. The results for acceptor concentration as a function of flow rate with the three BRB permeability coefficients are shown in Figure 4.11A. The sensitivity is presented by the dotted line. The concentration is above the sensitivity with the two higher permeabilities within the simulated flow rate range. However, it is clearly seen, that with $P_{BRB,c} = 1 \times 10^{-5} \text{ cm s}^{-1}$ the concentrations will decline under the sensitivity when $m_{fr} > 10 \text{ } \mu\text{l min}^{-1}$. For $P_{BRB,c} = 1 \times 10^{-6} \text{ cm s}^{-1}$, the acceptor concentration decreases below the sensitivity when $m_{fr} = 1 \text{ } \mu\text{l min}^{-1}$.

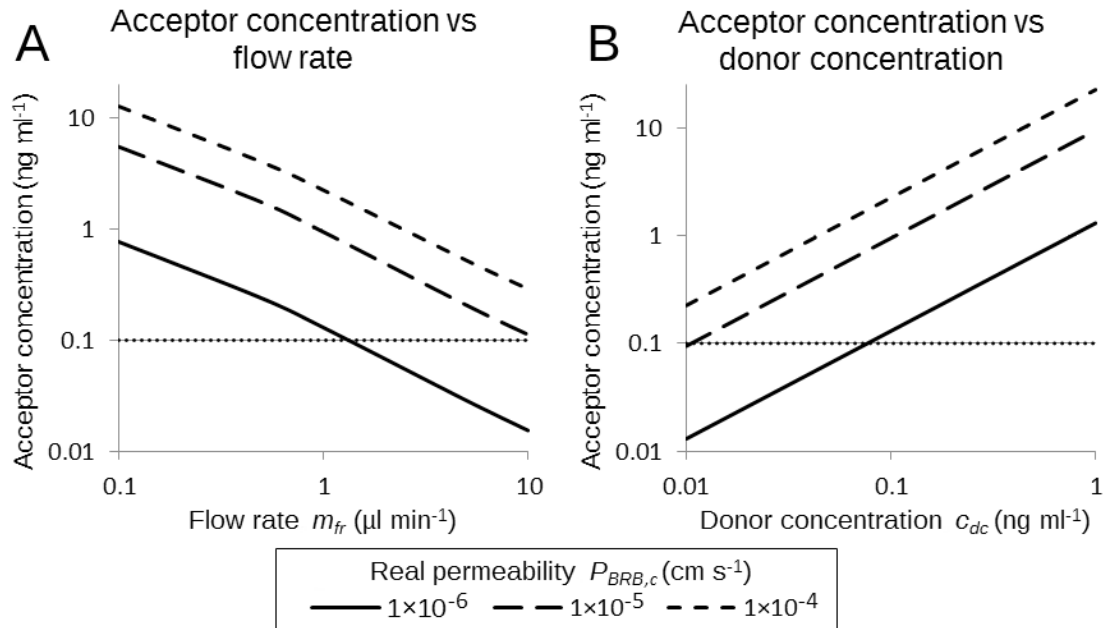


Figure 4.11: The effect of flow rate (m_{fr}) (A) and donor chamber concentration (c_{dc}) (B) to the acceptor chamber concentration, with the three real permeability coefficients (P_{BRB}). The sensitivity of the analysis technique is represented by the dashed line. Note the logarithmic axes.

The results between acceptor and donor chamber concentrations with the three permeabilities are shown in Figure 4.11B. Again, with the two higher permeabilities the acceptor concentrations stay above the sensitivity. However, with $P_{BRB,c} = 1 \times 10^{-5} \text{ cm s}^{-1}$, the acceptor concentration declines below the sensitivity just at the lower limit of the simulated donor concentration range. With $P_{BRB,c} = 1 \times 10^{-6} \text{ cm s}^{-1}$, the acceptor concentration becomes unmeasurable as the donor concentration drops below $c_{dc} = 0.1 \text{ ng ml}^{-1}$.

5 DISCUSSION

In this thesis, two mathematical models related to BRB permeability and its measurement system were constructed. The main aim of the models is to predict the barrier properties of the outer blood-retinal barrier (BRB) and the functionality of a permeability measurement system. In the first model, the diffusion barrier formed by the BRB was modeled. The aims of this BRB model were to construct and validate it as well as to determine the importance of different parts of BRB to the barrier function. The second model was of a half-perfusion chamber setup for the BRB barrier property studies. The model was used to study the effects of certain system dimensions and other parameters to the system's functionality.

5.1 BRB model

The BRB model presented in this thesis is the first model of its kind for BRB, based on the literature review. There is a need for this kind of model to explain experimental results, as it can link the solute permeability to the state of the BRB, be it normal or diseased (Ranta & Urtti 2006). It can be used to facilitate the experimental permeability studies, as it enables the linking of permeability coefficient with the physicochemical properties of the BRB. Thus, it may reveal why certain drugs have a certain permeability coefficient. Basically, the model relates the molecular properties to the interactions between the molecule and structures that form the BRB, and calculate how much they hinder the diffusion rate.

The model includes a much more detailed description of the BRB than any of the preceding pharmacokinetic models, such as those by Mac Gabhann et al. (2007), Amrite et al. (2008) and Ranta et al. (2010). There are similar models for other biological barriers, though, like for the cornea (Edwards & Prausnitz 1998; 2001) and the skin (Mitragotri 2003). This model uses mostly the same theory as those models for the other barriers, but some components, such as the model of RPE TJs, are more accurate than in any of the preceding ones.

To enable the use of the BRB model in further studies, the functionality of the model has to be evaluated. This is done in the following chapters, where first the results of the calculations are discussed, followed by the discussion how different assumptions and simplifications in the model may have affected the results. Finally, the discussion is summarized and future prospects of the model are considered.

5.1.1 Assessment of the results

To evaluate the functionality of the model, four different analyses were conducted. First, the different methods of determining the solute radius were compared. Then, the behavior of the model in relation to solute radius, charge and lipophilicity was investigated, followed by the model validation by comparing the calculated and measured permeability values. Finally, a sensitivity analysis concerning specific model parameters was carried out.

Comparison between the solute radii

The compared methods to calculate the solute radius were Stokes-Einstein Equation (2.3), Sutherland Equation (2.4) and van der Waals radii based on the solute volume. The radii were compared with actual solute size approximated by molecule's average projection radius. It is evident that Equation (2.4) is clearly a better method compared to Equation (2.3), as it follows much more closely to the real molecular size. Equation (2.3) produces consistently smaller radii and should not be used for small molecules, as it underestimates the radius.

The accuracy of solute radius is important for several reasons. First of all, it affects the permeabilities in different geometries. For example, if Equation (2.3) was used to calculate the solute radius, the permeabilities from fiber matrix model would be much higher with the same matrix parameters. Another important factor is the surface charge density. With smaller radius the surface charge density increases compared to the larger one.

Parameter behavior analysis

The permeability behavior of BRB and its parts in relation to solute lipophilicity and radius was studied. RPE was further divided into paracellular and transcellular pathways and modeled with and without melanin binding. The RPE permeability is mainly governed by the paracellular pathway regardless of solute properties and especially with melanin. As the normal mode of permeation should be somewhere between the two melanin modes, the real significance of transcellular pathway – and solute lipophilicity – according to this model, is very small. Edwards & Prausnitz (2001) also concluded that this kind of transcellular pathway has a little effect in the epithelial scale. Their model worked better as a whole, as they also included the pathway of diffusion within the cell membrane. With increasing solute radius, the paracellular permeability does clearly decrease, but not nearly in the same extent as the transcellular permeability. The discontinuity in paracellular permeability at $r_s = 8.9 \text{ \AA}$, is caused by the TJ pore radius ($r_{Tjp} = 8.9 \text{ \AA}$). This is quite similar behavior as seen in experimental measurements by Van Itallie et al. (2008).

The behavior of the BrM permeability with increasing solute radius is very similar in shape to the experimental measurements by Hussain et al. (2010) and Zauas-Santiago et al. (2011). The effect of negative molecular charge is intuitive, as objects with the

same charge repel each other, which in turn retards the diffusion rate. However, the accelerated diffusion of positively charged solutes may not be realistic as the proteoglycans bind these solutes in some extent, which also slows down the diffusion. The CE model is quite simple and the resulting behavior as a function of solute radius comes straight from the pore model. There is no measured data to compare the CE permeability behavior to. As the solute size is probably the only main factor affecting the permeation in the real case, the model can be estimated to be fairly accurate.

When the components of the BRB are studied together, it is clear that the RPE contributes most to the total permeability, especially with melanin. This aligns well with the literature (Pitkänen et al. 2005; Kadam et al. 2011). BrM does form a significant permeability barrier with highly lipophilic molecules. This behavior is quite similar to the one produced by the cornea model by Edwards & Prausnitz (2001), in which the corneal stroma becomes the least permeable component with highly lipophilic molecules.

In the literature, there are contradicting results about the relationship between permeability and solute lipophilicity. Pitkänen et al. (2005) found that the BRB permeability increases with increasing lipophilicity, and the finding of Kadam et al. (2011) were contradictory. One possible reason for this difference in behavior might be that Kadam et al. normalized their results with tissue thicknesses and melanin content. However, the differences in permeability within each study was small. This might mean that actually with lipophilic molecules, the enhanced cell membrane permeability is countered with enhanced melanin binding, thus decreasing the impact of lipophilicity on the total permeability. In addition, the standard deviations calculated by Kadam et al. (2011) are significantly smaller than those calculated by Pitkänen et al. (2005), which might indicate to differences in calculation methods between the two studies.

The orders of magnitude between the permeabilities of different BRB components are large. In the model between the RPE and BrM, the difference is around 25-fold for medium sized solutes. Pitkänen et al. (2005) concluded that this difference should be around 70- to 170-fold for 4 kDa FITC-dextran. Of course, FITC-dextran are linear molecules and much bigger than drug molecules, so this comparison might not be feasible. In the present model, the difference between the BrM and CE is around 40- to 190-fold, depending on the solute radius. It is difficult to estimate the accuracy of this difference, as there is no data available from the CE.

As a summary, the RPE forms the most significant component in the BRB. Due to its small significance of the transcellular pathway. As this is the only lipophilicity-dependent part of the model, lipophilicity has very little effect. Thus, the whole BRB model depends mainly on the paracellular pathway, which further depends only the solute radius. This leads to a narrow value range of permeability values.

Validation with the measured data

The model was validated by comparing the calculated permeabilities with the measured values. The calculated BRB permeability values are within a very narrow permeability range regardless of the properties of the solute. The measured values vary within much

larger range. The issues in the model behavior leading to the narrow range, such as the transcellular pathway, were discussed in the preceding section. The differences between species are not noticeable, which can be contributed to comparability of different experimental studies.

The comparison for just the BrM model shows better results than the comparison with the BRB model. Only few permeabilities differ more than one order of magnitude, namely the bovine Ch-BrM. Again the values reside within small permeability range, which indicates a flaw in the BrM model. Although the choroid ECM is more permeable than BrM, its larger thickness does make significant part of the measured permeability values. Because of this, the present BrM model probably underestimates the real BrM permeability, as do the measured results. In addition, the choroid contains melanin (Pescina et al. 2012), which in turn decreases the comparability.

There are some complications concerning the comparability of the calculated and experimentally measured values. First of all, the number of the experimental studies is low. Most of these studies use either bovine or porcine eyes, but the present model is based on the human BRB. Kadam et al. studied the permeabilities of choroid-RPE in the eyes from multiple species, including human, and concluded that the differences between species are noticeable. Bovine and porcine are close to each other, but humans have about 3-10 times higher permeabilities depending on the molecule. The differences between species leveled out as the permeabilities were normalized with tissue thickness and melanin content. (Kadam et al. 2011.) Secondly, there actually is a lack of data about the permeability of only the BRB. Although RPE forms the most significant barrier in Ch-BRB and BrM in Ch-BrM system, choroid still does affect the permeability due to its larger thickness. The comparability between different experimental studies may be a problem due to different study conditions and methods. These issues should be taken into account when viewing the validation results. In addition, it is more important to predict the magnitude and behavior of the permeability, not the exact absolute value, which is difficult to measure experimentally due to the varying experimental conditions.

Sensitivity analysis

The importance of five parameters from both the RPE and BrM models was studied by changing their value by 25 % to both directions and calculating the change in permeability. Large effect in permeability caused by these changes indicates the importance of the parameter. For RPE, the studied parameters were from the paracellular pathway, and two different sizes of solutes were used. TJ open part size (ϵ_{open}) has a significant effect on the larger solutes which are unable to diffuse through the TJ pores. For small molecules, ϵ_{open} has a little effect as they mainly diffuse through the pores. The effect of the TJ region half-width (W_{TJ}) is noticeable with larger solutes, as the slit affect more the diffusion rate of large molecules. TJ pore radius (r_{Tjp}) is very important parameter. For small solutes, the value change has only a small effect, but for large solutes the effect is very significant. This is caused by the fact that the value of r_{Tjp} increases above the large solute radius when increased by 25 %, which leads to considerable increase in perme-

ability (approximately 120 %). Lateral space half-width (W_{LS}) and TJ pore separation (d_{TJp}) are both insignificant. As a summary, the most important parameters in the paracellular pathway are the TJ open part size, TJ region half-width and TJ pore radius.

For BrM, the studied parameters were the proteoglycan surface charge density (q_{PG}) as well as proteoglycan and collagen fibril volume fractions in both the ICL and OCL ($\phi_{PG,ICL}$, $\phi_{CF,ICL}$, $\phi_{PG,OCL}$ and $\phi_{CF,OCL}$). The values of the volume fractions were estimated, as there was no data available. Four solutes with two different radii and charges were used. Parameter $\phi_{PG,ICL}$ is the most important parameter studied in the BrM model, as the change in its value leads to the largest change in the BrM permeability. For large solutes, the effect is even more significant than for small ones, as it is more difficult for them to diffuse through the fiber matrix. Although the changes caused by the variation of $\phi_{CF,ICL}$ are also large, they are similar to all the solutes. The differences between solutes with the changes of $\phi_{PG,ICL}$ arise from the fact that the radius of the proteoglycans is in similar scale as that of the solutes. With $\phi_{CF,ICL}$, the size difference is larger. Because of the significance of $\phi_{PG,ICL}$ and $\phi_{CF,ICL}$, the underestimation of the BrM permeability discussed earlier is partly caused by too high values of these two volume fractions. The effect of q_{PG} , $\phi_{PG,OCL}$ and $\phi_{CF,OCL}$ are insignificant.

5.1.2 Model assumptions and simplifications

Many assumptions and simplifications of the BRB anatomy had to be made during the model construction. Next, their justification and possible impact on the model functionality and the limitations of the model are discussed.

Assumptions and simplifications of the RPE model

It is quite clear that the transcellular pathway of the RPE model has many problems, which stem from multiple reasons. The transcellular model, especially cell membrane permeation, is different from the rest of the model. It calculates the permeability based on fitted equation, whereas the other parts of the model use the free diffusion coefficient and multiply it with different coefficients. This means that there may be large differences between permeabilities. Of course, the cell membrane forms a quite different barrier compared to the other parts of the model, as there are a lot of different interactions between the membrane and solute molecules. Edwards & Prausnitz (2001) concluded that their model tends to overestimate the cell membrane permeability by approximately two orders of magnitude. One thing that might affect the transcellular permeability is how van der Waals volume is calculated, as Edwards & Prausnitz (2001) used different software for this.

The applicability of the diffusion pathway within the cell membrane used by Edwards & Prausnitz (2001) was tested in the present model, but it led to too high permeabilities, and was thus ignored. This partly balances out the overestimation in the cell membrane permeability model concluded by Edwards & Prausnitz. The relationship between the cell membrane permeation and diffusion pathways within the cell membrane

is difficult. In the present model, lipophilic molecules readily permeate through the whole membrane. However, in reality a lipophilic molecule might not partition out of the hydrocarbon core into the cytosol, as this is energetically more unfavorable environment. This would mean that the diffusion pathway within the cell membrane is significant, but as mentioned, difficult to model.

In addition to the cell membrane permeability, the melanin binding has a huge effect on the total transcellular permeability. The present model of melanin binding is very simple, but it would have been difficult to model it more accurately in the scope of this thesis. Melanin binding is a complex process influenced by many other things than just lipophilicity, like the atom scale molecular properties (Lowrey et al. 1997).

In the present model, the effects of basal infoldings and apical microvilli in the RPE and the increased cell membrane area were ignored. They would not have made the transcellular pathway more significant, as they would have only multiplied the transcellular permeability with a small constant that describes the increased area. The effect of active transport is one source of error when comparing predicted and experimentally measured permeabilities. For example some solutes, such as carboxyfluorescein (Kimura et al. 1996), are actively transported from apical to basal direction, which might decrease the measured permeability in the other direction.

The paracellular pathway is modeled with a novel method compared to preceding models. The TJ structure in the present model more accurately follows the real TJ structure than for instance the model by Edwards & Prausnitz (2001). The biggest simplifications are the omission of the web-like structure of the TJs and the TJ pore charge selectivity, which would needlessly increase the complexity of the model. Also, both the slit and pore models – with which the paracellular pathway model is based – assume that the geometry is perfect and that there is no binding with the walls, which may be incorrect but difficult to model.

Assumptions and simplifications of the BrM model

With BrM, the most important simplification is the modeling of only the ICL and OCL. For example, both basal laminae may be significant barriers, as one fourth of proteoglycans in BrM is primarily located in the RPE-BL (Inatani & Tanihara 2002). This would probably form a barrier against diffusion, but also increase the number of parameters. Due to the lack of data, the number of parameters estimated was kept at minimum. The present model only takes into account the collagen fibrils and proteoglycans. In reality, BrM includes many other biomolecules, such as other types of collagens and fibronectin, with different properties. Also, with increasing age, lipids accumulate into BrM, which would relate its permeability to solute's lipophilicity. However, it would be difficult to model the other biomolecules or lipids with the models and equations utilized in the present model.

The fiber matrix model itself has some simplifications. The fibers in the model are randomly oriented, homogeneously distributed, immobile and rigid. In reality, the ECM geometry is not this strict. The fibers can move about and there might be inhomogeneous

geneities in the fiber distribution, because of which the fiber matrix model tends to underestimate the diffusion rate. (Phillips 2000.)

Another question is the applicability of the fiber matrix model to the BrM model. It is derived for diffusion in hydrogels, whose volume fractions are mainly under 0.10 (Phillips 2000). The high volume fractions used in the present model are well above this. So, the correctness of the fiber matrix model at higher volume fractions is difficult to estimate. For perfect square array of fibers, the diffusion is blocked when fibers touch each other and the volume fraction can be calculated to be 0.79. The volume fraction for random matrix that totally blocks diffusion is probably not so much different and using values as high as used in the present model (0.60) might lead to incorrect results, due to the limits of the fiber matrix model.

In addition to the hydrodynamic and steric interactions between the solute and fibers, also the accuracy of electrostatic interactions depends on the fiber volume fraction. The model created by Johnson & Deen is most accurate when the interactions are only between one particle and one fiber. (Johnson & Deen 1996.) The issue with this is that the high fiber volume fraction might lead to more complex interactions between the solute and multiple fibers. The unrealistic behavior of attractive electrostatic forces mentioned earlier is caused by the fact that the electrostatic solute-fiber model was derived only for repulsive interactions (Stylianopoulos et al. 2010a).

Assumptions and simplifications of the CE model

With the CE model, the paracellular and transcellular pathways were ignored, and only the diaphragmed fenestrations were modeled. The transcellular pathway would have been modeled similarly to the RPE model. In the paracellular pathway, the parameters concerning the TJs would have been adapted to the CE. Nevertheless, these pathways would have become very tight compared with the fenestrations, as can be seen from the RPE model permeability results. As the magnitude of the CE model results seems correct, these simplifications seem justified.

Assumptions and simplifications of the solutes

The main simplification with the solutes was the spherical shape. Some molecules are not spherical, so for example the orientation of a molecule trying to diffuse through a TJ pore becomes significant. However, slit, pore and fiber matrix models assume this geometry, and it would be impractical to take into account the individual shapes of each molecule. Also, the molecular size is limited to under 1000 Da as it is calculated with Sutherland equation.

The solute sizes were calculated as molecules without hydration. With charged solutes, water molecules attracted by the charge form a hydration layer around the solute, which increases the molecular size (Hämäläinen et al. 1997) and makes diffusing through pores and membranes energetically more unfavorable (Nelson 2008).

The solute's charge was taken as the charge of the most common chemical species. However, as practically with all the molecules, the most common species was around 99 % of all the molecules, this simplification has no impact on the model. There are multiple databases including tabulated lipophilicity values. Some include measured values and some calculated values. The problem with most of the databases is that none of them includes all the molecules needed for this model. Due to different study methods and conditions, values from different studies vary. This makes combining data from different databases undesirable. Because of these reasons, all the lipophilicity values are calculated using Marvin Calculator Plugins.

5.1.3 Summary and future prospects

The BRB model is the first model of its kind for BRB and it is more accurate than the existing pharmacokinetic models. As already discussed, there are some areas of improvement with the model. The main issue in the BRB model is the lack of experimental data. In spite of its problems, it is able to predict the right magnitude for the permeabilities. However, the more accurate behavior based on the molecular properties is not seen. The same theory with different parameter values could easily be extended for other species, although it was constructed for the human BRB.

The model forms a good platform for the refinement of the different components. In the future, there are several directions this model can be taken and application it can be used for. One interesting direction is more dynamic behavior of the BRB. The BRB permeability can be regulated with different methods, for example by different claudins in the TJs or with changes in active transport. The integration of these into the model could enable the simulation of the dynamic behavior of the BRB in different scenarios, such as AMD. The changes in solute permeability caused by AMD could be traced back to the structural and behavioral changes caused by it. Additionally, by changing the system parameters the model shows the effect on permeability, which can be compared to the changes caused by AMD. Also, one possible direction is to try to join together the molecular permeability studied in this model with the TER values across the BRB. This kind of model would enable more complete description of the BRB barrier function.

The model can be used to design new drugs for AMD, as it is possible to predict the permeability of a drug based on its properties. Other possible uses for the model are the prediction and guidance of experimental *in vitro* drug analyses. In addition, the model can be used to replace the constants describing permeability in the pharmacokinetic models. This would enable much more accurate modeling and simulations of drug delivery from a periocular implant or blood circulation. In addition to the pharmacological and pathological applications, the BrM model can be utilized to study the diffusional properties of polymer biomaterials for the replacement of BrM in RPE transplantation.

5.2 Chamber model

The finite element method (FEM) model was constructed and used to simulate the effects of different parameters to the functionality of a half-perfusion chamber concept. The idea is to study how certain system parameters affect the functionality of the system and to find out what causes the possible measurement errors. This kind of models of experimental measurement tools are important, as they show where the errors in the systems come from.

5.2.1 Assessment of the results

The functionality of the chamber was studied by varying the values of certain parameters and monitoring how these changes affect the system function. First, the errors caused by the parameters to the permeability measured from the system were simulated. Following that, the measurability of the acceptor chamber concentration was studied.

Parameter-based errors in permeability

The effects of four parameters to the chamber-based measurement error were simulated. The parameters were the chamber-BRB distance (l_{dcBRB}), BRB-channel distance (l_{BRBpc}), channel height (h_{pc}), perfusion flow rate (m_{fi}) and BRB permeability coefficient ($P_{BRB,c}$). Two errors were considered: BRB error representing the system's ability to reach the real BRB permeability and outlet error representing the system's ability to actually measure the real BRB permeability. The simulations were done by varying one or two of the investigated parameters and keeping the others constant. Three values of $P_{BRB,c}$ were used to study the chamber's ability to measure the permeability of different membranes.

First of all, the effect of the real permeability coefficient $P_{BRB,c}$ to both the BRB and outlet errors is very significant regardless of all the other parameters. At least two reasons can be considered for this remarkable dependence of both the BRB and outlet errors on $P_{BRB,c}$. The first reason is more important to the BRB error than to the outlet error. In the beginning of the measurement, the concentration gradient between the sides of the membranes is at its maximum. When the measurement proceeds, the concentration above the BRB decreases and below the BRB increases, thus decreasing the gradient. However, Equation (3.20) uses the time average concentration above the BRB and assumes zero concentration below the BRB. Because this assumption is never actually true, there is a small error. This error can be seen as a BRB error and it is under 10 %. The second reason for the increasing error with increasing value of $P_{BRB,c}$ is diffusion rate. As an example, if the permeability of water-filled channel with the length of 2 mm is calculated with equation (2.7), the result is $3.75 \times 10^{-5} \text{ cm s}^{-1}$. This value is in similar scale with the higher values of $P_{BRB,c}$. If this channel is connected in series with the BRB, its importance increases with increasing $P_{BRB,c}$. Because of this, the system can never measure the actual value of $P_{BRB,c}$. Even if both l_{dcBRB} and l_{BRBpc} are zero, the diffusion rate within the donor chamber limits the flux across the BRB.

Basically the value of $P_{BRB,c}$ sets the base level for both the BRB and the outlet errors, but the more precise changes are caused by the changes in the parameters of chamber geometry. The effect of l_{dcBRB} is relatively small to both the BRB and the outlet errors with the smallest value of $P_{BRB,c}$, as the BRB remains as the rate-limiting part. But as $P_{BRB,c}$ increases the importance of l_{dcBRB} increases as it partly defines the permeability of the upper part of the channel. The differences between the BRB and the outlet errors are small and mainly caused by the constant values of the other three parameters.

Parameter l_{BRBpc} is more significant than l_{dcBRB} , especially for the outlet error and lower permeabilities. When l_{BRBpc} is short, perfusion flow facilitates the solute movement, also near BRB. As l_{BRBpc} increases, the distance a molecule has to diffuse without perfusion increases. This does not have a significant effect on the BRB error with lowest value of $P_{BRB,c}$, but the effect on the outlet error is noticeable as the lower part of the BRB forms an additional permeability component to the system, as discussed earlier. The small increase in the BRB error as l_{BRBpc} increases is probably due to the fact that the solutes do not diffuse very fast away from the BRB without perfusion. This decreases the concentration gradient over the BRB. As the value of $P_{BRB,c}$ increases, the differences between the BRB and outlet errors begins to vanish. This is because of the decreasing relevance of the BRB as a permeability component. With $P_{BRB,c} = 1 \times 10^{-4} \text{ cm s}^{-1}$, the behavior of both errors is mainly influenced by the diffusion rate, not $P_{BRB,c}$.

As clearly shown in Figure 4.9 the effect of channel height h_{pc} to both the BRB and the outlet errors is quite insignificant. There are only small differences between different values of h_{pc} , apart from $h_{pc} = 0.15 \text{ mm}$. As solutes diffuse into the perfusion channel, the preferred method of transport changes from diffusion to convection. The channel height is less important, as convection is a much faster method of transport than diffusion and as the transport does not occur in vertical direction. The different behavior of $h_{pc} = 0.15 \text{ mm}$ might be a result of changed flow pattern within the BRB channel. Another option is that the FEM mesh within the perfusion channel is too rough, so the channel is only a few elements high, which may affect the calculated results.

Increasing the flow rate (m_{fr}) in the perfusion channel does decrease the error to some extent. This can be explained by the fact that as the value of m_{fr} increases, its influence on the BRB channel reaches higher. This leads to faster transport of solutes away from the BRB, which in turn increases the concentration gradient over the BRB. However, as the changes in both the BRB and outlet errors are quite small, the behavior might be a result of COMSOL, as there are some variation in the calculations.

As a summary, the BRB permeability coefficient is the parameter with the largest effect on the measurement errors, which follows from the importance of the free diffusion coefficient to the measured values. The differences in errors when the other model parameters are changed follow from the changes in diffusion distances.

Measurability of the acceptor chamber concentration

The solute concentration of the acceptor chamber (c_{ac}) was studied by varying m_{fr} and donor chamber concentration (c_{dc}). As discussed with the error analysis, the effect of m_{fr}

to the outlet error is not important. However, for the measurability of c_{ac} , it has a large role. The increasing value of m_{fr} deteriorates the measurability fast, especially with small permeabilities, as there is smaller solute a flux going through the outlet. As the donor and acceptor concentrations are directly proportional to each other, it is quite clear that a large donor concentration leads to a large acceptor concentration.

5.2.2 Model limitations

Using FEM to model the diffusion imposes some limitations for the accuracy of the model. First of all, the accuracy of the mesh is an important factor. This can especially be seen with the smallest values of channel height, as in these cases the channel is only a few elements in height. This means that the changes and gradients in flow rates and concentrations, which can probably be quite drastic in such small channel, are not modeled correctly. However, the increasing the element number would lead to very high computational loads in larger channel heights.

In addition to the mesh, the physics used in the simulations are simplifications of the real situations. The physics for the diffusion only represent the diffusing molecules as concentrations. This means that the model does not take into account any real interactions between the diffusing molecule and the system or BRB. For example, the molecules may bind to the chamber walls and especially to the melanin in the BRB. However, the problems with the physics are probably smaller than the mesh, as Fick's second law captures the rate limiting step of the molecular movement: the diffusion. Also, as Fick's second law is an idealized model of diffusion, the present chamber model at most overestimates the molecular transport rate in the system. This is because all the interactions would hinder the diffusion rate. So, even if the model is not entirely correct, the real situation with all the interactions not modeled here is probably worse.

5.2.3 Summary

As the importance of different dimensional and measurement-based parameters to the functionality of the chamber was studied, it was quite surprising that the most important parameter concerning the functionality of the chamber is not any of these, but actually the free diffusion coefficient. Basically, the slow movement of molecules over large distances creates the error in the system. The four different parameters create some error, which mainly follows from the fact that they define the diffusion distances. The greatest effect on error was seen when the permeability coefficient of the BRB was varied. This change can be traced back to the free diffusion coefficient. It is quite clear, that with larger permeability coefficients, the measured permeability is not as much based on the BRB permeability as it is to the permeability – or error – of the chamber. The measurability of the concentration in the acceptor chamber is important for the usage of this kind of a system, and the concentration is highly dependent on the flow rate and donor concentration.

Based on a literature review, there are no published models of the chamber functionality. Thus this model may be the first to show the challenges in the ability of diffusion chambers to measure the membrane permeability. The problems this model revealed presumably affect most of the diffusion chambers, and especially those that depend at least partly on passive diffusion. Generally, the ability of these chambers to measure the actual absolute values of permeability and the results obtained with them should be considered with caution.

5.3 The models together

Physiological models, and especially mathematical models, have a great importance when studying the properties of the BRB in health and disease. Although the two models are very different in nature, they aim to create a comprehensive understanding of both the barrier function of the BRB as well as the methods and tools for studying it. Both models can together be used to guide the experimental research by combining our knowledge about the diffusion in the BRB and in the measurement tools. There are no published models that include both the subject of the measurement and the measurement tool. In the end, the main objective of these models in a larger context is to mediate the research on AMD and other similar diseases and facilitate the development of new treatment options.

6 CONCLUSION

Modeling is a significant part of the research of physiological systems. Models complement and direct the experimental studies towards the important objectives. To develop new treatments for AMD – such as drug therapies or RPE transplantation – the properties of the BRB in the normal eye and in the diseased eye has to be studied. Modeling gives simple methods for this. Also, to be able to study the barrier properties of the BRB, there has to be suitable tools, such as the diffusion chambers. When utilizing these tools, the user must understand how the measurement setup behaves and what are the possible sources of error.

To meet these needs, two mathematical models were constructed in this thesis. The first model is a passive diffusion model of the BRB based on the physicochemical properties of the diffusing molecule and the barrier itself. The author combined physical theories of hindered diffusion and dimensional parameters of the BRB from the literature. The model was constructed, validated and its properties were studied in multiple ways. The second model was of a conceptual half-perfusion chamber meant for the BRB permeability studies, and it was used to study how system dimensions and parameters affect the results measured with the system. This model was a FEM model and the author constructed it by using the existing physics models in COMSOL Multiphysics software.

The results show that the BRB model does predict the correct magnitude of the BRB permeabilities, but fails to show the more specific behavior based on the properties of the diffusing molecules. The TJ model in the present BRB model is novel and more accurate than in the previously published models. Furthermore, this also the first model of BRB to include the melanin binding. The BRB model also shows that RPE forms the major barrier against diffusion, as predicted in the literature. However, BrM limits the diffusion of highly lipophilic molecules. The effect of choroid to the measured permeability values should also be considered as a noteworthy permeability component due to its thickness. The largest problem with the model is the transcellular pathway of the RPE, which is the most difficult part to model due to the complex interactions between the solute and the structures of the RPE. Nevertheless, the model does form a good platform for future refinements.

The chamber model shows that the functionality of the half-perfusion chamber addressed in this thesis is limited by the diffusion rate. As for the dimensions and other parameters, the system will function at its best when the free diffusion distances are minimized. Generally, the ability of the diffusion chambers to measure the actual absolute values of permeability and the results should be considered with caution.

REFERENCES

- Alberts, B., Johnson, A., Lewis, J., Raff, M., Roberts, K. & Walter, P. 2008. *Molecular Biology of the Cell*. 5th ed. New York, USA, Garland Science. 1601 p.
- Amrite, A., Edelhauser, H. & Kompella, U. 2008. Modeling of corneal and retinal pharmacokinetics after periocular drug administration. *Investigative Ophthalmology & Visual Science* 49, 1, pp. 320–332.
- Amsden, B. 1998. Solute Diffusion within Hydrogels. Mechanisms and Models. *Macromolecules* 31, 23, pp. 8382–8395.
- Anand-Apte, B. & Hollyfield, J.G. 2011. Developmental Anatomy of the Retinal and Choroidal Vasculature. In: Besharse, J.C. & Bok, D. (ed.). *The Retina and Its Disorders*. Oxford, UK, Academic Press. pp. 179–185.
- Anderson, J.M. & Van Itallie, C.M. 2009. Physiology and Function of the Tight Junctions. *Cold Spring Harbor perspectives in biology* 1, 2, pp. 1–16.
- Augood, C.A., Vingerling, J.R., de Jong, P.T.V.M., Chakravathy, U., Seland, J., Soubrane, G., Tomazzoli, L., Topouzis, F., Bentham, G., Rahu, M., Vioque, J., Young, I.S. & Fletcher, A.E. 2006. Prevalence of age-related maculopathy in older Europeans: the European Eye Study (EUREYE). *Archives of Ophthalmology* 124, 4, pp. 529–535.
- Avdeef, A. 2010. Leakiness and Size Exclusion of Paracellular Channels in Cultured Epithelial Cell Monolayers – Interlaboratory Comparison. *Pharmaceutical Research* 27, 3, pp. 480–489.
- Balachandran, R. & Barocas, V. Computer modeling of drug delivery to the posterior eye: effects of active transport and loss to choroidal blood flow. *Pharmaceutical Research* 25, 11, pp. 2685–2696.
- Ban, Y. & Rizzolo, L.J. 2000. Differential regulation of tight junction permeability during development of the retinal pigment epithelium. *American Journal of Physiology. Cell Physiology* 279, 3, pp. 744–750.
- Barar, J., Asadi, M., Mortazavi-Tabatabaei, S.A. & Omid, Y. 2009. Ocular Drug Delivery; Impact of *in vitro* Cell Culture Models. *Journal of Ophthalmic and Visual Research* 4, 4, pp. 238–252.
- Beaber, E.L. & Orci, L. 1985. Endothelial Fenestral Diaphragms: A Quick Freeze, Deep-Etch Study. *The Journal of Cell Biology* 100, 2, pp. 418–428.
- Bernstein, M.H. & Hollenberg, M.J. 1965. Fine structure of the choriocapillaris and retinal capillaries. *Investigative Ophthalmology & Visual Science* 4, 6, pp. 1016–1025.

- Bhutto, I. & Luty G. 2012. Understanding age-related macular degeneration (AMD): Relationships between the photoreceptor/retinal pigment epithelium/Bruch's membrane/choriocapillaris complex. *Molecular Aspects of Medicine* 33, 4, pp. 295–317.
- Booij, J.C., Baas, D.C., Beisekeeva, J., Gorgels, T.G.M.F. & Bergen, A.A.B. 2010. The dynamic nature of Bruch's membrane. *Progress in Retinal and Eye Research* 29, 1, pp. 1–18.
- Boulton, M. & Dayhaw-Barker, P. 2001. The role of the retinal pigment epithelium: topographical variation and aging changes. *Eye* 15, 3, pp. 385–389.
- Brady, J. 1994. Hindered Diffusion. Extended Abstracts, AIChE Annual Meeting, San Francisco, USA, p. 320.
- Brodin, B., Steffansen, B. & Nielsen, C.U. 2009. Passive diffusion of drug substances: the concepts of flux and permeability. In: Steffansen, B., Brodin, B. & Nielsen, C.U. (ed.). *Molecular Biopharmaceutics*. London, UK, Pharmaceutical Press. pp. 135–152.
- Brown, R. 1828. A brief account of microscopical observations made on the particles contained in the pollen of plants. *Philosophical Magazine* 4, pp. 161–173.
- Cheruvu, N.P.S. & Kompella, U.B. 2006. Bovine and Porcine Transscleral Solute Transport: Influence of Lipophilicity and the Choroid-Bruch's Layer. *Investigative Ophthalmology & Visual Science* 47, 10, pp. 4513–4522.
- Clague, D.S. & Phillips, R.J. 1996. Hindered diffusion of spherical macromolecules through dilute fibrous media. *Physics of Fluids*, 8, 7, pp. 1720–1731.
- Clarke, L.L. 2009. A guide to Ussing chamber studies of mouse intestine. *American Journal of Physiology. Gastrointestinal and Liver Physiology* 296, 6, pp. G1151–1166.
- Claude, P. 1978. Morphological Factors Influencing Transepithelial Permeability: A Model for the Resistance of the Zoluna Occludens. *The Journal of Membrane Biology* 39, 2–3, pp. 219–232.
- Cobelli, C. & Carson, E. 2008. *Introduction to Modeling in Physiology and Medicine*. London, UK, Academic Press. p. 328.
- Cu, Y. & Saltzman, W.M. 2009. Mathematical modeling of molecular diffusion through mucus. *Advanced Drug Delivery Reviews* 61, 2, pp. 101–114.
- Cunha-Vaz, J.G. 1997. The blood-ocular barriers: past, present, future. *Documenta Ophthalmologica* 93, 1–2, pp. 149–157.

Cunha-Vaz, J.G. 2004. The blood-retinal barrier system. Basic concepts and clinical evaluation. *Experimental Eye Research* 78, 3, 715–721.

Cunha-Vaz, J.G. 2009. The Blood-Retinal Barrier in Retinal Disease. *European Ophthalmic Review* 3, 2, pp. 105–108.

Cussler, E.L. 2009. *Diffusion – Mass Transfer in Fluid Systems*. 3rd ed. New York, USA, Cambridge University Press. 631 p.

Dechadilok, P. & Deen. W.M. 2006. Hindrance Factors for Diffusion and Convection in Pores. *Industrial & Engineering Chemistry Research* 45, 21, pp. 6953–6959.

Del Amo, E.M. & Urtti, A. 2008. Current and future ophthalmic drug delivery systems. A shift to the posterior segment. *Drug Discovery Today* 13, 3-4, pp. 135–143.

Edwards, A. & Prausnitz, M. 1998. Fiber Matrix Model of Sclera and Corneal Stroma for Drug Delivery to the Eye. *AIChE Journal* 44, 1, pp. 214–225.

Edwards, A. & Prausnitz, M. 2001. Predicted permeability of the cornea to topical drugs. *Pharmaceutical Research* 18, 11, pp. 1497–508.

Essner, E. & Gordon, S.R. 1983. Observations on the permeability of the choriocapillaris of the eye. *Cell and Tissue Research* 231, 3, pp. 571-577.

Federman, J. 1982. The fenestrations of the choriocapillaris in the presence of choroidal melanoma. *Transactions of the American Ophthalmological Society* 80, pp. 498–516.

Friedman, D.S., O'Colmain, B.J., Muñoz, B., Tomany, S.C., McCarty, C., de Jong, P.T., Nemesure, B., Mitchell, P., Kempner, J. & Eye Diseases Prevalence Research Group. 2004. Prevalence of age-related macular degeneration in the United States. *Archives of Ophthalmology* 122, 4, pp. 564–572.

Gallo, J.M. 2003. *Pharmacokinetics: Model Structure and Transport Systems*. In: Amidon, G.L., Lee, P.I. & Topp, E.M. *Transport Processes in Pharmaceutical Systems*. New York, USA, Marcel Dekker, Inc. pp. 219–316.

Garron, L.K. 1963. The Ultrastructure of the Retinal Pigment Epithelium with Observations on the Choriocapillaris and Bruch's Membrane. *Transactions of the American Ophthalmological Society* 61, pp. 545–588.

Gavaghan, D., Garny, A., Maini, P.K. & Kohl, P. 2006. Mathematical models in physiology. *Philosophical Transactions of the Royal Society A* 364, 1842, pp. 1099–106.

Goldbaum, M.H. & Madden, K. 1982. A new perspective on Bruch's membrane and the retinal pigment epithelium. *British Journal of Ophthalmology* 66, 1, pp. 17–25.

Griep, L.M., Wolbers, F., de Wagenaar, B., ter Braak, P.M., Weksler, B.B., Romero, I.A., Couraud, P.O., Vermes, I., van der Meer, A.D. & van der Berg, A. 2013. BBB on chip: microfluidic platform to mechanically and biochemically modulate blood-brain barrier function. *Biomedical Microdevices* 15, 1, pp. 145–150.

Guymer, R., Luthert, P. & Bird, A. 1998. Changes in Bruch's Membrane and Related Structures with Age. *Progress in Retinal and Eye Research* 18, 1, pp. 59–90.

Hewitt, A. T., Nakazawa, K. & Newsome, D.A. 1989. Analysis of Newly Synthesized Bruch's Membrane Proteoglycans. *Investigative Ophthalmology & Visual Science* 30, 3, pp. 478–486.

Hillenkamp, J., Hussain, A.A., Jackson, T.J., Constable, P.A. Cunningham, J.R. & Marshall, J. 2004. Compartmental analysis of taurine transport to the outer retina in the bovine eye. *Investigate Ophthalmology & Visual Science* 45, 11, 4099-4105.

Hirsch, M., Prenant, G. & Renard, G. 2001. Three-dimensional Supramolecular Organization of the Extracellular Matrix in Human and Rabbit Corneal Stroma, as Revealed by Ultrarapid-freezing and Deep-etching Methods. *Experimental Eye Research* 72, 2, pp. 123–135.

Ho, N.F.H., Raub, T.J., Burton, P.S., Adson, A., Audus, K.L. & Borchardt, R.T. 2003. Quantitative Approaches to Delineate Passive Transport Mechanisms in Cell Culture Monolayers. In: Amidon, G.L., Lee, P.I. & Topp, E.M. *Transport Processes in Pharmaceutical Systems*. New York, USA, Marcel Deccer, Inc. pp. 219–316.

Hogan, M.J. & Alvarado, J. 1967. Studies on the Human Macula IV. Aging Changes in Bruch's Membrane. *Archives of Ophthalmology* 77, 3, pp. 410–420.

Hosoya, K., Yamamoto, A., Akanuma, S. & Tachikawa, M. 2010. Lipophilicity and Transporter Influence on Blood-Retinal Barrier Permeability: A Comparison with Blood-Brain Barrier Permeability. *Pharmaceutical Research* 27, 12, pp. 2715–2724.

Hudspeth, A.J. & Yee, A.G. 1973. The intercellular junctional complexes of retinal pigment epithelia. *Investigative Ophthalmology & Visual Science* 12, 5, pp. 354–365.

Hulmes, D.J.S. 2008. Collagen Diversity, Synthesis and Assembly. In: Fratzl, P. (ed.). *Collagen Structure and Mechanics*. New York, USA, Springer. pp. 15–48.

Hussain, A.A., Rowe, L. & Marshall, J. 2002. Age-related alterations in the diffusional transport of amino acids across the human Bruch's-choroid complex. *Journal of the Optical Society of America. A, Optics, Image Science, and Vision* 19, 1, pp. 166–172.

Hussain, A.A., Starita, C., Hodgetts, A. & Marshall, J. 2010. Macromolecular diffusion characteristics of ageing human Bruch's membrane: Implications for age-related macular degeneration (AMD). *Experimental Eye Research* 90, 6, pp. 703–710.

Hutton, D.V. 2003. *Fundamentals of Finite Element Analysis*. New York, USA, McGraw-Hill Science. pp. 494.

Hynes, S.R. & Lavik, E.B. 2010. A tissue-engineered approach towards retinal repair: Scaffolds for cell transplantation to the subretinal space. *Graefe's Archive for Clinical and Experimental Ophthalmology* 248, 6, pp. 763–778.

Hämäläinen, K.M., Kontturi, K., Auriola, S., Murtomäki, L. & Urtti, A. 1997. Estimation of pore size and pore density of biomembranes from permeability measurements of polyethylene glycols using an effusion-like approach. *Journal of Controlled Release* 49, 2–3, pp. 97–104.

Inatani, M. & Tanihara, H. 2002. Proteoglycans in retina. *Progress in Retinal and Eye Research* 21, 5, pp. 429–447.

Johansson, L. & Löfroth, J.-E. 1993. Diffusion and interaction in gels and solutions. 4. Hard sphere Brownian dynamic simulations. *The Journal of Chemical Physics* 98, 9, pp. 7471–7479.

Johnson, E.M., Berk, D.A., Jain, R.K. & Deen, W.M. 1995. Diffusion and partitioning of proteins in charged agarose gels. *Biophysical Journal* 68, 4, pp. 1561–1568.

Johnson, E.M., Berk, D.A., Jain, R.K. & Deen, W.M. 1996. Hindered diffusion in agarose gels: test of effective medium model. *Biophysical Journal* 70, 2, pp. 1017–1023.

Johnson, E.M. & Deen, W.M. 1996. Electrostatic Effects on the Equilibrium Partitioning of Spherical Colloids in Random Fibrous Media. *Journal of Colloid and Interface Science* 178, 2, pp. 749–756.

Jylhä, A. 2013. Researcher, Ophthalmology Group, Institute of Biomedical Technology, University of Tampere. Tampere. Personal communications 11.2.2013.

Kadam, R.S. & Kompella, U.B. 2009. Cassette analysis of eight beta-blockers in bovine eye sclera, choroid-RPE, retina, and vitreous by liquid chromatography-tandem mass spectrometry. *Journal of Chromatography B* 877, 3, pp. 253–260.

Kadam, R.S. & Kompella U.B. 2010. Influence of Lipophilicity on Drug Partitioning into Sclera, Choroid-Retinal Pigment Epithelium, Retina, Trabecular Meshwork, and Optic Nerve. *The Journal of Pharmacology and Experimental Therapeutics* 332, 3, pp. 1107–1120.

- Kadam, R.S., Cheruvu, N.P.S., Edelhauser, H.F. & Kompella, U.B. 2011. Sclera-Choroid-RPE Transport of Eight β -blockers in Human, Bovine, Porcine, Rabbit and Rat Models. *Investigative Ophthalmology & Visual Science* 52, 8, pp. 5387–5399.
- Kao, H.P., Abney, J.R. & Verkman, A.S. 1993. Determinants of the Translational Mobility of a Small Solute in Cell Cytoplasm. *The Journal of Cell Biology* 120, 1, pp. 175–184.
- Kimura, M., Araie, M. & Koyano, S. 1996. Movement of Carboxyfluorescein across Retinal Pigment Epithelium-Choroid. *Experimental Eye Research* 63, 1, pp. 51–56.
- Krug, S.M., Fromm, M. & Günzel, D. 2009. Two-Path Impedance Spectroscopy for Measuring Paracellular and Transcellular Epithelial Resistance. *Biophysical Journal* 97, 8, pp. 2202–2211.
- Leblanc, B., Jezequel, S. Davies, T., Hanton, G. & Taradach, C. 1998. Binding of Drugs to Eye Melanin Is Not Predictive of Ocular Toxicity. *Regulatory Toxicity and Pharmacology* 28, 2, pp. 124–132.
- Li, H., Sheppard, D.N. & Hug, M.J. 2004. Transepithelial electrical measurements with the Ussing chamber. *Journal of Cystic Fibrosis* 3, Supplement 2, pp. 123–126.
- Lieb, W. & Stein, W. 1986. Non-Stokesian Nature of Transverse Diffusion Within Human Red Cell Membranes. *Journal of Membrane Biology* 92, 2, pp. 111–119.
- Lowrey, A.H., Famini, G.R., Loumbev, V., Wilson, L.Y. & Tosk, J.M. 1997. Modeling Drug-Melanin Interactions With Theoretical Linear Solvation Energy Relationships. *Pigment Cell Research* 10, 1, pp. 251–256.
- Nelson, P. 2008. *Biological Physics – Energy, Information, Life*. New York, USA, W.H. Freeman and Company. 630 p.
- Mac Gabhann, F., Demetriades, A.M., Deering, T., Packer, J.D., Shah, S.M., Duh, E., Campochiaro, P.A. & Popel, A.S. 2007. Protein transport to choroid and retina following periocular injection: theoretical and experimental study. *Annals of Biomedical Engineering* 35, 4, pp. 615–630.
- Marieb, E.N. 2009. *Essentials of Human Anatomy and Physiology*. 9th ed. San Francisco, USA, Pearson Benjamin Cummings. 632 p.
- Marshall, J. 1987. The Ageing Retina: Physiology or Pathology. *Eye* 1, 2, pp. 282–295.
- Mattern, K.J., Nakornchai, C. & Deen, W.M. 2008. Darcy Permeability of Agarose-Glycosaminoglycan Gels Analyzed Using Fiber-Mixture and Donnan Models. *Biophysical Journal* 95, 2, pp. 648–656.

- Melamed, S., Ben-Sira, I. & Ben-Shaul, Y. 1980. Ultrastructure of fenestrations in endothelial choriocapillaris of the rabbit – a freeze-fracturing study. *British Journal of Ophthalmology* 64, 7, pp. 537–543.
- Michel, C.C. & Curry, F.E. 1999. Microvascular Permeability. *Physiological Reviews* 79, 3, pp. 703–761.
- Mitragotri, S. 2003. Modeling skin permeability to hydrophilic and hydrophobic solutes based on four permeation pathways. *Journal of Controlled Release* 86, 1, pp. 69–92.
- Moore, D.J., Hussain, A.A. & Marshall, J. 1995. Age-Related Variation in the Hydraulic Conductivity of Bruch's Membrane. *Investigative Ophthalmology & Visual Science* 36, 7, pp. 1290–1297.
- Moore, D.J. & Clover, G.M. 2001. The Effect of Age on the Macromolecular Permeability of Human Bruch's Membrane. *Investigative Ophthalmology & Visual Science* 42, 12, pp. 2970–2975.
- Mullins, R. & Sohn, E. 2012. Bruch's Membrane: The Critical Boundary in Macular Degeneration. In: Ying, G.-S. (ed.). *Age Related Macular Degeneration – The Recent Advances in Basic Research and Clinical Care*. Rijeka, Croatia, InTech. pp. 49–72.
- Mälkiä, A., Murtomäki, L., Urtti, A. & Kontturi, K. 2004. Drug permeation in biomembranes In vitro and in silico prediction and influence of physicochemical properties. *European Journal of Pharmaceutical Sciences* 23, 1, pp. 13–47.
- Ogston, A.G. 1958. The spaces in a uniform random suspension of fibers. *Transactions of the Faraday Society* 54, pp. 1754–1757.
- Ogston, A.G., Preston, B.N. & Wells, J.D. 1973. On the transport of compact particles through solutions of chain-polymers. *Proceedings of the Royal Society, Series A, Mathematical and Physical Sciences* 333, 1594, pp. 297–316.
- Pascolini, D. & Mariotti, S.P. 2012. Global estimates of visual impairment: 2010. *British Journal of Ophthalmology* 96, 5, pp. 614–618.
- Peng, S., Rahner, C. & Rizzolo, L.J. 2003. Apical and Basal Regulation of the Permeability of the Retinal Pigment Epithelium. *Investigate Ophthalmology & Visual Science* 44, 2, pp. 808–817.
- Peng, S., Rao, V.S., Adelman, R.A. & Rizzolo, L.J. 2011. Claudin-19 and the Barrier Properties of the Human Retinal Pigment Epithelium. *Investigative Ophthalmology & Visual Science* 52, 3, pp. 1392–1403.

- Perrins, W., McKenzie, D. & McPhedran, R. 1979. Transport Properties of Regular Arrays of Cylinders. *Proceedings of the Royal Society, Series A, Mathematical and Physical Sciences* 369, 1737, pp. 207–225.
- Pescina, S., Santi, P., Ferrari, G., Padula, C., Cavallini, P., Govoni, P. & Nicoli, S. 2012. *Ex vivo* models to evaluate the role of ocular melanin in trans-scleral drug delivery. *European Journal of Pharmaceutical Sciences* 46, 5, pp. 475–483.
- Phillips, R.J., Deen, W.M. & Brady, J.F. 1989. Hindered transport of spherical macromolecules in fibrous membranes and gels. *AIChE Journal* 35, 11, pp. 1761–1769.
- Phillips, R.J. 2000. A Hydrodynamic Model for Hindered Diffusion of Proteins and Micelles in Hydrogels. *Biophysical Journal* 79, 6, pp. 3350–3353.
- Pino, R.M. & Essner, E. 1981. Permeability of Rat Choriocapillaris to Hemeproteins. Restriction of Tracers by a Fenestrated Endothelium. *The Journal of Histochemistry and Cytochemistry* 29, 2, pp. 281–290.
- Pitkänen, L., Ranta, V.-P., Moilanen, H. & Urtti, A. 2005. Permeability of retinal pigment epithelium: effects of permeant molecular weight and lipophilicity. *Investigative Ophthalmology & Visual Science* 46, 2, pp. 641–646.
- Pitkänen, L., Ranta, V.-P., Moilanen, H. & Urtti, A. 2007. Binding of Betaxalol, Metoprolol and Oligonucleotides to Synthetic and Bovine Ocular Melanin, and Prediction of Drug Binding to Melanin in Human Choroid-Retinal Pigment Epithelium. *Pharmaceutical Research* 24, 11, pp. 2063–2070.
- Prausnitz, M. & Noonan, J. 1998. Permeability of cornea, sclera and conjunctiva: a literature analysis for drug delivery to the eye. *Journal of Pharmaceutical Sciences* 87, 12, pp. 1479–1488.
- Rahner, C., Fukuhara, M., Peng, S., Kojima, S. & Rizzolo, L.J. 2004. The apical and basal environments of the retinal pigment epithelium regulate the maturation of tight junctions during development. *Journal of Cell Science* 117, 15, pp. 307–318.
- Rajasekaran, S.A., Hu, J., Gopal, J., Gallemore, R., Ryazantsev, S., Bok, D. & Rajasekaran, A.K. 2003. Na,K-ATPase inhibition alters tight junction structure and permeability in human retinal pigment epithelial cells. *American Journal of Physiology. Cell Physiology* 284, 6, pp. C1497–1507.
- Ramrattan, R.S., van der Schaft, T.L., Mooy, C.M., de Bruijn, W.C., Mulder, P.G.H. & de Jong, P.T.V.M. 1994. Morphometric Analysis of Bruch's Membrane, the Choriocapillaris, and Choroid in Aging. *Investigative Ophthalmology & Visual Science* 35, 6, pp. 2857–2864.

- Ranta, V.-P., Toropainen, E., Talvitie, A., Auriola, S. & Urtti, A. 2002. Simultaneous determination of eight β -blockers by gradient high-performance liquid chromatography with combined ultraviolet and fluorescence detection in corneal permeability studies in vitro. *Journal of Chromatography B* 772, 1, pp. 81–87.
- Ranta, V.-P. & Urtti, A. 2006. Transscleral drug delivery to the posterior eye: prospects of pharmacokinetic modeling. *Advanced Drug Delivery Reviews* 58, 11, pp. 1164–1681.
- Ranta, V.-P., Mannermaa, E., Lummeppuro, K., Subrizi, A., Laukkanen, A., Antopolsky, M., Murtomäki, L., Hornof, M. & Urtti, A. 2010. Barrier analysis of periocular drug delivery to the posterior segment. *Journal of Controlled Release* 148, 1, pp. 42–48.
- Rizzolo, L.J. 2007. Development and role of tight junctions in the retinal pigment epithelium. *International Review of Cytology* 258, pp. 195–234.
- Rizzolo, L.J., Peng, S., Luo, Y. & Xiao, W. 2011. Integration of tight junctions and claudins with the barrier functions of the retinal pigment epithelium. *Progress in Retinal and Eye Research* 30, 5, pp. 296–323.
- Sanders, B., Larsen, M., Moldow, B. & Lund-Andersen, H. 2001. Diabetic Macular Edema: Passive and Active Transport of Fluorescein through the Blood-Retina Barrier. *Investigative Ophthalmology & Visual Science* 42, 2, pp. 433–438.
- Sasaki, H., Matsui, C., Furuse, K., Mimori-Kiyosue, Y., Furuse, M. & Tsukita, S. 2003. Dynamic behavior of paired claudin strands within apposing plasma membranes. *Proceedings of the National Academy of Sciences* 100, 7, pp. 3971–3976.
- Schneeberger, E.E. & Lynch R.D. 2003. The tight junction: a multifunctional complex. *American Journal of Physiology. Cell Physiology* 286, 9, pp. C1213–1228.
- Starita, C., Hussain A.A., Patmore, A. & Marshall J. 1997. Localization of the Site of Major Resistance to Fluid Transport in Bruch's membrane. *Investigative Ophthalmology & Visual Science* 38, 3, pp. 762–767.
- Steuer, H., Jaworski, A., Elger, B., Kaussmann, M., Keldenich, J., Schneider, H., Stoll, D. & Schlosshauer, B. 2005. Functional Characterization and Comparison of the Outer Blood-Retina Barrier and the Blood-Brain Barrier. *Investigative Ophthalmology & Visual Science* 46, 3, pp. 1047–1053.
- Stevenson, B.R., Anderson, J.M., Goodenough, D.A. & Mooseker, M.S. 1988. Tight Junction Structure and ZO-1 Content Are Identical in Two Strains of Madin-Darby Canine Kidney Cells Which Differ in Transepithelial Resistance. *The Journal of Cell Biology* 107, 6, pp. 2401–2408.

- Strauss, O. 2005. The Retinal Pigment Epithelium in Visual Function. *Physiological Reviews* 85, 3, pp. 845–881.
- Stylianopoulos, T., Poh, M.-Z., Insin, N., Bawendi, M.G., Fukurama, D., Munn, L.L. & Jain, R.K. 2010a. Diffusion of particles in the Extracellular Matrix: The Effect of Repulsive Electrostatic Interactions. *Biophysical Journal* 99, 5, pp. 1342–1349.
- Stylianopoulos, T., Diop-Frimpong, B., Munn, L.L. & Jain, R.K. 2010b. Diffusion Anisotropy in Collagen Gels and Tumors: The Effect of Fiber Network Orientation. *Biophysical Journal* 99, 10, pp. 3119–3128.
- Sutherland, W. 1905. A Dynamic Theory of Diffusion for Non-Electrolytes and the Molecular Mass of Albumin. *Philosophical Magazine* 9, 6, pp. 781–785.
- Thrimawithana, T.R., Young, S., Bunt, C.R., Green, C. & Alany, R.G. 2011. Drug deliver to the posterior segment of the eye. *Drug Discovery Today* 16, 5-6, pp. 270–277.
- Van Itallie, C.M. & Anderson, J.M. 2004. The molecular physiology of tight junction pores. *Physiology (Bethesda)* 19, pp. 331-338.
- Van Itallie, C.M., Holmes, J., Bridges, A., Gookin, J.L., Coccaro, M.R., Proctor, W., Colegio, O.R. & Anderson, J.M. 2008. The density of small tight junction pores varies among cell types and is increased by expression of claudin-2. *Journal of Cell Science* 121, 3, pp. 298–305.
- Yu, L.X. & Amidon, G.L. 2000. Analytical Solutions to Mass Transfer. In: Amidon, G.L., Lee, P.I. & Topp, E.M. (ed.). *Transport Processes in Pharmaceutical Systems*. New York, USA, Marcel Dekker. 727 p.
- Zayas-Santiago, A., Marmorstein, A.D. & Marmorstein, L.Y. 2011. Relationship of Stokes Radius to the Rate of diffusion across Bruch's Membrane. *Investigative Ophthalmology & Visual Science* 52, 7, pp. 4907–4913.

APPENDIX 1: MOLECULES OF THE BRB MODEL, THEIR PROPERTIES AND MEASURED PERMEABILITIES

Table A1.1. The parameter values in the validation of the BRB model. (M_s : molecular mass; V : van der Waals volume; r_s : radius; D_0 : free diffusion coefficient; $\log K_p$: partition coefficient; $\log K_D$: distribution coefficient; K_a : association constant; q_s : charge)

Molecule	M_s (Da)	V (\AA^3)	r_s (\AA)	D_0 ($10^{-6} \text{ cm}^2 \text{ s}^{-1}$)	$\log K_p$	$\log K_D$	K_a (μM^{-1})	q_s
Atenolol	266.34	261.34	6.24	7.89	0.70	-1.65	0.141	+1
Betaxolol	307.43	313.49	6.66	7.39	2.53	0.31	0.243	+1
Carboxyfluorescein	376.32	299.15	7.30	6.74	3.54	0.16	0.235	-1
Cimetidine	252.34	226.82	6.09	8.08	-0.29	-0.34	0.209	0
Clonidine	230.10	177.15	5.84	8.43	2.49	1.66	0.313	+1
Fluorescein	332.07	271.40	6.90	7.14	3.88	3.86	0.428	0
Gabapentin	171.24	176.16	5.11	9.63	-1.27	-1.27	0.161	0
Levofloxacin	361.37	309.99	7.17	6.87	0.65	-0.28	0.212	-1
Mannitol	182.17	165.06	5.25	9.37	-3.73	-3.73	0.033	0
Memantine	179.30	194.54	5.22	9.44	2.07	-0.78	0.186	+1
Methylene blue	284.40	262.13	6.43	7.66	2.61	2.61	0.363	+1
Methylprednisolone	374.47	356.94	7.28	6.76	1.56	1.56	0.308	0
Metoprolol	257.36	274.24	6.14	8.01	1.75	-0.47	0.202	+1
Nadolol	309.40	305.19	6.68	7.37	0.85	-1.44	0.152	+1
Nicotine	162.12	164.23	4.98	9.88	1.16	-0.31	0.211	+1
Phenylalanine	165.19	155.62	5.03	9.79	-1.18	-1.19	0.165	0
Pindolol	248.32	269.33	6.05	8.14	1.69	-0.53	0.199	+1
Probenecid	285.36	260.88	6.44	7.64	2.44	-0.92	0.179	-1
Propranolol	259.34	257.56	6.17	7.98	2.58	0.36	0.246	+1
Rhodamine 123	345.37	301.75	7.02	7.01	4.01	4.01	0.435	+1
Rhodamine 6G	443.47	420.09	7.89	6.26	5.35	5.33	0.504	0
Sotalol	272.36	252.38	6.30	7.81	-0.40	-2.12	0.117	+1
Timolol	316.42	292.07	6.75	7.29	1.33	-0.97	0.176	+1
Verapamil	454.60	458.65	7.95	6.19	5.04	2.79	0.372	+1

Table A1.2. *The measured permeability coefficients used in the validation of the BRB model.*

Molecule	Measured mean P (10^{-6} cm s $^{-1}$)	Tissue	Reference
Atenolol	2.00	Bovine choroid and BRB	Pitkänen et al. 2005
	0.01	Bovine choroid and BRB	Steuer et al. 2004
	1.47	Bovine choroid and BRB	Kadam et al. 2011
	2.71	Porcine choroid and BRB	Kadam et al. 2011
	5.67	Human choroid and BRB	Kadam et al. 2011
	8.09	Bovine choroid and BrM	Cheruvu & Kompella 2006
Betaxolol	10.3	Bovine choroid and BRB	Pitkänen et al. 2005
	0.19	Bovine choroid and BRB	Kadam et al. 2011
	0.3	Porcine choroid and BRB	Kadam et al. 2011
	3.49	Human choroid and BRB	Kadam et al. 2011
Carboxyfluorescein	0.96	Bovine choroid and BRB	Pitkänen et al. 2005
Cimetidine	0.293	Bovine choroid and BRB	Steuer et al. 2004
Clonidine	5.04	Bovine choroid and BRB	Steuer et al. 2004
Fluorescein	0.18	Bovine choroid and BRB	Steuer et al. 2004
	1.94	Human BRB (<i>in vivo</i>)	Sander et al. 2001
	0.92	Bovine choroid and BRB	Cheruvu & Kompella 2006
Gabapentin	0.959	Bovine choroid and BRB	Steuer et al. 2004
Levofloxacin	59.7	Porcine choroid and BrM	Pescina et al. 2012
Mannitol	3.33	Human RPE	Rajasekaran et al. 2003
	21.34	Bovine choroid and BrM	Cheruvu & Kompella 2006
Memantine	31.7	Bovine choroid and BRB	Steuer et al. 2004
Methylene blue	21.0	Porcine choroid and BrM	Pescina et al. 2012
Methylprednisolone	50.2	Porcine choroid and BrM	Pescina et al. 2012
Metoprolol	10.6	Bovine choroid and BRB	Pitkänen et al. 2005
	0.4	Bovine choroid and BRB	Kadam et al. 2011
	0.65	Porcine choroid and BRB	Kadam et al. 2011
	4.53	Human choroid and BRB	Kadam et al. 2011
	2.03	Bovine choroid and BRB	Pitkänen et al. 2005
Nadolol	1.18	Bovine choroid and BRB	Kadam et al. 2011
	4.62	Porcine choroid and BRB	Kadam et al. 2011
	2.25	Human choroid and BRB	Kadam et al. 2011
Nicotine	16.5	Bovine choroid and BRB	Steuer et al. 2004
Phenylalanine	55.02	Human choroid and BrM	Hussain et al. 2002
Pindolol	3.48	Bovine choroid and BRB	Pitkänen et al. 2005
	0.13	Bovine choroid and BRB	Kadam et al. 2011
	0.11	Porcine choroid and BRB	Kadam et al. 2011
	3.32	Human choroid and BRB	Kadam et al. 2011
	0.952	Bovine choroid and BRB	Steuer et al. 2004
Propranolol	0.01	Bovine choroid and BRB	Kadam et al. 2011
	0.096	Porcine choroid and BRB	Kadam et al. 2011
Rhodamine 123	1.34	Human choroid and BRB	Kadam et al. 2011
	77.0	Porcine choroid and BrM	Pescina et al. 2012
	0.23	Bovine choroid and BRB	Steuer et al. 2004

Molecule	Measured mean P (10^{-6} cm s $^{-1}$)	Tissue	Reference
Rhodamine 6G	0.07	Bovine choroid and BrM	Cheruvu & Kompella 2006
Sotalol	1.31	Bovine choroid and BRB	Kadam et al. 2011
	2.24	Porcine choroid and BRB	Kadam et al. 2011
	6.03	Human choroid and BRB	Kadam et al. 2011
Timolol	8.41	Bovine choroid and BRB	Pitkänen et al. 2005
	0.37	Bovine choroid and BRB	Kadam et al. 2011
	0.37	Porcine choroid and BRB	Kadam et al. 2011
	3.99	Human choroid and BRB	Kadam et al. 2011
Verapamil	11.6	Bovine choroid and BRB	Steuer et al. 2004

APPENDIX 2: RESULTS OF THE BRB MODEL VALIDATION

Table A2.1. The calculated RPE (P_{RPE}), BrM (P_{BrM}), CE (P_{CE}) and total BRB (P_{BRB}) permeability values in the validation of the BRB model. P_{RPE} and P_{BRB} are shown with and without melanin. All the results have units of cm s^{-1} .

Molecule	P_{RPE} with melanin	P_{RPE} without melanin	P_{BrM}	P_{CE}	P_{BRB} with melanin	P_{BRB} without melanin
Atenolol	2.44	2.44	87.1	5340	2.37	2.37
Betaxolol	1.84	1.84	63.0	4780	1.79	1.79
Carboxyfluorescein	1.40	1.40	25.3	4030	1.32	1.32
Cimetidine	2.66	2.66	79.0	5600	2.57	2.57
Clonidine	3.05	38.33	119	6020	2.97	28.85
Fluorescein	1.52	35.28	42.6	4480	1.47	19.21
Gabapentin	4.35	4.35	167	7520	4.24	4.24
Levofloxacin	1.43	1.43	28.0	4170	1.36	1.36
Mannitol	4.06	4.06	150	7180	3.95	3.95
Memantine	4.13	4.14	193	7270	4.05	4.05
Methylene blue	2.17	3.65	75.3	5090	2.11	3.48
Methylprednisolone	1.40	1.40	31.6	4050	1.34	1.34
Metoprolol	2.58	2.58	93.9	5510	2.51	2.51
Nadolol	1.81	1.81	62.1	4750	1.76	1.76
Nicotine	4.62	4.83	232	7820	4.52	4.73
Phenylalanine	4.52	4.54	178	7720	4.41	4.43
Pindolol	2.73	2.73	101	5670	2.65	2.65
Probenecid	2.15	2.15	48.5	5080	2.06	2.06
Propranolol	2.55	2.55	92.4	5480	2.48	2.48
Rhodamine 123	1.48	7.67	47.6	4340	1.43	6.59
Rhodamine 6G	1.26	1.33	20.2	3490	1.19	1.25
Sotalol	2.34	2.34	83.0	5270	2.28	2.28
Timolol	1.72	1.72	58.8	4670	1.67	1.67
Verapamil	1.24	1.24	22.9	3420	1.18	1.18